LBL-1183
Preprint

HIGH TEMPERATURE CREEP IN METALS AT INTERMEDIATE AND LOW STRESSES

Farghalli Abdel Rahman Mohamed
(Ph.D. thesis)

November 1972

AEC Contract No. W-7405-eng-48

LBL-1183

DISCLAIMER

Dedicated

to

Professor John E. Dorn

HIGH TEMPERATURE CREEP IN METALS
AT INTERMEDIATE AND LOW STRESSES

Contents

HIGH TEMPERATURE CREEP IN METALS AT INTERMEDIATE AND LOW STRESSES

Farghalli Abdel Rahman Mohamed

Inorganic Materials Research Division, Lawrence Berkeley Laboratory and Department of Materials Science and Engineering, College of Engineering; University of California, Berkeley, California

ABSTRACT

High-temperature creep has been studied in aluminum-3% magnesium (solid solution alloy), aluminum, lead and tin in the stress range of 10^{-6} - 10^{-3} G using double-shear type specimen at temperatures near the melting point. The experimental data reveal two important transitions in the rate controlling mechanism:

(i) For aluminum-3% magnesium there is a transition from viscous glide behavior to climb-controlled mechanism at $\tau \sim 6 \times 10^{-5}$ G. The identification of such a transition was determined from the stress exponent, n, the type of the creep curve observed and the activation energy for creep.

(ii) For aluminum-3% magnesium, lead and tin at $\tau \leqslant 10^{-5}$ G the dominant creep mechanism changes from climb mechanism to Harper-Dorn creep, a type of viscous deformation first reported in pure aluminum at high temperature and low stress. It is characterized by a creep rate which is linearly dependent on the applied stress and apparently independent of grain size. The identification of Harper-Dorn behavior in the metals tested was determined from the linear stress exponent, the discrepancy between the experimental values of the creep rate and that obtainable from various mechanisms of viscous deformation and the close correspondence between the experimental data and the

earlier results on pure aluminum. The experimental results on aluminum reproduce the data of Harper and Dorn almost exactly, despite a significant difference in the sample and load geometries.

The experimental evidence of Harper-Dorn creep in aluminum-3% magnesium, lead and tin along with data indicating the occurrence of the same creep behavior in other materials suggests that Harper-Dorn creep might be a general mechanism for creep at high temperature and low stress. Available microstructural evidence on the mechanism of Harper-Dorn is reviewed. While the details of the process are unknown, available data may be interpreted as due to climb of "saturated" dislocations. The simple Harper-Dorn creep behavior disappears when the applied stress exceeds a critical value or when sample grain size becomes sufficiently small. In the first case, the rate controlling mechanism changes to climb behavior while in the second case Nabarro-Herring mechanism dominates.

I. INTRODUCTION

A. General Review

The time-dependent plastic deformation of materials under constant stress is known as creep. Creep can take place only as a result of thermal activation of the deformation process (Fig. 1). Consequently, the shear strain rate of creep, $\dot{\gamma}$, for the ith mechanism can be written formally in terms of the probability of a thermal fluctation[1] as

$$\dot{\gamma}_i = f_i^+ \{\tau, st, T\} \exp -h_i^+ (\tau, st, T)/kT \qquad (1)$$

$$-f_i^- \{\tau, st, T\} \exp -h_i^- (\tau, st, T)/kT$$

where k is the Boltzmann constant and T is the absolute temperature. The enthalpy of activation, h_i, depends on the applied shear stress which assists the forward reaction (+) and hinders the reverse reaction (-), thus giving magnitude and directionality to the strain-rate. The frequency term f_i represents the strain per second per successful fluctuation, into which the activation entropy has been incorporated. Both the frequency factor, f_i, and the enthalpy of activation, h_i, could be a function of the applied shear stress, τ, the instantaneous structure of the material, st, and the temperature, T. As in all kinetics of reaction problems, the net forward rate is determined by the total contribution to the forward rate minus the total contribution to the reverse rate, which gives rise to the two terms of Eq. (1).

Occasionally, several mechanisms operate simultaneously. If they operate in sequence, such that the second can take place after the first mechanism has occurred, creep for the sequence is dictated by the slowest process. When the total creep rate arises from a series of parallel,

and independently operative mechanisms, the total creep rate is given by the sum of the contributions over all such independent processes. The objective of fundamental investigation on creep, is the determination of the rate-controlling mechanisms. When the mechanisms of creep are uncovered in sufficient detail, it should be possible to predict the shape of the creep curve and thus facilitate creep testing as well as design for creep resistance. Furthermore, when the mechanisms are known, it may be possible to introduce factors that block the prominent mechanisms and thereby reduce the creep rate. Frequently, over certain regions of stress, structure, and temperature, the creep rate arises principally from a single mechanism.

The analyses here will be limited to discussion of high temperature creep phenomena that are controlled by diffusion mechanisms. Such diffusion-controlled processes assume significance at temperature above about one-half of the melting point. In this range of temperatures, the creep rate is almost always determined by one or more of several diffusion-controlled mechanisms. In addition, above $T_m/2$ diffusion becomes reasonably rapid, and dislocations acquire a new degree of freedom in their motion; edge-components of dislocations are no longer confined to glide exclusively on their original slip planes and may climb to new planes. The most important diffusion-controlled mechanisms suggested for high temperature creep include

(i) stress-directed diffusion of vacancies in polycrystals

(ii) thermally activated motion of jogged screw dislocations

(iii) climb of edge dislocations

(iv) solute atom diffusional processes and viscous drag.

The viscous creep mechanism concerned with the stress-directed diffusion of vacancies in grain boundaries,[2] superplastic mechanism,[3] and dispersion hardened creep[4] will not be considered here.

(i) Stress-directed diffusion of vacancies in polycrystals

Creep by the stress-directed diffusion of vacancies, formulated originally by Nabarro[5] and further elaborated by Herring,[6] is one of the best understood mechanism for high temperature creep. Three steps are involved in the original stress-directed diffusion model for creep: (1) The formation of a vacancy in the grain volume near the grain boundary under a positive stress. (2) Its migration to the boundary that is under a negative stress. (3) Its annihilation at that boundary.

The flow of vacancies will be matched by an equal and opposite flow of atoms resulting in a longitudinal extension and lateral contraction of the grain with time under stress (Fig. 2). The shear creep rate, $\dot{\gamma}_s$, is given by

$$\dot{\gamma}_s = A_{NH} \frac{Db^3\tau}{d^2kT} \tag{2}$$

where b is the Burgers vector, τ the applied shear stress, d the mean grain diameter, and kT the Boltzmann constant times the absolute temperature. The diffusivity, D, is obtained from the tracer diffusivity D^*. For pure metals

$$D = \frac{D^*}{f} \tag{3a}$$

and for binary solution alloys[7]

$$D = \frac{D_A^* D_B^*}{(N_B D_A^* + N_A D_B^*) f} \tag{3b}$$

where N_A and N_B are the atomic fractions of A and B atoms, and f is the correlation factor. The dimensionless constant A_{NH} depends insensitively on the geometry of grains, but is generally estimated to have an average value of 14.

Nabarro creep applies only to polycrystalline aggregates at very high temperature, fine grain size and very low stresses.[8] It provides an independent deformation mechanism which does not involve the motion of dislocations. Nabarro creep is characterized by a creep rate that increases linearly with stress and inversely with the square of grain diameter, and has an activation energy that is nearly equal to that for self diffusion. Limitations of Nabarro creep will be discussed in more detail later in this thesis.

(ii) Creep due to the motion of jogged screw dislocations

Jogs in edge dislocations do not materially restrain the motion of an edge dislocation because the jogs also lie in slip planes, but jogs on screw dislocations are edge jogs, and if the screw dislocation is forced to move, such jogs must move from one slip plane to the next adjacent slip plane. This is only possible as a result of atom transfer (see Fig. 3). In view of the high energy of formation of interstitials, it has generally been conceded that the vacancy mechanism is much more probable. Vacancy generation and absorption models fall into two major categories, those that are based on thermal activation, e.g., Mott's original model,[9] and those that are diffusion controlled, as suggested by Friedel,[10] Hirsch and Warrington[11] and Barrett and Nix.[12] Although the various models differ somewhat in detail from one another and are

frequently given special interpretations, the factors of major interest here are at least sufficiently similar in all cases to permit a description of this process in terms of the recent dislocation theory by Gibbs[13] who has shown that to a good approximation,

$$\dot{\gamma}_e = 6 \rho_s D\{\exp(L_j b^2/kT)-1\} \qquad (4)$$

where $\dot{\gamma}_e$ is the secondary shear strain rate and the subscript e refers to the case of exclusively vacancy-emitting jogs. The term ρ_s, τ, L_j and D refer respectively to the density of the "mobile" screw dislocations, the applied shear stress, the mean distance between jogs, and the diffusivity. As will be illustrated in the discussion of this thesis, the screw dislocation models suffer from various handicaps, and major modifications are needed to obtain the correct activation energies and stress laws for the high stress-low temperature creep behavior. However, for the case of low stress-high temperature creep, the screw dislocation models with some modifications could be one of the possible rate controlling mechanisms.

(iii) Creep due to climb of edge dislocation

The theory for creep due to climb of edge dislocations is much more difficult to formulate accurately than that due to the motion of a jogged screw dislocation. This arises from the fact that the rate at which edge dislocations climb depends intimately on the geometric details of dislocation patterns that are produced under stress in the vicinity of the climbing dislocation. These patterns have not yet been sufficiently well documented to provide unambiguous guides to formulation of the climb process in detail. The theory for climb of dislocations has been discussed

by Mott,[14] Seeger,[15] and Weertman.[16,17] However, the first serious formulation dislocation-climb theory for steady-state creep was presented by Weertman in 1955.[16] It constituted a major advance in the rationalization of the mechanical behavior of metals at high temperatures. The first version, which postulated dislocation arrays piled up against Lomer-Cottrell dislocations, was limited to fcc metals. Only the second[17] and more generally applicable model will be discussed here. Weertman assumed that dislocation loops were emitted from fixed and more or less uniformly distributed Frank-Read sources. Screw dislocations of opposite sign from adjacent sources could cross-slip with ease and thus annihilate each other. In contrast, however, the leading edge dislocations from adjacent sources would block each others motion as a result of their mutual interactions (Fig. 4). Additional dislocations, however, would continue to issue from the sources until the back stress on the source equaled the applied stress. It was further tacitly assumed that the piled-up arrays were completely analogous to arrays piled-up against rigid barriers. Further deformation could then only take place when the two lead dislocations of opposite sign climbed together and annihilated each other this relieved the back stresses on the two sources and permitting another dislocation to be generated and move out from each source. The climb rate was assumed to be diffusion-controlled with distances of about the separation of the arrays. On this basis Weertman estimated that

$$\dot{\gamma}_s = \frac{\pi^2 \tau^2 D}{G^2 b^2} \sinh \frac{\sqrt{3}\, \tau^{2.5} b^{1.5}}{8\, G^{1.5} \sqrt{N}\, kT} \qquad (5)$$

where N is the number of dislocation sources per unit volume. The major virtue of Weertman's theory is that it correlates quite well with most of the mechanical data on high-temperature creep. It accounts for the observed apparent activation energies, the effect of the modulus of elasticity, and gives almost the observed stress law. However, several objections have been raised against the theory. These objections will be reviewed in the discussion section. Nevertheless, it seems inevitable that climb itself must necessarily play a role in any model for high-temperature creep; it need not, however, be the rate-controlling mechanism.

(iv) Solute atom diffusional process and viscous drag

A number of different dislocation-solute atom interaction mechanisms may be responsible for producing viscous glide creep in solid solution alloys. Any interaction mechanism[18,19,20] that can reduce the rate of gliding dislocation motion to a value which is so low that glide becomes slower than dislocation-climb recovery, can produce such creep behavior. For instance, when solute atoms are bound to dislocations through the Co-trell atmosphere,[20] glide can proceed no faster than the rate of solute atom diffusion.

A derivation for the rate of glide-controlled creep, which does not invoke fixed dislocation sources or glide of dislocation arrays, was made for the simple case where all dislocations within a crystal drag Cottrell atmospheres.[21] It was assumed that as each solute atom jumps forward one Burgers vector under the action of the applied stress, the dislocation also moves forward one Burgers vector (Fig. 5). Therefore, as shown by Bird, et al.,[21] the steady-state creep rate can

be approximated by

$$\frac{\dot{\gamma}kT}{DGb} = 6\left(\frac{\tau}{G}\right)^3 \tag{6}$$

This result is similar to that originally derived by Weertman.[22] The only difference is that the pre-exponential term is independent of solute concentration and independent of the details of the Cottrell interaction mechanism. A review of the literature shows that viscous glide creep is rate controlling in some solid solutions such as Al-Mg, Cu-Zn, and Au-Ni. Up to the present it has not been possible to predict which solid solution alloys should creep by the viscous glide mechanism and which should creep by dislocation climb.

There are two comments concerning the steady-state creep rate predicted from Eq. (6). First, the diffusivity (D) differs from that given for the climb mechanism (vacancy diffusivity) since it refers to the chemical interdiffusivity of the alloy, $\tilde{D}$, or equivalently to the Darken expression[23] for interdiffusivity for binary solutions

$$\tilde{D} = (N_A D_B^* + N_B D_A^*)\left(1 + \frac{\partial \ln \gamma_A}{\partial \ln N_A}\right) \tag{7}$$

where N_A and N_B are the atomic fractions of A and B atoms, γ_A is the activity coefficient of the A species, and D^* is the tracer diffusivity. Secondly, the stress exponent, n, is often greater than the theoretically suggested value of three. The Au-Ni and Al-Mg alloys demonstrate the usually observed effect of solute concentration on the stress exponent.[24] As alloying content increases, n decreases from values characteristic of climb-controlled creep (4-6) towards the limiting value of three that is predicted from a simple model of viscous creep.

1. Semi-Empirical Approach to Creep Mechanisms

A recent survey by Bird, Mukherjee and Dorn[21] (hereafter referred to as BMD) concluded that the steady-state rate of creep of a metal deforming at high temperature through any diffusion controlled mechanism is given by the dimensionless relation

$$\frac{\dot{\gamma}kT}{DGb} = A\left(\frac{\tau}{G}\right)^n \qquad (8)$$

In this equation A and n are constants depending upon the particular operating mechanism.

At high temperature ($\geq 0.5\ T_m$) creep in metals is controlled by dislocation climb. In such cases A has a mean value of 6×10^7 and the parameter n takes a range of values depending on the crystal structure. For fcc metals n lies in the range 4.2 to 5.5 and increases with Gb/Γ where Γ is the stacking fault energy. For bcc metals n lies in the range 4.0 to 5.5, and is near 4.5 in the majority of cases. For hcp metals, n is between 3.0 and 5.5. In solid solution alloys such as Al-Mg, creep is controlled by viscous glide motion of dislocations, and these alloys display values of n from 3 to 3.6. However, for the Nabarro-Herring mechanism A is dependent on the inverse of the square of grain size, and $n = 1$.

2. Typical Creep Curves

The curve in Fig. 6a illustrates the idealized shape of a creep curve. The slope of this curve ($\frac{d\gamma}{dT}$ or $\dot{\gamma}$) is referred to as the creep rate. Following an initial rapid elongation of the specimen, γ_o, the creep rate decreases with time (primary creep), then reaches a steady state (secondary creep), and finally the creep increases rapidly with time until

fracture occurs (tertinary creep). Major differences between the creep curves of various materials, however, are noted over the primary creep stage. Accordingly, there are two important types of creep curves (Fig. 6b).

a. Type A (usual type). It is obtained for all annealed metals and some alloys. It exhibits a decelerating primary creep rate, illustrating the continued formation of a more creep resistant substructure during the transient stage. Climb-controlled mechanism gives creep curve of this type.

b. Type B. It enters the steady-state almost immediately, is typical of materials in which the substructure pertinent to creep remains substantially constant. Such a creep curve has been observed whenever the rate-controlling mechanism is Nabarro-Herring in metals or viscous glide in solid solutions.

The same steady-state creep rate is obtained in metals and alloys regardless of their previous mechanical behavior. It is clear, therefore, that the secondary creep rate is obtained when a balance is reached between the rate of generation of the creep-resistant substructure and the rate of its thermal recovery under the applied stress.

B. Thesis Objective

A common method of presenting creep data is to plot the logarithm of the stress against the logarithm of the steady creep rate. With this type of plot straight lines will be obtained for the higher stresses. Frequently high-temperature strength data are needed for conditions for which there is no experimental information, i.e., very low stresses. Obviously, in such situations extrapolation of the data to very low

stresses is one alternative. However, reliable extrapolation can be made only when it is certain that no change to another rate-controlling mechanism occurs in the region of extrapolation which would produce a change in the slope of the straight line (log τ-log $\dot{\gamma}$ plot). The effort in this thesis is devoted to three cases where there is a change in the predominant mechanism as the stress is decreased or the grain size is made smaller. The first case deals with the transition from viscous glide controlled to climb controlled mechanism, while the second illustrates that the rate controlling mechanism at very low stresses changes from climb process to behavior of the Harper-Dorn type. The third case demonstrates that a transition from Harper-Dorn creep to Nabarro creep is expected as the grain size is made small.

1. Transition from Viscous Glide Process to Climb Mechanism at Intermediate Stresses

For metals and alloys in which dislocations glide readily, the creep mechanism is climb-controlled as typified by the nickel curve in Fig. 7a. When solid solution alloying results in a viscous glide, the viscous creep mechanism controls as typified by the nickel-50% gold. However, climb always occurs in alloys where the creep rate is viscous glide-controlled (the two mechanisms are sequential). As can be seen in Fig. 7a the value of $\dot{\gamma}_s kT/DGb$ for climb mechanism falls below that for the viscous mechanism for $\tau/G \leq 5 \times 10^{-5}$. Since the climb-controlled and the viscous glide-controlled mechanisms are mutually exclusive, only the slower can control the creep rate. Consequently, it is anticipated that alloys which exhibit viscous glide mechanism at high values of τ/G will revert to climb-controlled mechanisms when τ/G is

decreased somewhat below 5×10^{-5}. Experimental verfication of such a transition is unavailable. Therefore, the first objective of the present research was undertaken to test this prediction. The material selected for such a purpose is aluminum-3% magnesium. It was chosen for two reasons: First, it has been established that this alloy is one of the solid solutions which exhibit viscous creep at higher stresses. Secondly, it is cheaper than nickel-gold alloy and a useful industrial material.

As will be shown, the transition in creep mechanism from viscous glide to climb process occurs in this alloy. In addition, a third creep mechanism was found to govern creep at very low stresses. In fact, the second transition was unexpected and therefore partially motivated the research toward the second objective of the thesis.

2. Transition from Climb Mechanism to Harper-Dorn Creep at Very Low Stresses

Harper-Dorn creep refers to the anomalous creep behavior first reported by Harper and Dorn[25] in their studies on pure aluminum in the region of low stress and high temperature. Although the observed creep behavior was in harmony with two characteristics of Nabarro-Herring model (stress law and the activation energy of creep), the creep rate was established to be orders of magnitude higher than expected and it was independent of grain size (Fig. 7b). Consequently, this fact, along with several substructural observations, led Harper and Dorn to the conclusion that such a creep behavior cannot be ascribed to stress-assisted diffusion models. Since that time, no major effort has been devoted to test whether Harper-Dorn creep is a significantly

new mechanism of creep, or perhaps an experimental or material anomaly. Accidentally, in the study on aluminum-magnesium (as mentioned before) a behavior, which is phenomenologically identical to that previously found by Harper and Dorn, was observed. At the time when the observation on aluminum-magnesium was reported, Muehleisen[26] found no evidence for behavior of the Harper-Dorn type in low-stress creep of pure copper. These results raised the possibility that Harper-Dorn creep is unique to aluminum and its alloys.

This possibility motivated the work reported here, in which the low stress-high temperature creep of pure lead and tin were investigated. These two metals were chosen because of their low melting points (allowing good temperature control in tests at temperatures near T_m) and their differing crystal structures (lead is face-centered cubic, tin is body centered tetragonal). Both metals were found to exhibit a creep behavior which appears to be of the Harper-Dorn type.

Since the load and sample geometrics employed in this research differ significantly from those used in the earlier work,[25,27] creep rates for bulk samples of pure aluminum, polycrystals as well as single crystals, were measured to test consistency with the data of Harper and Dorn.

In addition, it will be demonstrated that Harper-Dorn creep is a dislocation-dominated process with unique substructural features. Such a dislocation-dominated process will be speculated as climb of "saturated" dislocations.

3. Transition from Harper-Dorn Creep to Nabarro-Herring Mechanism

As will be demonstrated later, Harper-Dorn creep and Nabarro-Herring creep are independent parallel mechanisms. Therefore, the total creep rate at very small stresses, provided no third mechanism intervenes, is given by the sum of the contribution over both processes. However, under certain conditions it is expected that Nabarro-Herring mechanism becomes the dominant mechanism. Such a condition will be specified, and new evidence[28] for the expected transition will be discussed.

II. EXPERIMENTAL PROCEDURE

Aluminum-3% magnesium was supplied by Kaiser Aluminum and Chemical Corporation. The final product contained the following elements in atomic percent: Mg-3.29, Si-0.003, Fe-0.003, Mn-0.006, Cu-0.005, Cr-<0.001, Zn-0.003, Ti-<0.005. The remainder is aluminum. The cast ingots were soaked at 783°K for 48 hours and air cooled. After scalping ~0.2 in. per surface they were flush heated to 686°K and stabilized at that temperature for about an hour. The ingots which initially measured about 3 1/4 in. thick were hot rolled to the final thickness of 0.875 in. in five passes. Ultra high purity lead and tin (99.999%) were procured from the United Mineral and Chemical Corporation. High purity aluminum was obtained from Cominco American Incorporated. Single crystals of aluminum were grown in this laboratory using a modified Bridgman technique.

Double-shear specimens of the shape and dimensions shown in Fig. 8 (inset) were prepared from the experimental materials. Prior to testing the specimens were annealed for the dual purpose of relaxing internal stress and stabilizing the grain size. Aluminum-3% magnesium specimens were annealed in situ for a minimum of 2 hours at a temperature slightly above the planned test temperature prior to testing. The lead samples were annealed at 590°K for 48 hours, resulting in a mean grain size of approximately 1.5 mm. The tin samples were annealed for 96 hours at 498°K, yielding a mean grain size of 2 mm. The polycrystalline aluminum samples were annealed for 5 days at 927°K, giving a grain size of about 9 mm.

Tests were carried out either on an Instron testing machine (aluminum-magnesium for high stresses) or on a suitably designed creep testing machine at constant load; for this specimen configuration, constant load implied constant stress. The creep testing machine is shown in Fig. 9. Tests on aluminum-3% magnesium and pure aluminum were conducted in air in an electric furnace, while tests on lead and tin were performed in stirred silicon oil baths. Temperatures were monitored with Chromel-Alumel thermocouples held in direct contact with the specimen (Fig. 8) and were held constant to better than ±1° by a proportional controller. The length changes were recorded by a linear variable differential transformer, and were accurate to $\pm 5 \times 10^{-5}$ inches. By using double-shear type test specimens, uniform elongations and constant steady-state strain-rates were observed to shear strains beyond 0.80.

For aluminum-3% magnesium the range of the stresses from 8×10^{-3} G to 10^{-6} G was employed (Table I.a). The range of stresses from ~1 to ~35 psi was scanned at a temperature of about 923°K (0.99 T_m) for pure aluminum (Table I.b). Three single crystal specimens (aluminum) were used to cover the Harper-Dorn region. In the case of lead, the range of stresses from ~1 to ~100 psi was investigated at two temperatures: 587°K (0.98 T_m) and 554°K (0.93 T_m). Tests at two additional temperatures were conducted to determine the activation energy for creep (Table I.c). During the tests at higher stresses complications were encountered due to sample recrystallization. In this case the minimum strain-rate was taken as the steady-state value as discussed by elsewhere.[29] This may have caused the relatively high scatter in the lead data. For tin, the stress-range from ~5 to ~100 psi was scanned at 495°K (0.98 T_m). Tests

at three additional temperatures were conducted for use in determining the activation energy (Table I.d).

III. EXPERIMENTAL RESULTS

A. Creep Behavior of Aluminum-3% Magnesium

As noted in the earlier section, data were obtained through both creep and Instron tests. In any creep test at the steady state, there are three variables related by one equation. These variables are the applied stress, τ, the strain-rate, $\dot{\gamma}$, and the temperature, T. On the Instron machine, both the strain-rate and the temperature are externally imposed. The measured parameter is the stress for the steady state, and the technique is known as strain-rate cycling technique (Fig. 9). Whereas, on the creep machine, the measured variable is the steady state strain-rate since the stress as well as the temperature are the independent parameters. In this case, the technique is named differential stress. However, in both these cases the specimens were left to achieve the steady state before changing the stress or the strain-rate. Figure 10 clearly domenstrates three regions with two transitions, the first at $\tau = 100$ and the second at $\tau = 20$ psi. Important differences were noted in the creep curves corresponding to various regions. Figure 11 is a schematic representation of the important features of the curves observed in the three regions.

Creep curves in region III are typical of solid solution alloys with no extensive initial strain upon loading. They are characterized by brief transient creep, indicating that the substructure pertinent to creep remains substantially constant. Additional support of these findings is obtained through intermittent loading experiments. In one of the tests the specimen was unloaded after it crept to a certain strain in the steady state and left for about 3 hours at the test

temperature. Upon reloading to the original stress the steady state was achieved immediately and no transient was observed (Fig. 12). It may be noted that sometimes inverted creep curves may be observed in the viscous glide region. An example is shown in Fig. 13 for aluminum-5% magnesium where normal primary creep was observed before deformation while inverted curves were observed after deformation. In no case were such inverted transients found in the present study of aluminum-3% magnesium.

In contrast to these observations, extensive normal primary creep regions were noted for specimens crept in region II. The decelerating primary creep illustrates the continued formation of a more creep resistant substructure during the transient stage. When the stress was removed and reapplied after an hour, a region of primary creep was again observed following a small instantaneous strain (Fig. 14). However, the final steady-state creep rate was exactly the same as the original value.

Creep curves obtained in region I are similar to curves obtained previously from tests of pure aluminum in the same stress range. The transients observed in the annealed samples were present even after prior deformation.

Plot of log $\dot{\gamma}$ vs log τ at constant temperature gives the stress law for creep. Figure 15 represents such a plot for viscous glide with average slope ~3.14, while Fig. 10 gives slope of 4.2 for region II, and a slope of ~1 for region I.

The temperature dependence of the steady-state creep rate was studied in each of the three regions. Effective activation energies

were obtained from the slope of the Arrhenius plots shown in Figs. 16a, b and c. To compensate for the effect of the shear modulus and temperature,[21] $\log \dot{\gamma} G^{n-1} T$ vs $\frac{1000}{T}$ is used in lieu of the usual plot of $\log \dot{\gamma}$ vs $\frac{1000}{T}$ (where n is stress exponent). Figure 16a shows plots of $\log \dot{\gamma} G^2 T$ vs $\frac{1000}{T}$ at constant stresses of 300 and 600 psi. These data fall in region III and give a value of 33.10 ± 2.16 kcal/mole for the activation energy. $\text{Log } \dot{\gamma} G^3 T$ vs $\frac{1000}{T}$ is plotted for region II in Fig. 16b. These data yield a value of 31.08 ± 0.52 kcal/mole for the activation energy for creep. A similar plot for the region I is presented in Fig. 16c where $\log \frac{\dot{\gamma} T}{\tau}$ is plotted against $\frac{1000}{T}$ since temperature variation in this region covers a small range. The line drawn through the datum points yields a value of 35.7 ± 5.78 kcal/mole. These three values for the effective activation energies for creep are also included in Table II. An average value of 33 kcal/mole was obtained for the activation energy.

The data obtained are plotted in Fig. 17 as $\log \frac{\dot{\gamma} kT}{DGb}$ vs $\log \tau/G$ with $D = 1.86 \exp\left(-\frac{34,230}{RT}\right)$. The unavailability of interdiffusivity data on aluminum-3% magnesium forced the choice of the value of the diffusivity of pure aluminum. The diffusivity of aluminum is taken from least squares fit to the composite high temperature diffusion data[30,31] (Fig. 32). The shear stresses employed range from about 2×10^{-6} G to 10^{-3} G. The equivalence of the creep and tension testing is apparent from the overlap of the datum points obtained from these tests (Fig. 17). The lowest available cross head speed of the machine restricted the data to stresses greater than or equal to about 4×10^{-5} G. Three distinct regions appear in Fig. 17: region III extending from stresses of about 6×10^{-5} G and beyond, region II from 10^{-5} G to 6×10^{-5} G and region I

below 10^{-5} G. The values of the stress exponent (n) and pre-exponential factor (A) obtained in these 3 regions are tabulated in Table II.

B. Creep Behavior of Aluminum

The results of creep tests on pure aluminum are plotted in Fig. 18 together with the results obtained by Harper and Dorn.[25,27] The parameters used for this plot are a non-dimensional strain rate, $\dot{\gamma}kT/DGb$, and a non-dimensional stress, (τ/G). The Harper-Dorn data were rephrased in terms of these variables by transforming the tensile stresses and tensile strains they reported according to the relations

$$\dot{\gamma} = \frac{3}{2}\dot{\varepsilon}$$
$$\tau = \frac{1}{2}(\sigma - \sigma_o) \qquad (9)$$

The value σ_o appearing in the second of these relations is a correction term Harper and Dorn found necessary to account for an apparent back stress presumably due to surface effects in their thin platelet samples. Since the present research used bulk samples, no correction term is necessary; the data extrapolated naturally to zero strain rate at zero applied stress.

As is apparent from Fig. 18, the agreement between the present results and those of Harper and Dorn is excellent both in the Harper-Dorn creep region at low stress and the conventional creep region beyond the knee of the curve. The single and polycrystalline data lie on the same curve, showing the independence of creep rate and grain size. For comparison, the predicted rate of creep via the Nabarro-Herring mechanism[5,6] has also been plotted, using the relation

$$(\dot{\gamma}kT/DGb) = A_{NH}(b/d)^2 (\tau/G) \qquad (2\text{-}b)$$

where A_{NH} is a constant equal to approximately 14. The measured values for low-stress creep in aluminum lie several orders of magnitude above the Nabarro-Herring estimate.

Primary creep was noted in all tests conducted during this research, both in single crystal and polycrystalline samples. This observation also agrees with the results of Harper and Dorn.

C. Creep Behavior of Lead and Tin

1. Stress Dependence of Creep Rate

The experimental results obtained from isothermal creep tests at 4 different temperatures are presented in Figs. 19 and 20 for lead and tin respectively. Because of the time limitation on the measurement of shear strain-rates below about 2×10^{-9} sec^{-1}, the entire range of stresses could be scanned only at the higher temperatures. The data at these higher temperatures do indicate a transition from a higher slope (~4.9 for lead and ~6.6 for tin) to a lower one (~1 for both metals). The transition from high stress region to low stress region was observed at shear stress values of ~14.5 and ~16.0 psi for lead at 0.98 T_m and 0.93 T_m respectively. A value of ~32 psi was found for this transition-stress at 0.98 T_m for tin.

2. Creep Curves

Typical creep curves observed in both the regions are shown in Figs. 21 and 22 for lead and tin respectively. As is clear from these, normal primary creep regions were noted in the entire stress range for both the metals. It is important to note the presence of this primary creep in Harper-Dorn creep region (where the creep-rate is proportional

to the applied stress), since the diffusional creep mechanisms[2,5,6] which predict linear creep behavior are characterized by the absence of this primary creep region.

3. Temperature Dependence of Creep Rate

To determine the activation energy for creep, the logarithm of the modulus-compensated steady-state strain-rate ($\dot{\gamma}G^{n-1}T$) vs the reciprocal of the absolute temperature was plotted at constant stresses of ~30 psi and ~100 psi for lead and tin respectively (Fig. 23). Here values of ~4 and ~6 are used respectively for lead and tin for (n-1), since the averages of the slopes of the lines in Figs. 19 and 20 were found respectively to be ~5 and ~7. These data for both the metals fall in the high stress region. The least square analyses of the data presented in Fig. 23 yielded values, for the activation energy for deformation, of 22,920 ± 180 cal/mole for lead and 23,070 ± 1,820 cal/mole for tin. These are in essential agreement with the self diffusion data, namely

$$D = 0.28 \exp(-24{,}200/RT) \quad \text{for lead}^{32}$$

and

$$D = 0.78 \exp(-22{,}350/RT) \quad \text{for tin}^{33}$$

No attempt was made to determine the activation energy for creep in the low stress region. However, a value of 24,945 cal/mole was inferred from the data at temperatures 587°K and 554°K presented in Fig. 19. Thus the activation energy for creep appears to be essentially identical to that for volume self-diffusion throughout the employed stress range. Similar findings were reported earlier in pure aluminum. In addition, the same behavior was observed in aluminum-3% magnesium.

The creep data for lead and tin presented in Figs. 19 and 20 were analyzed in terms of Eq. (8) and Fig. 24 is a plot of log $\frac{\dot{\gamma}kT}{DGb}$ vs log (τ/G) for both the metals. As is clear from this figure, the data at various temperatures coalesced into a single line for each metal. Again the data reveal transitions from high stress region to low stress region at stresses of $\sim 10^{-5}$ G for tin and 2×10^{-5} G for lead. Values of A and n obtained from the least squares analyses of the data are tabulated in Table III, along with the values predicted from the governing equation of Nabarro-Herring creep (Eq. (2-b)).

IV. DISCUSSION

The various diffusion controlled creep mechanisms documented in Table IV, can be classified into two groups. The first group includes Nabarro-Herring,[5,6] Coble,[2] and perhaps superplastic creep[3,21] as well and these mechanisms are due to changes in grain shape arising directly from vacancy fluxes under chemical-potential gradients. The second group includes creep by climb[17] and viscous glide,[22] and in contrast to the mechanisms of the first group, the creep behavior is due to average rates of slip displacements of dislocations released by climb. At the steady state, a balance must necessarily be obtained between the rate of accumulation of dislocations and their rate of removal by climb-recovery. To account for continuing steady-state creep, recovery by dislocation climb must always be operative at high temperatures. In solid solution alloys, however, as noted earlier, although climb always occurs the creep rate is controlled by viscous glide motion of dislocations when it gives the slower rate. Since dislocation glide and climb are in series, the total creep rate in solid solutions is due to the rates ascribable to either climb or viscous glide, dependent on which is controlling, plus the sum of rates from all remaining mechanisms. As will be clear, although many parallel mechanisms can be operable at one time, usually one exhibits the highest creep rate and therefore becomes dominant over special ranges of τ/G and T. Transient creep seems to occur only when dislocation cells and entanglements are produced as a result of the initial plastic straining that take place upon the application of stress.[34] In the absence of initial plastic straining, however, the steady-state creep rate is

achieved almost immediately following stressing. Obviously, Nabarro, Coble, superplastic and viscous glide mechanisms do not exhibit transient stages (in some cases a very brief transient appears). This is also true for the recently proposed Nabarro-Bardeen-Herring mechanism[35] based on climb of dislocations from Bardeen-Herring sources (hereafter N-B-H). The correlation of the present experimental results with the thus far documented theories will be discussed next.

A. Region III (Only in Some Solid Solutions)

A value of 3.2 for the stress exponent (n) in this stress-range in aluminum-3% magnesium discounts the possibility of climb (A) and Nabarro (D) creep mechanisms (Table IV). Further elimination is achieved through the pre-exponential factor, A. The experimental value of A (Table II) refutes (B(a)) as the controlling mechanism since even if L_j is taken conservatively as "10b", this factor is too large compared to 51, while the Nabarro-subgrain[36] and N-B-H mechanism[35] can be ruled out since they predict too small a value for A. In addition, it is questionable on theoretical grounds whether the Nabarro creep in subgrains and N-B-H creep can even take precedence over viscous glide and/or climb mechanisms.[21] This isolates the viscous glide mechanism and the experimental results are in line with the predictions based on this model. As was mentioned, the expression for the creep-rate presented here for glide was taken from BMD[21] and this differs slightly from Weertman's,[22] in that the latter theory predicts solute-concentration-dependence of the pre-exponential factor. Moreover, such an expression can be derived in a more straightforward way as given below.

For the case where all dislocations within a crystal drag Cottrell atmospheres, the shear strain-rate is given by[36]

$$\dot{\gamma} = \rho b v = \rho b \frac{\nu b}{\lambda} b \exp\left(\frac{-f_d}{kT}\right)\left\{\exp\left(\frac{\tau\lambda b^2}{kT}\right) - \exp\left(-\frac{\tau\lambda b^2}{kT}\right)\right\} \qquad (34)$$

where v is the dislocation velocity, ν the Debye frequency, ρ the dislocation density, λ the distance between solute atoms and f_d the free energy of activation for solute atom diffusion. Since $\tau\lambda b^2 \ll kT$ and $D = \nu b^2 \exp(-f_d/kT)$,

$$\dot{\gamma} = 2\rho D \frac{\tau b^3}{kT} \qquad (35)$$

and, since $$\rho = \frac{\tau^2}{\alpha^2 G^2 b^2} \quad \text{(Ref. 21)} \qquad (36)$$

with $\alpha = 0.6$ $$\therefore \quad \frac{\dot{\gamma} kT}{DGb} = 6(\tau/G)^3 \qquad (6)$$

It is important to note that the proper diffusivity applicable here is the chemical interdiffusivity of the alloy as given by Eq. (7). The paucity of data on the chemical interdiffusivity and the activity coefficient makes accurate correlation of the expression with the present experimental findings difficult. However, as noted by BMD[21] this should not make too much difference in the present case of aluminum-3% magnesium solid solution alloy. As is clear from Table II, experimental results in region III correlate well with Eq. (6).

B. Region II

The experimental values for the pre-exponential factor and the stress exponent for aluminum-magnesium, aluminum, lead and tin are documented in Table II and Table III respectively. This region illustrates creep behavior generally attributed to the climb-controlled process.

As was mentioned in the introduction, jogs on screw dislocations may impede the conservative motion of the dislocations and further slip is possible only by the nonconservative motion of these jogs in the direction of the advance of screw dislocations. One of the primary difficulties of the jogged-screw dislocations models is the prediction of the stress dependence of creep. At lower values of stress, when the value of $\frac{\tau L_j b^2}{kT}$ is small, the bracketed expression in Eq. (4) reduces to just this term. In order to arrive at the observed stress power law (~4.2 in aluminum-magnesium, 4.5 in pure aluminum, 4.9 in lead and 6.9 in tin) with average value for $n \approx 5$, it follows the ρ_s must increase approximately as τ^4, if the reasonable assumption is made that L_j is independent of the stress. But it might be expected that ρ_s is a fraction of ρ (total dislocation density) and therefore increases only as $\tau^{2.21}$ This reveals that the actual creep rate at high stresses is much greater than that suggested by Eq. (4). It was concluded that the jogged screw dislocation models suffer from various inaccuracies and require major repairs in order to account correctly for the activation energies and stress laws that are obtained.

If the motion of jogged screw dislocation is not the rate-controlling mechanism in region II, some other slower mechanism must be sought. The recent investigations by Clauer, Wilcox and Hirth[37] on Bcc molybdenum show that a majority of the dislocations which they observed in crept specimens in an edge orientation. Thus a mechanism based on some kind of edge dislocation climb seems more reasonable. The first serious formulation of a dislocation-climb theory for steady-state creep was presented by Weertman.[17] The derived equation (Eq. (5)) at lower

values of stress, reduces to

$$\dot{\gamma} = C_W \frac{\tau^{4.5}}{G^{3.5}} \frac{D}{kT} \frac{1}{\sqrt{N}} \tag{37}$$

where N is the number of dislocation sources per unit volume and C_W is constant. The major virtue of Weertman's theory is that it correlates quite well with most of the mechanical data on high-temperature creep. It accounts for the observed apparent activation energies, the effect of the modulus of elasticity, and gives almost the observed stress law.

Despite its excellence, many of the assumptions on which it was based are now questionable. First, it is not evident why the number of Frank-Read sources should be constant despite theoretical attempts to justify this assumption. Secondly, piled up arrays of dislocations are not seen in metals that were in the secondary stage of creep. A probable reason is that the thinning techniques may result in their dispersal. However, calculations by Head,[38] Li[39] and Hazzeldine[40] have shown that even in the absence of climb, piled up arrays of dislocations of opposite signs on nearby parallel slip planes are unstable; they decompose into widely spaced dipoles. Therefore, Mukherjee, et al.[29] indicated that the assumption of piled up arrays of dislocations seems to have been invoked in order to obtain a predicted creep rate that increases with a sufficiently high powef of the stress to approach the experimental values. Several approaches have recently been suggested, such as dipole annihilation[41] and N-B-H[35] creep, to correlate the creep behavior in region II. However, none of these approaches predict the correct exponent as well as the pre-exponential factor. Mukherjee, et al.[41] observed that although Chang's theory[41] based on

dipole annihilation does not predict the correction values for (n) and (A), it nevertheless has very attractive features and further modifications along these lines may prove valuable.

In an attempt to present a unified picture of high-temperature creep, BMD[21] suggested a semi-empirical approach to correlate the creep data. Such an approach considers the effect of modulus of elasticity, subgrain size and stacking-fault energies. Four steps are involved in arriving at Eq. (8). The first step assumes that the secondary creep rate can usually be represented as a power of the stress according to

$$\dot{\gamma}_s = f\{T\}\tau^n \tag{38}$$

In general the exponent (n) is substantially constant over a wide range of stress and temperature. At high stresses the secondary creep rate appears to increase more rapidly than that given by constant value of n. The second step deals with the temperature dependence of the creep rate. Since Creep is a thermally-activated process, it was assumed that its temperature dependence arises principally from an Arrhenius type of expression,

$$\dot{\gamma}_s = F\{\tau\}e^{-\frac{Q_c'}{RT}} \tag{39}$$

The apparent activation energy, Q_c', has been shown to be insenitive to the stress; it has been shown to be in very close agreement with the activation energy for self diffusion. When Eqs. (38) and (39) are combined, the empirical relationship results

$$\dot{\gamma}_s \, e^{\frac{Q_c'}{RT}} = A'\tau^n \tag{40}$$

The third step concerns the incorporation of the modulus effect into the analysis. It was found that the value (A') differs greatly from metal to metal, and that variation in A' seems to depend systematically on the modulus of elasticity.[42] On this basis, it was suggested that a better correlation of the secondary creep rates among the various metals is possible when Eq. (40) is rewritten as

$$\dot{\gamma}_s \, e^{\frac{Q_c}{RT}} = A'' \left(\frac{\tau}{G}\right)^n \tag{41}$$

where G is the shear modulus of elasticity. Since $D = D_o \, e^{-H_D/RT}$ and $Q_C \simeq H_D$, Eq. (41) becomes

$$\frac{\dot{\gamma}_s}{D} = A''' \left(\frac{\tau}{G}\right)^n \tag{42}$$

The final step was carried out for two purposes; first, to make Eq. (42) consistent with the requirements for thermally-activated or diffusion-controlled mechanisms of creep; secondly, to put the expression in dimensionless form. The fact that the activation energy of creep is insensitive to the applied stress merely illustrates that the usual exponential terms in the free energy gradient expression reduce to a linear term. This suggests a relationship such as

$$\dot{\gamma}_s = A'''' \left(\frac{\tau}{G}\right)^{n-1} \left(\frac{\tau V}{kT}\right) e^{-\frac{H_c}{RT}} \tag{43}$$

for simple cases where the entropy is not a function of temperature and where V is an activation volume and H_C is the activation enthalpy for creep. Equation (43) can be rewritten as

$$\frac{\dot{\gamma}_s kT}{DG} = A_1 \left(\frac{\tau}{G}\right)^n \tag{44}$$

To permit unbiased comparisons, the term preceeding the equality sign should be divided by some significant length. Burgers vector b was tentatively taken to be the significant dimension in either diffusion or deformation to provide the required dimensionless expression,

$$\frac{\dot{\gamma}kT}{DGb} = A\left(\frac{\tau}{G}\right)^n \qquad (8)$$

In the first survey,[29] it was suggested that n is a universal constant and the reported variations in n are due to random scatter, while A depends on the stacking fault energy. The alternative possibility, however, which was presented in the second and more general review[21] is that A is a universal constant and the remaining parameter, n of Eq. (8), increases with the dimensionless quantity Gb/Γ where Γ is the stacking-fault energy.

For aluminum-3% magnesium, the very fact that at higher stresses (region III) a smaller n value (~3 compared to ~4 of region II) was observed indicates that the mechanisms responsible for the region III (viscous glide) and region II act in series. The added observation of the equality of the activation energies for creep in both regions with that for self diffusion leaves no doubt that the viscous glide motion of dislocations and dislocation climb control creep in region III and region II respectively. In addition, a strong evidence for such a transition is provided by the transition in the type of the creep curve. In region III (viscous glide), the creep curve immediately enters the steady state, while in region II there is extensive primary creep. Such an observation is in harmony with the characteristics of the creep curve expected, if viscous glide and climb

mechanisms control region III and region II respectively.

The present experimental results on aluminum-3% magnesium in the climb region region can be compared with the climb expression for pure aluminum given by Eq. (8) with $A = 6\times10^7$ and $n = 4.2$. Such a comparison is shown in Fig. 17 where it is clear that aluminum-magnesium data fall below the aluminum curve. There are three possibilities for this difference. The first possibility might have arisen from the diffusion frequency factor (D_o) since the appropriate diffusivity is given by Eq. (3-b) in lieu of the simpler D^*/f for pure aluminum. The second possibility might be due to the strengthening effect introduced by magnesium solute atoms on the aluminum matrix. The last possibility might arise if the magnesium reduces the stacking fault energy of pure aluminum. However, the last effect is disqualified due to the observation that stacking fault width in pure aluminum is insensitive to magnesium additions.[43]

The present data on aluminum in region II (Fig. 18) are in line with BMD's predictions[21] as well as the earlier work by Servi, et al.,[44] Weertman[45] and Sherby, et al.[46] For lead, their prediction suggested an exponent n of the order of 4.7, compared to the present experimental value of 4.9.

Earlier studies by Dorn and co-workers[47] on the creep of tin indicate that the activation energy for creep is about 22,700 cal/mole, while Breen and Weertman[48] found a value of 26,000 cal/mole for the same. These values are in essential agreement with the present one of 23,070 cal/mole as well as the more recent value for self diffusion in polycrystalline tin.[33] A re-evaluation of the data of Breen and Weertman at higher temperatures where a value of 26,000 cal/mole was obtained for the activation energy, yielded a value of 5.91 ± 0.31 for n and

$(1.03 \begin{smallmatrix} + 14.74 \\ - 9.96 \end{smallmatrix}) \times 10^{15}$ for A. These values should be compared with 6.59 and 3.55×10^{17} obtained in the present investigation. The fact that the above values of A for tin are orders of magnitude larger than those based on the predictions by BMD on fcc, Bcc, and HCP metals, illustrates that yet unknown factors concerning the crystal structure also play a significant role in high temperature-creep.

C. Region I

In this region ($\tau/G \leqslant 10^{-5}$) the stress exponents were found to be near unity for aluminum, aluminum-3% magnesium, lead and tin. Mechanisms which predict viscous deformation such as Nabarro-Herring[5,6] yield values for the strain-rates which are orders of magnitude lower than those observed (Table V). However, as shown in Fig. 25, the present results fall very close to the earlier observation of the Harper-Dorn creep on pure aluminum.

Harper-Dorn creep was first reported in pure aluminum by Harper and Dorn,[25] and Harper, Shepard and Dorn.[27] The new creep behavior was manifested by several characteristics. The most important of these are: (1) the creep rate is linearly proportional to the applied stress; (2) the activation energy for creep is nearly equal to that for self diffusion; (3) single crystals exhibit almost the same creep rate as polycrystals. The first and second characteristics suggested that such a creep behavior might be ascribed to the Nabarro-Herring creep mechanism. However, the third observation was incompatible with the Nabarro-Herring model, since that model predicts negligible creep rate for single crystals.

The present experimental work on bulk samples of aluminum in shear confirms the earlier work by Harper and Dorn[25,28] who tested thin platelets of both single and polycrystalline aluminum samples in tension. In spite of the difference in the kind of specimen used, the type of the stressing and the grain size of polycrystalline specimen (d ~ 9 mm in this investigation and 3 mm in Harper-Dorn study), the agreement between these distinct investigations is excellent. The same creep behavior in pure aluminum has been recently confirmed by another investigation conducted by Barrett, et al.[49] who tested bulk tensile specimen of both single and polycrystalline (d ~ 10 mm) in tension. The aggregate results of the three investigations (present, Barrett, et al.[49] and Harper, et al.[25,28]) are shown in Fig. 26, where a non-dimensional shear strain rate $\left(\frac{\dot{\gamma}kT}{DGb}\right)$ against a non-dimensional shear stress (τ/G) was plotted on a log scale. To obtain this plot, the tensile data of Harper and Dorn and Barrett, et al. were transformed to shear data using Eq. (9). The scatter about the Harper-Dorn line is due principally to a small consistent deviation between the results of Barrett, et al. and the results of this thesis. The data also scatter somewhat near the knee of the curve where the mechanism of creep is changing. For comparison, Fig. 26 also contains a plot of the creep rate predicted from the Nabarro-Herring model for the grain size (9 mm) used in this investigation. As can be seen from Fig. 26, the predicted rate of Nabarro-Herring creep is roughly three orders of magnitude lower. Moreover, the single and polycrystalline data lie on the same curve showing the independence of creep rate and grain size. Consequently, the basic conclusion from such extensive work on aluminum is that the existence of Harper-Dorn creep in pure

aluminum is well established experimentally.

The first clear evidence for Harper-Dorn creep in a material other than pure aluminum was found by Ziling[50] in studies of the creep of silver foils under low stress. The curve through his data is plotted in Fig. 27. The data were taken at a single temperature, 950°C, on foils having thickness ~600μ and grain diameters ~200μ. The creep rates found in region I of this curve are, in fact, comparable to those predicted from the Nabarro-Herring model for this grain size. However, Ziling obtained direct measurements of grain elongation during creep, using both marker and surface interferometric techniques, and concluded that grain elongation can account for no more than 30% of the total deformation. The remainder, he concludes, must be attributed to deformation in the interior of grains, presumably through creep of the Harper-Dorn type. As can be seen from Fig. 28, the dimensionless creep rates of these specimens coincide exactly with those observed in Harper-Dorn creep of aluminum.

The experimental results on aluminum-3% magnesium reveal a change in creep behavior at $\tau \sim 10^{-5}$ G. Below this transitional stress the strain rate depends linearly on the stress and the activation energy for creep approximates that for self diffusion. The creep rates observed in region I are two orders of magnitude above those predicted on the basis of Nabarro-Herring model (Table V). Moreover, a normal primary creep is evident in tests conducted within region I. These findings, coupled with the observation that the observed dimensionless creep rates in region I are reasonably close to those found for pure aluminum, lead to the conclusion that Harper-Dorn creep is dominant in aluminum-3% magnesium at low stresses.

In case of lead, the creep rates in region I lie considerably above those predicted from the Nabarro-Herring model for the grain size (1.5 mm) for the lead samples used (Table V), but are within a factor of about 1.5 of the dimensionless creep rates found in the Harper-Dorn region of pure aluminum. In addition, lead undergoes an appreciable primary creep at low stresses and the activation energy for creep is approximately the activation energy for self diffusion.

The strain rates obtained in region I for tin are uniformly more than two orders of magnitude above the Nabarro-Herring prediction for the grain size (2 mm) of the samples used, but are within a factor of two of the creep rates of pure aluminum. Normal primary creep is observed in region I. The activation energy for creep in this region I is assumed to agree with self diffusivity, but has not been checked since the very low absolute strain rates in region I of tin have restricted measurements to $T > 0.98\ T_m$. This gives an insufficient temperature range to determine valid activation energies.

Hence there is now persuasive evidence for Harper-Dorn creep in four materials other than pure aluminum: Al-3Mg, silver, lead and tin. To make this evidence definitive one should demonstrate that the strain rates in region I of these materials are independent of grain size. Previous work indicates this lack of dependence, since small variations in mean grain size from sample to sample have no apparent effect on the creep rates obtained. Attempts to gather more definitive data have been complicated by sample preparation problems and by recrystallization problems in high temperature tests on very large grain samples of lead and tin.

The data on aluminum, silver, aluminum-3% magnesium, lead and tin for Harper-Dorn creep are well represented by a linear relation

$$\frac{\dot{\gamma}kT}{DGb} = A_{HD} (\tau/G) \qquad (45)$$

where A_{HD}, a dimensionless constant, ranges from 1.39×10^{-11} for aluminum-3% magnesium to 7.24×10^{-11} for tin. The values of A for all metals which show apparent Harper-Dorn creep are given in Table V.

The apparent success in finding Harper-Dorn creep in other materials suggests that Harper-Dorn creep may be an important general mechanism of creep at high temperature and low stress. However, not all attempts to find Harper-Dorn creep behavior have been successful. Muehleisen[26] saw no evidence of Harper-Dorn creep in studies of creep in compression specimens of copper at low stress. His measurements extended down to stresses $\tau \sim 5.10^{-6}$ G and non-dimensional strain rate $\frac{\dot{\gamma}kT}{DGb} \sim 10^{-16}$. As can be seen from Fig. 28, this range of conditions extends slightly into the range of apparent Harper-Dorn creep in other materials. Pines and Sirenko[51] may have observed Harper-Dorn creep in copper at $\tau \sim 5 \times 10^{-6}$ G, but the evidence is not clear.

1. Substructural Features of Harper-Dorn Creep

The body of available microstructural evidence indicates that Harper-Dorn creep is dislocation-dominated and characterized by a low density of dislocations dispersed through large subgrains. Evidence for a dislocation-dominated mechanism was noted in the original work of Harper and Dorn[25] and Harper, Shepard and Dorn.[27] This evidence included the observation of strain recovery following creep, the uniformity of strain inside the grain as well as across the grain boundary (marker

experiment) and the occurence of extensive primary creep. More recent work by Muchleisen[26] and by Barrett, Muehleisen, and Nix[49] established subgrain formation during Harper-Dorn creep and showed that the rate of Harper-Dorn creep can be significantly reduced by distributing a fine precipitate (in this case Al_3Fe) through the microstructure. Ziling[50] concluded that 70-90% of the total strain he observed during low-stress creep of silver was due to dislocation motion in the interior of grains.

Available evidence indicates that the dislocation density (ρ) during Harper-Dorn creep of aluminum is low ($<10^4$ cm^{-2}) and independent of the applied stress. This result was obtained both by Muehleisen from etch pit counts, and Nost and Nes,[52] who used X-ray topographic techniques. The data are plotted in Fig. 29 as the dimensionless parameter $\sqrt{\rho}\, b$ vs the normalized stress τ/G. At high stresses ($\tau/G \geq 10^{-5}$) the dislocation density increases as $\tau^{2.21}$. The transition in the stress dependence of dislocation density is extrapolated to be at a stress value of about 3×10^{-6} G. This finding is in agreement with the observed stress level ($\sim 4 \times 10^{-6}$ G) in aluminum, where the transition from the climb controlled to Harper-Dorn creep occurs.

The evidence on subgrain formation is less definitive. Harper, Shepard and Dorn did not observe subgrains either because the technique was not developed at that time or because of the large subgrain size which might have equaled their employed grain size (3 mm). Muehleisen noted subgrains and obtained data on the variation of subgrain size with applied stress. The stress data are ambiguous because of the appreciable scatter.

The work of Muehleisen[26] suggested that the subgrain size is independent of the stress, whereas Barrett, et al.,[49] using the same data, claimed the subgrain is inversely proportional to the stress. However, the subgrains are large, having diameters in the range 1-3 mm.

2. The Status of Present Theories on the Mechanism of Harper-Dorn Creep

Several suggested mechanisms of Harper-Dorn creep show promising agreement with the experimental data, though they require restrictive assumptions and hence less appealing hypotheses. These include creep through glide of jogged screw dislocations,[27] creep through unsaturated climb of jogged edge dislocations,[53] and creep of the Nabarro-Herring type within subgrains.[36] (See Table VI.)

Creep through the glide of jogged screw dislocations was the mechanism favored by Harper, Shepard and Dorn. By modifying the equation given by Hirth and Lothe[53] (Appendix A), an equation of the form (Eq. (43)) is obtained with

$$A_{JS} = 12 \quad L_j b \tag{46}$$

where L_j is the spacing between jogs. Equation (46) gives a creep rate of the order, the observed one if $L_j \sim b$, an extremely high job density and $\rho = 10^4$ cm^{-2}. If these jogs are of the same type, the dislocation will certainly saturate.* If the jogs are of opposite type they will tend to annihilate by climb and will lead to an overall activation energy for creep which is expected to show the effects of core diffusion.

Creep through the climb of jogged edge dislocations is governed by[53] an equation of the form (Eq. (45)) (Appendix B) with

*The velocity of diffusion of the dislocation is controlled by the diffusion of vacancies through the crystal, and no longer by their production from the jogs or absorption by them.

$$A_{JE} = 12\pi\rho b^3/L_j \qquad (47)$$

Equation (47) predicts a creep rate near the observed one if $L_j \sim 20$ b and $\rho = 10^4$ cm^{-2}, which is roughly the spacing expected for thermal jogs in aluminum near the melting point.[26] However, the assumption of a large population of nearly straight edge dislocations near the melting point is difficult to accept. If the dislocation did not saturate one would expect[53] core diffusion to influence the activation energy for creep, in apparent conflict with the experimental data.

Friedel[36] originally favored a Nabarro-Herring mechanism acting across subgrains as the mechanism of Harper-Dorn creep (Appendix C). This mechanism obeys an equation of the form Eq. (2-b) with the parameter d equals to the mean subgrain size. As has been pointed out,[26] the large subgrain size observed during Harper-Dorn creep of aluminum caused the creep rate predicted by this mechanism to fall well below the observed one. Moreover, the subgrain size in aluminum either decreases with the applied stress or at least shows appreciable scatter over the domain of Harper-Dorn creep. This variation would induce a scatter in measured creep rate considerably greater than that observed experimentally.

Finally, Barrett, et al.[49] have recently suggested a model based on a balance between the generation and annihilation of gliding dislocations. When the model is reformulated in dimensionless form (Appendix D), it gives a Harper-Dorn equation with

$$A_{DB} = 3\rho_o b^2 \delta_o \quad (\delta_o \text{ is constant } \sim 10) \qquad (48)$$

However, to arrive at the required stress exponent, it was assumed that

subgrain diameter depends on the stress, a condition which has not yet been well established (see Ref. 26 and 49).

3. A Proposed Mechanism for Harper-Dorn Creep

The available data may be plausibly explained as due to creep via climb of "saturated" dislocations,[53] that is, when the dislocation climb velocity is controlled by the rate at which vacancies can diffuse to (or from) the dislocation line. The consistency of this mechanism with the experimental data may be summarized as follows.

1. The strain rate due to creep at low stress is given, according to Hirth and Lothe[53] (see Appendix D), by an equation which may be rewritten in the form of the governing Eq. (45) of Harper-Dorn creep with

$$A_{CS} = - 6\pi\rho b^2/\ln(\sqrt{\rho}\, b) \qquad (49)$$

Given $\rho \cong 10^4$ cm^{-2} and $b = 2.86 \times 10^{-8}$ for aluminum, A_{cs} is computed as $A_{cs} = 1.2 \times 10^{-11}$, in excellent agreement with the experimental value, $A_{HD} = 5 \times 10^{-11}$.

2. At low stress the activation energy for creep via this mechanism is the activation energy for self diffusion.

3. The mechanism is dislocation-dominated. Consequently, its rate should be markedly decreased if a fine precipitate is dispersed through the matrix.[49]

4. The rate of creep via this mechanism will be independent of grain size for large grain sizes.

5. The low dislocation densities observed during Harper-Dorn creep ($\sim 10^3 - 10^4$ cm^{-2}) are sufficient to saturate any dislocation which

contains a preponderance of jogs of one type (vacancy-absorbing or vacancy-emitting). Friedel[36] predicts saturation for dislocation densities $\rho \lesssim 10^5$ cm^{-2}. It is evident that the last observation of the low dislocation density is the central point which gives the "saturated" mechanism advantage over the other speculated mechanisms since the jogged screw, climb of unsaturated dislocation and the dislocation balance mechanisms readily predict the first four observations. In addition, the saturated dislocation mechanism has little dependence on the type of the dislocation (i.e., it does not require pure edge or pure screw).

4. The Domain of Harper-Dorn Creep

Harper-Dorn creep is limited to stresses and strain rates below the knee of the log $\frac{\dot{\gamma}bT}{DGb}$ vs log τ/G plot. In the absence of established creep mechanism the position of this knee cannot be predicted. However, if it is speculated that this knee is due to a change in dislocation density from the low, constant value found in region I to the high, increasing values ($\rho \propto \tau^2$) found in region II, an interesting correlation may be drawn. Let the change in the dislocation density be due to activation of dislocation sources at a critical value of the applied stress, $(\tau/G)_c$. Let these sources be nodes in the array of dispersed dislocations, having an expected spacing $(\rho)^{-1/2}$ the characteristic length of the array. Then dislocation multiplication by the bow-out mechanism[36] gives

$$(\tau/G)_c \cong 2\sqrt{\rho}\, b \qquad (50)$$

or 5.6×10^{-6} for aluminum having $\rho \sim 10^4$ cm^{-2}, very close to the value observed.

Recent data indicate that Harper-Dorn creep is also limited by sample grain size. Burton[28] studied the low-stress, high-temperature creep of fine-grained aluminum foils. He measured creep rates which may be shown to obey an equation of the form (2-b) of the governing equation of Nabarro-Herring creep if d is replaced by the "effective" grain size of the foil of thickness t,

$$d' = \sqrt{td} \tag{51}$$

and if $A_{NH} \cong 130$. This number is large compared to the expected value of 14, but does not seem unreasonable due to the approximations inherent in the Nabarro-Herring model. His data are plotted together with the creep curve for large-grained aluminum in Fig. 30. The measured creep rates are uniformly higher than those observed in Harper-Dorn creep of bulk aluminum.

The effect of small grain size is anticipated on the basis of any one of the candidate mechanisms discussed above. These competing mechanisms may increase the rate of Nabarro-Herring creep at small grain size by providing vacancy sources and sinks which decrease the effective diffusion distance, but they cannot decrease the Nabarro-Herring creep rate. Since the relation governing Harper-Dorn creep (Eq. (45)) predicts a creep rate independent of grain sizes and the governing equation of Nabarro-Herring predict a creep rate which increases as d^{-2} (Eq. (2-b)), there exists a critical value of the grain size, d_c, such that;

(a) For $d \ll d_c$

Nabarro creep predominates, and the creep rate is dictated by the diffusion model

$$\frac{\dot{\gamma} kT}{DGb} \simeq A_{NH}\left(\frac{b}{d}\right)^2 \frac{\tau}{G}$$

(b) For $d = d_c$

Nabarro creep includes the contribution from Harper-Dorn mechanism, and the total creep rate is given by,

$$\frac{\dot{\gamma}kT}{DGb} = \left\{A_{NH}\left(\frac{b}{d}\right)^2 + A_{HD}\right\}\frac{\tau}{G} \tag{52}$$

(c) For $d \gg d_c$

Harper-Dorn creep predominates. The creep rate is represented by

$$\frac{\dot{\gamma}kT}{DGB} = A_{HD}\left(\frac{\tau}{G}\right)$$

These trends are schematically shown in Fig. 31. It is clear that the extreme limit of case (c) is testing of single crystals.

The experimental values for A_{HD} and A_{NH} in aluminum are 5×10^{-11} and 130 respectively. Hence, d_c is given by

$$A_{HD} = A_{NH}\left(\frac{b}{d_c}\right)^2 \tag{53}$$

$$\therefore \quad d_c' = 460\mu \tag{54}$$

Nabarro-Herring creep should be anticipated for foils of smaller grain size.

Of the foils tested by Burton only two had an effective grain size $d' > d_c'$ and they exhibited zero creep rate. The remainder of his data fall in the Nabarro-Herring region and show agreement with the Nabarro-Herring model. On the basis of these data, Burton phrased the general conclusion that the low-stress, high-temperature creep of pure aluminum follows the Nabarro-Herring model.

Of the two foils from Burton's set having $d' > d_c'$, the first had a thickness of 2.5 mm and a mean grain size of 15 mm, giving an effective grain size d' of approximately 6 mm. This sample was tested at effective

shear stress of 3.3×10^{-6} G, a value which falls in the transition region at the knee of the creep curve of bulk aluminum. Thick samples of coarse-grained aluminum show an apparent mixture of Harper-Dorn and climb-dominated creep at this stress level. However, Burton was unable to measure a creep rate for his specimen and reports creep rate zero.

The second coarse-grained specimen tested by Burton is described in Section 5 of his paper. The thickness of this foil is not given, but the grain size is reported to be 10 mm. This sample was tested at effective shear stress of 5.7×10^{-6} G. Reference to the creep curve of bulk aluminum shows that this value of the shear stress is well above the maximum value at which Harper-Dorn creep is observed. Thick samples of coarse grained aluminum show an appreciable creep rate governed by the climb mechanism at this stress level. However, Burton failed to observe creep in his specimen and reports creep rate zero.

It is difficult to base any general conclusion on two data points in creep, particularly when the limit of resolution of the test apparatus and the reproducibility of the results are unknown. However, there are only two possibilities: either the coarse-grained foils tested are thick enough to exhibit creep behavior typical of bulk aluminum or they are not.

If the foils are assumed thick, their low creep rates may be attributable to experimental problems, but certainly cannot be used to question the existence of Harper-Dorn creep. As mentioned above, the latter foil was tested at a shear stress well above the maximum at which Harper-Dorn creep is observed. At this stress level ($\tau = 5.1 \times 10^{-6}$ G) the climb mechanism acting alone would give a creep rate

higher than four of the values measured by Burton in fine-grained specimens. The other coarse-grained foil was tested at an effective shear stress which falls in the knee of the creep curve. Again at this stress level ($\tau = 3.3 \times 10^{-6}$ G) an extrapolation of the curve representing climb dominated creep of aluminum shows that the climb mechanism acting alone would cause a creep rate above at least one of the values measured by Burton for thinner foils. Burton's results are markedly inconsistent with the measured creep behavior of bulk aluminum whether or not Harper-Dorn creep exist.

On the other hand, thin foil effects may be responsible for the low creep rates of this sample. The annealing or pinning of dislocations at the free surfaces of a foil should influence the rate of creep by dislocation-dominated processes, and may have the effect of suppressing the rate of creep due to either the climb or Harper-Dorn mechanism to values below those measurable by Burton's technique. In this context, it is interesting that those of Burton's samples which appear to have undergone creep by the climb-dominated mechanism exhibit creep rates which are uniformly below the curve for bulk aluminum. While there is, unfortunately, only one relevant datum point, the deviation from bulk behavior is more pronounced for the thinner of the two fine-grained foils which appear to have crept by the climb mechanism.

V. CONCLUSIONS

1. High-temperature creep data on aluminum-3% magnesium analyzed in terms of the dimensionless parameters $\frac{\dot{\gamma}kT}{DGb}$ and τ/G revealed three distinct regions. Values for the stress exponents in the three regions were found to be 3.2, 4.1 and 0.9 respectively in the high (III), intermediate (II) and low (I) stress region. A value of 33 kcal/mole was obtained for the activation energy for creep in the three regions and this value is in good agreement with that for self-diffusion in pure aluminum. Viscous glide and dislocation climb mechanisms were found to be operative in region III and II. Such a transition from viscous glide to climb mechanism is favorable from a practical point of view since it gives creep rates lower than those predicted by simple extrapolation to high stress values.
2. The experimental results on low stress, high temperature creep of aluminum reproducd the data of Harper, et al. and Barrett, et al. almost exactly, despite a significant difference in the sample and loading geometry. Hence it is concluded that the existence of Harper-Dorn creep in pure aluminum is well established.
3. A creep behavior which appears to be of the Harper-Dorn type is observed in aluminum 3% magnesium, pure lead and pure tin over a range of normalized stress (τ/G) roughly identical to the range over which this type of creep had been found in aluminum and silver. Two interesting correlations may be drawn from this observation. First, Harper-Dorn may be an important general mechanism of creep at high temperature and low stress. Secondly, metals become weaker than expected in the limit of low stress and high temperature,

and a clear "danger" is involved in simple extrapolation from high stress region.

4. The body of available microstructural evidence, which is drawn almost entirely from research on pure aluminum, indicates that Harper-Dorn creep is a dislocation-dominated mechanism and characterized by a low dislocation density dispersed through rather large subgrains.

5. The available data on Harper-Dorn creep may be plausibly explained as due to creep via climb of "saturated" dislocations. Other candidate mechanisms have been suggested and showed promising agreement. However, many of the assumptions, on which they are based, are questionable.

6. Simple Harper-Dorn creep behavior disappears when the applied stress exceeds a critical value or when sample grain size becomes sufficiently small. A recent experiment reveals that if a sample of $d < d_c$ is tested and if no third mechanism intervenes, the Nabarro-Herring creep will dominate over the Harper-Dorn. Reasoning from these experimental data give $d_c \sim 460\mu$ in aluminum.

ACKNOWLEDGEMENTS

This thesis is the outgrowth of research inaugurated and guided by the late Professor John E. Dorn. Much of the experimental work reported was done under his supervision. The remainder shows his strong influence.

I am deeply indebted to Professor J. W. Morris, Jr. for his continued interest, support and many valuable contributions during the course of this project after the death of Professor Dorn. I also wish to express my appreciation to Professor F. Hauser and Professor S. Ravitz for reviewing the manuscript.

Thanks are due to Jean Wolslegel and Shirley Ashley for typing the manuscript; to Gloria Pelatowski for preparing the figures; to Lloyde Crawford, Al Lyle and Jack Wodei for their technical assistance; and to Chol Syn, my friend, for his help and cooperation. Lastly, I give my sincerest thanks to my beloved wife, Gamalat, for her unlimited patience and invaluable encouragement.

This work was done under the auspices of the U. S. Atomic Energy Commission.

APPENDIX A. GLIDE OF JOGGED SCREW DISLOCATIONS

Consider screw dislocation with vacancy-forming jogs at a spacing L_j and height b. For stresses below a critical value, the dislocation bows out between the jogs but is pinned at them. By means of thermal activation, vacancies are produced at the jogs and the dislocation glides forward. If the entire bowed-out dislocation configuration moves forward uniformly by the emission of one vacancy from each jog, the distance of advance is ~b.

The free-energy change per length L_j of dislocation segment is

$$dF = \text{chemical work--mechanical work} \tag{1A}$$

Chemical Work

The total increase in free energy upon introduction of n independent and noninteracting vacancies at random among n_A atom is

$$F = n f_f - kT \ln \frac{(n_A + n)!}{n_A!\, n!} \tag{2A}$$

where f_f is the free energy of formation of a vacancy and the last term arises from the configurational entropy of random mixing of n vacancies among n_A atom. Therefore, the average work that must be done in adding a vacancy to a random mixture of n vacancies and n_A atoms is

$$\frac{\partial F}{\partial n} = f_f - kT \ln \frac{n + n_A}{n} \tag{3A}$$

Since the free energy is min. at equilibrium, the equilibrium number of vacancies, n_o, is given by

$$\left(\frac{\partial F}{\partial n}\right)_{no} = 0$$

$$\frac{n_o}{n_s} = e^{-f_f/kT}$$

where

$$n_s = n_A + n$$

or

$$\frac{C_o}{C_s} = e^{-f_f/kT} \tag{4A}$$

C_o and C_s are concentrations.

The extra work that must be done in creating a vacancy in lattice that contains n vacancies as referred to one that contains the equilibrium number of vacancies is given by the chemical work

$$W_c = \left(\frac{\partial F}{\partial C}\right)_C - \left(\frac{\partial F}{\partial n}\right)_{C_o} = f_f - kT \ln \frac{C_s}{C} - 0$$

$$= kT \ln \frac{C_s}{C_o} - kT \ln \frac{C_s}{C} \tag{5A}$$

$$= kT \ln \frac{C}{C_o}$$

Mechanical Work

$$W_m = (\text{Force on dislocation/unit length}) \times \text{Jog spacing} \times \text{distance of advance} \tag{6A}$$

$$= \sigma b \cdot L_j \cdot b$$

Al local equilibrium dF = 0, so that

$$W_C = W_m$$

$$C/C_o = \exp \frac{\sigma b^2 L_j}{kT} \tag{7A}$$

where C/C_o is the vacancy superconcentration

If $\sigma b^2 L_j < kT$ (very low stress), (Eq. (7A) becomes

$$C - C_o \cong C_o \frac{\sigma b^2 L_j}{kT} \tag{8A}$$

now, assume that the vacancy superconcentration C/C_o is in quasi-equilibrium with jogs over spheres of radius ~ b. Fick's second law for spherical coordinates in case of steady state gives

$$\frac{1}{r^2}\frac{\partial}{\partial r}\left(r^2 D \frac{\partial C}{\partial r}\right) = \frac{\partial C}{\partial t} = 0 \tag{9A}$$

Integrating twice (assume diffusivity, D, is constant)

$$C = -\frac{K_1}{r} + K_2 \tag{10A}$$

where K_1 and K_2 are constants to be determined from the boundary conditions

$$\begin{aligned} C &= C_o \quad \text{at} \quad r \to \infty \\ C &= C_o\left(1 + \frac{\sigma b^2 L_j}{kT}\right) \quad \text{at} \quad r = b \end{aligned} \tag{11A}$$

solving for K_1 and K_2, the solution is

$$C = C_o \frac{\sigma b^3 L_j}{kTr} + C_o \tag{12A}$$

The total flux of vacancies is

$$\begin{aligned} J &= \text{area of sphere} \times (\text{flux/unit area}) \\ &= 4\pi r^2\left[-D_v \frac{d}{dr}(C - C_o)\right] \end{aligned} \tag{13A}$$

where D_v is vacancy diffusivity.

The velocity of jog equals the velocity of the dislocation

$$V_j = V_d = J \cdot b = 4\,(C_o\, b^3\, D_v)\frac{b\, L_j}{kT}\sigma \tag{14A}$$

Since

$$\text{lattice diffusivity, } D, \cong C_o\, b^3\, D_v$$

$$V_d = 4\pi b L_j \frac{D}{kT}\ \sigma \tag{15A}$$

and

$$\dot{\varepsilon} = \rho b V_d \tag{16A}$$

Then

$$\dot{\varepsilon} = 4\pi b^2 L_j \frac{D}{kT}\,\sigma \tag{17A}$$

the last equation can be written in the form of Harper-Dorn equation as follows using the transformation of $\dot{\varepsilon}$ and σ to the equivalent values of $\dot{\gamma}$ and τ (Eq. (9))

$$\frac{\dot{\gamma} kT}{DGb} = 12\pi b L_j (\tau/G) \tag{18A}$$

Comparing Eq. (18A) with Eq. (45) gives

$$\left(A_{HD}\right)_{JS} = 12\pi b L_j \tag{19A}$$

APPENDIX B. CLIMB OF JOGGED EDGE DISLOCATION

Consider a single jog on straight edge dislocation. If a climb force $\frac{\sigma b^2}{L_j}$ acts on dislocation per unit length, the force on the jog is

$$F_j = \frac{\sigma b^2}{L_j} \cdot b \text{ (it is assumed the jog height } \sim b) \tag{1B}$$

The work done to emit a vacancy by jog motion is

$$W \cong \frac{\sigma b^2}{L_j} \cdot b \cdot b = \frac{\sigma b^4}{L_j} \tag{2B}$$

The vacancy superconcentration in local equilibrium with a jog is given by similar expression to Eq. (8A)

$$C - C_o \cong C_o \frac{\sigma b^4}{L_j kT} \tag{3B}$$

If it is assumed that jog is a point source where quasi-equilibrium is maintained with a surface of radius $\sim b$ around the jog, and Fick's second law is applied for the case of spherical coordinates at the steady state, a similar procedure to the one used in Appendix A can be carried out. First, the solution of Fick's second law with the same two boundary conditions specified in Appendix A gives

$$C - C_o = C_o \frac{\sigma b^5}{r L_j kT} \tag{4B}$$

Secondly, the net flux of vacancies is written as

$$J = 4\pi b^2 D \frac{\sigma}{L_j kT} \tag{5B}$$

and the velocity of climb is,

$$V_C = J \cdot b = 4\pi b^3 D \frac{\sigma}{L_j kT} \tag{6B}$$

Finally, the creep rate, $\dot{\varepsilon}$, is obtained as

$$\dot{\varepsilon} = \rho bV = \rho b^2 J = 4\pi b^4 \rho D \frac{\sigma}{L_j kT} \tag{7B}$$

If the Eq. (7B) is rearranged in the form of Harper-Dorn equation, the final expression is

$$\frac{\dot{\gamma} kT}{DGb} = \frac{12\pi b^3 \rho}{L_j} (\tau/G) \tag{8B}$$

with

$$\left(A_{HD}\right)_{JE} = \frac{12\pi b^3 \rho}{L_j} \tag{9B}$$

APPENDIX C. SUBGRAIN CREEP

Subgrain creep can be derived by formulating Nabarro-Herring equation with subgrain diameter, δ, replacing the grain size d.

Consider a subgrain dimension δ stressed as shown in Fig. 2. It is assumed that the subgrain boundaries are regions which act as sources and sinks for vacancies. When a tensile stress is applied normal to a sub boundary, it can assist in the formation of a vancancy since it will do work $\sigma\Omega_v$ per vacancy produced, where Ω_v the volume of a vacancy. At sub boundary subjected to tensile stress, the probability of finding a vacancy is

$$n_v^+ = n_s \left(\exp - f_f/kT\right)\left(\exp \frac{\sigma\Omega v}{kT}\right) \tag{1C}$$

while the probability of finding a vacancy at sub boundary subjected to compressive stress is

$$n_v^- = n_s\left(\exp - f_f/kT\right)\left(\exp - \frac{\sigma\Omega_v}{kT}\right) \tag{2C}$$

The difference in concentration of vacancies between the two subgrain boundaries is

$$C^+ - C^- = \frac{1}{\Omega} \exp - f_f/kT\left[\exp \frac{\sigma\Omega_v}{kT} - \exp - \frac{\sigma\Omega_v}{kT}\right] \tag{3C}$$

The diffusion path is approximately $\pi/2\ \frac{\delta}{4}$ and therefore the conc. gradient for this path is about

$$\frac{C^+ - C^-}{\frac{\pi\delta}{\delta}} = \frac{16}{\Omega\pi\delta} \exp - f_f/kT\left[\exp \frac{\sigma\Omega_v}{kT} - \exp - \frac{\sigma\Omega_v}{kT}\right] \tag{4C}$$

Since $\frac{\sigma\Omega}{kT} < 1$ for the usual values of the applied stress,

$$\text{conc. gradient} = \frac{16\,\Omega_v\, e^{-f_f/kT}\,\sigma}{\Omega\pi\delta kT} \tag{5C}$$

If h is taken as the height of an atom, the area of an atom is $\frac{\Omega}{h}$. Then, the flux of atoms across an atomic area is given by

$$J = \frac{\Omega}{h} \cdot D_v \cdot (\text{conc. gradient}) \tag{6C}$$

where D_v = diffusivity of vacancy.

For each atom transferred (in opposite direction to vacancy flow), the strain is

$$\gamma = \frac{2h}{\delta} \tag{7C}$$

and the strain rate, $\dot{\varepsilon}$, is

$$\dot{\gamma} = (\text{strain/atom}) \times \text{total flux/sec}$$

$$= \frac{2h}{\delta} \cdot \frac{\Omega}{h} \cdot D_v \cdot \frac{16\,\Omega_v \exp^{-f_f/kT}}{\Omega\pi\delta kT}\,\sigma \tag{8C}$$

$$\dot{\gamma} = \frac{32}{\pi} \cdot \frac{\Omega_v}{\delta^2}\,\frac{D_v}{kT}\,\exp^{-f_f/kT} \cdot \sigma$$

Since $\sigma = \tau$ for this case of loading

and $D = D_v \exp^{-f_f/kT}$

$\Omega_v = b^3$

Equation (8C) can be written as

$$\dot{\gamma} = A' \frac{b^3}{\delta^2}\,\frac{D}{kT}\,\tau \tag{9C}$$

where A' is dimensionless constant which depends on the geometry of subgrain, but is generally estimated to have a value of 14 for the case of Nabarro-Herring creep. Comparing Eq. (9C) with Harper-Dorn creep

gives A_{HD} as

$$\left(A_{HD}\right)_{SG} = 14 \left(\frac{b}{\delta}\right)^2 \qquad (10C)$$

APPENDIX D. DYNAMIC BALANCE OF DISLOCATIONS

(a) Dislocation generation.

It is assumed that the dislocation multiplication occurs at a fixed number of sources by a diffusion controlled climb mechanism. The rate of dislocation generation, $\frac{d\rho^+}{dt}$ is written as,

$$\frac{d\rho^+}{dt} = \rho_o \frac{V_C}{h} \tag{1D}$$

where ρ_o is the fixed dislocation source length per unit volume, h is the climb distance required to create a dislocation and V_C is the climb velocity. The expression for climb velocity, V_C, is the same given by Eq. (6B) in Appendix B

$$V_C \cong D \frac{\sigma b^2}{kT} \tag{2D}$$

and

$$h = \frac{Gb}{\sigma} \tag{3D}$$

Therefore,

$$\frac{d\rho^+}{dt} = \rho_o b \frac{D}{kT} \frac{\sigma^2}{G} \tag{4D}$$

(b) Dislocation annihilation.

Dislocation annihilation is assumed to occur only at subgrain boundaries.

$$\frac{d\rho^-}{dt} = \rho \frac{V_g}{\delta} \tag{5D}$$

where ρ is the mobile dislocation density, V_g is the glide velocity and δ is subgrain diameter. Subgrain size, δ, can be approximated as (according to Barrett, et al.)

$$\frac{\delta}{b} = \delta_o \left(\frac{G}{\sigma}\right) \tag{6D}$$

Equation (6D) is slightly different from that assumed by Barrett, et al. since it is written here in dimensionless form. Combining Eq. (5D) and Eq. (6D) gives

$$\frac{d\rho^-}{dt} = \rho \frac{V_g \sigma}{\delta_o G b} \tag{7D}$$

At the steady state

$$\frac{d\rho^+}{dt} - \frac{d\rho^-}{dt} = 0 \tag{8D}$$

solving for ρ,

$$\rho = \rho_o b^2 \frac{D}{kT} \frac{\sigma}{V_g} \tag{9D}$$

The creep process is controlled by climb, but the strain is produced by glide. Therefore, the creep rate is given by,

$$\dot{\varepsilon} = \rho b V_g \tag{10D}$$

Substitute for ρ from Eq. (9D)

$$\dot{\varepsilon} = \rho_o \delta_o b^3 \frac{D}{kT} \sigma$$

or

$$\dot{\gamma} = 3\rho_o \delta_o b^3 \frac{D}{kT} \tau \tag{11D}$$

Equation (11D) can be written in Harper-Dorn type as follows,

$$\frac{\dot{\gamma} kT}{DGb} = 3\rho_o b^2 \delta_o (\tau/G) \tag{12D}$$

with

$$\left(A_{HD}\right)_{DB} = 3\rho_o b^2 \delta_o \tag{13D}$$

APPENDIX E. CLIMB OF SATURATED DISLOCATION

Consider the case of edge dislocation near the center of a cylinder and parallel to its axis (the same treatment can equally be applied to a mixed dislocation with almost the same final answer). The shear stress exerts a force σb per unit length on the dislocation. Therefore, the local equilibrium vacancy concentration near the core is given by an equation similar to Eq. (8A) (Appendix A).

$$C \cong C_o\left(1 + \frac{\sigma b^3}{kT}\right) \tag{1E}$$

Fick's second law for cylindrical coordinates at the steady state is,

$$\frac{1}{r}\ \frac{\partial}{\partial r}\left(rD\ \frac{\partial C}{\partial r}\right) = \frac{\partial C}{\partial t} = 0 \tag{2E}$$

(the derivatives with respect to θ and z are zero by symmetry)
To solve Eq. (2E), it is assumed that C_o and D are constant. These simplifying assumptions are reasonable except in a region very close to the core. The solution of Eq. (2E) gives,

$$C = K_1 \ln r + K_2 \tag{3E}$$

to determine K_1 and K_2, two boundary conditions are needed. These are;

$$\begin{aligned} C &= C_o \quad \text{at} \quad r = R \\ C &\cong C_o\left(1 + \frac{\sigma b^3}{kT}\right) \text{ at} \quad r = b \end{aligned} \tag{4E}$$

The solution to Eq. (2E) which satifies the above conditions is,

$$C = C_o + C_o\ \frac{\sigma b^3}{kT}\ \frac{\ln\ (R/r)}{\ln\ (R/b)} \tag{5E}$$

The net flux per unit length of dislocation J is given by

J = area of cylinder X flux per unit area

$$= - 2\pi r D_v \frac{\partial}{\partial r} (C - C_o) \tag{6E}$$

Combining Eq. (5E) and Eq. (6E), we obtain

$$J = 2\pi b^3 C_o \frac{D}{kT \ln R/b} \sigma \tag{7E}$$

The velocity of dislocation (climb)

$$\frac{v}{b^2} = J \tag{8E}$$

then,

$$V = 2\pi b^5 C_o \frac{D}{kT \ln R/b} \sigma \tag{9E}$$

Since

$$\dot{\varepsilon} = \rho b V \tag{10E}$$

and

$$D \cong b^3 C_o D_v$$

The creep rate, $\dot{\varepsilon}$, is

$$\dot{\varepsilon} = \frac{2\pi b^3 \rho D}{\ln R/b \; kT} \sigma \tag{11E}$$

Equation (11E) can be rearranged in the form of Harper-Dorn equation (transform $\dot{\varepsilon}$ and σ to $\dot{\gamma}$ and τ)

$$\frac{\dot{\gamma} kT}{DGb} = \frac{6\pi \rho b^2}{\ln R/b} \left(\frac{\tau}{G}\right) \tag{12E}$$

since $R = \frac{1}{\sqrt{\rho}}$ the final form of Eq. (12E) becomes

$$\frac{\dot{\gamma} kT}{DGb} = - \frac{6\pi \rho b^2}{\ln \sqrt{\rho} b} \left(\frac{\tau}{G}\right) \tag{13E}$$

with

$$\left(A_{HD}\right)_{CS} = - \frac{6\pi \rho b^2}{\ln \sqrt{\rho} b} \tag{14E}$$

APPENDIX F. SHEAR MODULUS AND DIFFUSIVITY

(a) Shear modulus.

The unrelaxed shear modulus of most metals can be represented by

$$G = A - BT \tag{1F}$$

where G is the shear modulus (Dynes/cm^2), T is the absolute temperature (°K), and A and B are materials constants. The values of the shear modulus for the metals considered in this thesis are,

$$G = 3.02 \times 10^{11} - 1.6 \times 10^{8} \quad T \quad \text{For aluminum}^{54} \tag{2F}$$

$$G = 9.94 \times 10^{10} - 8.83 \times 10^{7} \times T \quad \text{For lead}^{55} \tag{3F}$$

$$G = 2.61 \times 10^{11} - 1.86 \times 10^{8} \times T \quad \text{For tin}^{56} \tag{4F}$$

and

$$G = 3.04 \times 10^{11} - 1.27 \times 10^{8} \times T \quad \text{For silver}^{57} \tag{5F}$$

For aluminum-3% magnesium, the modulus of pure aluminum was used since an experimental evidence shows that the shear modulus is independent of the concentration of magnesium[58] up to 10%.

(b) Diffusivity.

The diffusivity of metals can be represented by the following Arrhenius relation

$$D = D_o \exp(-H_D/RT) \tag{6F}$$

where D_o is the preexponential factor (cm^2/sec), H_D is the enthalpy of diffusion (cal/mole) and RT is the gas constant times the absolute temperature.

The values of the diffusivity for lead,[32] tin[33] and silver[59] are respectively,

$$D_{Pb} = 0.28 \exp(-24,200/RT) \quad (7F)$$

$$D_{Sn} = 0.78 \exp(-22,350/RT) \quad (8F)$$

$$D_{Ag} = 0.4 \exp(-44,100/RT) \quad (9F)$$

For pure aluminum, the diffusivity is taken from a least squares fit to the composite high temperature diffusion data of Lundy and Murdock[31] and Beyeler and Adda.[30] The value estimated is given by

$$D = (1.86 \pm 0.25) \exp(-34,230 \pm 211/RT) \quad (10F)$$

It might be noted that the value of D_o is different from that estimated by Robinson and et al.[60] using the same data. Their estimated value is 2.25. The tracer diffusivity data have an advantage over the other investigations since they represent the actual values of the diffusivity at the submelting temperatures. It is clear, from Fig. 32, that the theoretical prediction[61] is a factor of 2 below the tracer data. While the data by Volin, et al.[62] converge to the tracer data for $T > 0.95\ T_m$, the discrepancy between the tracer data and NMR[63] (Nuclear Magnetic Resonance) results increases as the temperature approaches the melting point.

APPENDIX G. COMPUTER PROGRAM

Definitions of Terminology Used

M = Metal or alloy tested

T = Absolute temperature °K

R = Creep rate, $\dot{\gamma}$ sec^{-1}

S = Applied stress, τ psi

G = Shear modulus = $Dyne/cm^2$

D = Diffusivity cm^2/sec

DO = Diffusivity factor cm^2/sec

Q = Activation energy for self diffusion cal/mole

V = Burgers vector cm

AL = Constant for each metal $Dyne/cm^2$

BL = Constant for each metal $Dyne/cm^2$ - °K

$BB_i = \dot{\gamma}_i kT_k/D_i G_i b$

$CC_i = \tau_i/G_i$

$YY_i = \log \dot{\gamma}_i kT_i/D_i G_i b$

$XX = \log \tau_i/G_i$

N = Number of experimental points

SN = Stress power

SDI = Standard deviation in stress power

SC = log (the intercept of straight line)

SD2 = log (standard deviation of the intercept)

C1 = Intercept of the straight line

C2 = The upper limit for the value of the intercept

C3 = The low limit for the value of the intercept

SUM = Σ

AVE = Average

```
      PROGRAM CREEP (INPUT,OUTPUT)
      DIMENSION T(100),R(100),S(100),G(100),D(100),BB(100),CC(100),YY(10
     A0),XX(100)
      PRINT 2
    2 FORMAT (1H1,30X*DETERMINATION OF STRESS LAW FOR HIGH TEMPERATURE
     CREEP*/59X*IN*/50X*PURE M*)
      DO 11 IZ = 1,2
      READ 34,N,(R(I) , I = 1,N)
   34 FORMAT (I3/(2X,7E10.3))
      READ 36,(S(I) , I = 1,N)
   36 FORMAT (2X,14F5.3)
      READ 35,(T(I) , I = 1,N)
   35 FORMAT (24F3.0)
      CON = (1.38054E-08)/V
      DO 10 I = 1,N
      G(I) = AL-BL*T(I)
      D(I) = DO*Exp(-Q/(1.987*T(I))
      BB(I) = CON*R(I)*T(I)/(D(I)*G(I))
      CC(I) = (S(I)/G(I))*6.8947E+04
      YY(I) = ALOG10(BB(I))
      XX(I) = ALOG10(CC(I))
   10 CONTINUE
      CALL LEAST(YY,N,XX,SN,SC,SD1,SD2)
   17 PRINT 444,SN,SD1,SC,SD2
  444 FORMAT (/10X*SLOPE=*2XF11.6*  +CR-*F9.6/10X*INTERCEPT=*E16.6*  +CR
     A-*E13.6
      C1 = 10.**SC
      C2 = 10. ** (SC+SD2)
      C3 = 10. ** (SC - SD2)
      PRINT 777 , C1,C2,C3
  777 FORMAT (10XE16.6,5XE13.6,5XE13.6)
   11 CONTINUE
      END

      SUBROUTINE LEAST(Y,N,X,SL,CI,SDL,SDT)
      DIMENSION Y(1),X(1)
      SUM1 = 0.
      SUM2 = 0.
     DO  13 I = 1,N
      SUM1 = SUM1 + Y(I)
   13 SUM2 = SUM2 + X(I)
      AVE1 = SUM1/N
      AVE2 = SUM2/N
      SUM3 = 0.
      SUM4 = 0.
      SUM5 = 0.
      SUM6 = 0.
      DO 15 I = 1,N
      SUM3 = SUM3 + (X(I) - AVE2)*(Y(I) - AVE1)
      SUM4 = SUM4 + (X(I) - AVE2)**2
      SUM5 = SUM5 + (X(I))**2
```

```
15 SUM6 = SUM6 + X(I))**2
   SL = SUM3/SUM4
   CI = (AVE1*SUM5 - AVE2*SUM6)/SUM4
   SUM7 = 0.
   SUM8 = 0.
   DO 18 I = 1,N
   SUM7 = SUM7+(X(I)-AVE2)**2*((Y(I)-AVE1)/(X(I)-AVE2)-SL)**2
18 SUM8=SUM8+(X(I)-AVE2)**2*((AVE1*X(I)-AVE2*Y(I))/(X(I)-AVE2)-CI)**2
   RN = N
   AN = SUM4*RN
   SDL = SQRT(SUM7/AN)
   SDT = SQRT(SUM8/AN)
   RETURN
   END
```

REFERENCES

1. G. Schoeck, Theories of Creep, in Mechanical Behavior of Materials at Elevated Temperature (McGraw-Hill Book Co., Inc., New York, 1961) p. 79.
2. R. L. Coble, J. Appl. Phys. 34, 1679 (1963).
3. A. Ball and M. M. Hutchison, Metal Sci. J. 3, 1 (1969).
4. P. Guyot, Act. Met. 14, 955 (1966).
5. F. R. N. Nabarro, Report of a Conference on the Strength of Solids, (The Physical Society, London, 1948) p. 75.
6. C. Herring, J. Appl. Phys. 21, 437 (1950).
7. E. R. Gilbert and D. E. Munson, Trans. AIME 233, 429 (1965).
8. A. L. Pranatis and G. W. Pound, Trans. AIME 203, 664 (1955).
9. N. F. Mott, A Discussion of Some Models of the Rate-Determining Process in Creep, in Creep and Fracture of Metals at Elevated Temperatures, (H. M. Stationary Office, London, 1956) p. 21.
10. J. Friedel, Phil. Mag. 46, 1169 (1956).
11. P. B. Hirsch and D. H. Warrington, Phil. Mag. 6, 735 (1961).
12. C. R. Barrett and W. D. Nix, Acta Met. 13, 1247 (1965).
13. J. B. Gibbs, Equilibrium Velocities of Defect-Emitting Jogs, RD/B/N884, Berkeley Nuclear Laboratory, England (1967).
14. N. F. Mott, The Mechanical Properties of Metals, Proc. Phys. Soc., London, 64B, 729 (1951).
15. A. Seeger, Phil. Mag. 46, 1194 (1955).
16. J. Weertman, J. Appl. Phys. 26, 1213 (1955).
17. J. Weertman, J. Appl. Phys. 23, 362 (1957).
18. H. Suzuki, Sci. Rep. Res. Inst. Tohoku Univ. (Japan) 7A, 194 (1955).

19. R. L. Fleischer, Acta Met. 9, 996 (1961); 11, 203 (1963).

20. A. H. Cottrell, Dislocations and Plastic Flow in Crystals, (Claredon Press, Oxford, 1953) p. 136.

21. J. E. Bird, A. K. Mukherjee and J. E. Dorn, Correlations Between High-Temperature Creep Behavior and Structure, in Quantitative Relation Between Properties and Microstructure (Israel University Press, Jerusalem, 1969).

22. J. Weertman, J. Appl. Phys. 28, 1185 (1957).

23. L. Darken, Trans. AIME 174, 184 (1948).

24. J. Weertman, Trans. AIME 218, 207 (1960).

25. J. G. Harper and J. E. Dorn, Acta Met. 5, 654 (1957).

26. E. C. Muehleisen, Ph.D. thesis, Stanford University (1969).

27. J. G. Harper, L. A. Shepard and J. E. Dorn, Acta Met. 6, 507 (1958).

28. B. Burton, Phil. Mag. 25, 645 (1972).

29. A. K. Mukherjee, J. E. Bird and J. E. Dorn, Experimental Correlations for High-Temperature Creep, presented at the Detroit Materials Engineering Congress of ASM, 1968, p. 16.

30. M. Beyeler and Y. Adda, J. de Phys. 29, 345 (1968).

31. T. S. Lundy and J. F. Murdock, J. Appl. Phys. 33, 1671 (1962).

32. N. Nachtrieb and G. Handler, J. Chem. Phys. 23, 1569 (1956).

33. W. Lange, A. Hassnet and I. Berthold, Phys. Status Solidi (Germany) 1, No. 1, 50 (1961).

34. K. E. Amin, A. K. Mukerjee and J. E. Dorn, J. Mech. Phys. Solids 18, 413 (1970).

35. F. R. N. Nabarro, Phil. Mag. 16, 231 (1967).

36. J. Friedel, Dislocations (Pergamon Press, London, 1964).

37. A. H. Clauer, B. A. Wilcox and J. P. Hirth, Acta Met. 18, 381(1969).

38. A. K. Head, Phil. Mag. 4, 295 (1959).

39. J. C. M. Li, Discussions of Faraday Society 38, 138 (1964).

40. P. M. Hazzledine, J. de Physique 27, 210 (1966).

41. R. Chang, in The Physics and Chemistry of Ceramics, (Gordon and Breach, New York, 1963).

42. D. McLean and H. F. Hale, The Stress Sensitivity of Creep, in Structural Processes in Creep (Iron and Steel Institute, London, 1961) p. 19.

43. V. C. Kannan and G. Thomas, J. Appl. Phys. 37, No. 6, 2363 (1966).

44. I. S. Servi and N. J. Grant, Trans. AIME 191, 909 (1951).

45. J. Weertman, J. Mech. and Phys. Solids 4, 230 (1956).

46. O. D. Sherby, J. L. Lytton and J. E. Dorn, Acta Met. 5, 219 (1957).

47. R. F. Frenkel, O. D. Sherby and J. E. Dorn, Acta Met. 3, 470 (1955).

48. J. E. Breen and J. Weertman, Trans. AIME 207, 1230 (1955).

49. C. R. Barrett, E. C. Muhleisen and W. D. Nix, Mat. Sci. Eng. 10, 33 (1972).

50. K. K. Ziling, Fiz. Metal. Metalloved. 22, 931 (1966).

51. B. Ya. Pines and A. F. Sirenko, Fiz. Metal. Metalloved. 15, 584 (1963).

52. B. Nost and E. Nes, Acta Met. 17, 13 (1969).

53. J. P. Hirth and J. Lothe, Theory of Dislocations (McGraw-Hill, New York, 1968).

54. P. M. Sutton, Phys. Rev. 91, 816 (1953).

55. J. Weertman, Tran. ASM 61, 681 (1968).

56. W. Köster, Z. Metallkunde 39, 1 (1948).

57. Y. A. Chang and L. Himmel, J. Appl. Phys. 37, 3567 (1956).

58. W. Köster and W. Rauscher, National Advisory Committee for Aeronautics (USA), Tech. Memo No. 1321 (1951).

59. C. Tomizuka and E. Sonder, Phys. Rev. 103, 1182 (1956).

60. S. L. Robinson and O. D. Sherby, Phys. Stat. Sol. (a)1, 119 (1970).

61. A. S. Nowick, J. Appl. Phys. 22, 1182 (1951).

62. T. E. Volin and R. W. Baluffi, Phys. Sat. Sol. 25, 163 (1968).

63. F. Y. Fradin and T. J. Rowland, Appl. Phys. Lett. 11, 207 (1967).

Table I.a. Aluminum-3% magnesium data.

Temperature (°K)	Applied Stress Psi	Creep Rate Sec^{-1}	Region
798	194.7	6.613×10^{-5}	III (Instron)
798	242.8	1.323×10^{-4}	"
798	297.8	2.645×10^{-4}	"
797	297.8	2.645×10^{-4}	"
800	298.0	2.645×10^{-4}	"
797	394.0	6.613×10^{-4}	"
802	366.5	6.613×10^{-4}	"
797	494.8	1.323×10^{-4}	"
797	490.2	1.323×10^{-4}	"
802	609.3	2.645×10^{-4}	"
802	613.9	2.596×10^{-4}	"
841	220.0	6.490×10^{-4}	"
840	293.0	1.298×10^{-3}	"
839	358.3	2.596×10^{-3}	"
838	450.2	2.596×10^{-3}	"
842	445.6	6.490×10^{-3}	"
842	579.0	2.66×10^{-3}	"
868	347.6	1.33×10^{-4}	"
868	284.5	2.66×10^{-4}	"
869	168.7	1.33×10^{-4}	"
877	362.4	1.33×10^{-3}	"
853	208.5	2.67×10^{-4}	"
853	278.57	6.67×10^{-4}	"
853	333.15	1.33×10^{-3}	"
853	413.79	2.67×10^{-3}	"
863	363.3	2.66×10^{-3}	"
864	296.5	1.33×10^{-3}	"
862	249.3	6.67×10^{-4}	"
725	1792.0	6.67×10^{-3}	"
725	1287.0	2.33×10^{-3}	"
725	1010.0	1.33×10^{-3}	"

Table 1.a continued

Temperature (°K)	Applied Stress Psi	Creep Rate Sec^{-1}	Region
725	808.0	6.67×10^{-4}	III (Instron)
725	599.5	2.66×10^{-4}	"
725	515.0	1.33×10^{-4}	"
672	2207.9	2.66×10^{-3}	"
672	1768.0	1.33×10^{-3}	"
672	1442.0	6.67×10^{-4}	"
672	1051.0	2.66×10^{-4}	"
672	902.7	1.33×10^{-4}	"
635	402.5	1.33×10^{-3}	"
635	320.0	6.67×10^{-4}	"
635	240.0	2.66×10^{-4}	"
635	200.0	1.33×10^{-4}	"
635	155.0	6.67×10^{-5}	"
854	241.95	4.96×10^{-4}	III (Creep)
857	170.00	5.95×10^{-4}	"
857	240.00	5.97×10^{-4}	"
704	513.00	1.09×10^{-4}	"
624	672.15	9.20×10^{-6}	"
630	672.15	1.286×10^{-5}	"
630	672.15	1.300×10^{-5}	"
630	702.00	1.342×10^{-5}	"
630	468.00	4.92×10^{-6}	"
625	423.8	2.56×10^{-6}	"
625	423.8	2.86×10^{-6}	"
800	146.6	2.645×10^{-5}	III-II (Instron)
870	146.1	1.33×10^{-4}	"
871	114.4	6.67×10^{-5}	II (Instron)
853	114.04	2.67×10^{-5}	"
865	102.6	2.67×10^{-5}	II (Creep)
866	27.86	1.73×10^{-7}	"

Table 1.a. continued

Temperature (°K)	Applied Stress Psi	Creep Rate Sec^{-1}	Region
866	27.86	1.77×10^{-7}	II (Creep)
866	36.9	2.95×10^{-7}	"
857	42.55	8.88×10^{-7}	"
857	42.55	7.33×10^{-7}	"
855	60.70	1.94×10^{-6}	"
834	123.5	2.93×10^{-5}	"
842	72.2	4.20×10^{-6}	"
838	85.7	6.66×10^{-6}	"
838	53.0	1.06×10^{-6}	"
834	99.0	1.16×10^{-6}	"
856	53.1	1.89×10^{-6}	"
856	53.1	1.59×10^{-6}	"
858	33.56	2.31×10^{-7}	"
858	33.56	2.82×10^{-7}	"
858	20.52	5.1×10^{-8}	II-I (Creep)
868	24.0	6.98×10^{-8}	"
866	4.98	1.5×10^{-8}	I (Creep)
868	6.8	2.35×10^{-8}	"
866	8.84	2.71×10^{-8}	"
866	15.17	4.21×10^{-8}	"
854	8.45	2.2×10^{-8}	"
857	14.0	3.29×10^{-8}	"
857	7.0	1.9×10^{-8}	"

Table I.b. Aluminum data.

Temperature (°K)	Applied Stress Psi	Creep Rate Sec^{-1}	Region
923	37.5 (P)	1.46×10^{-4}	II
923	28.2 (P)	4.00×10^{-5}	II
923	21.5 (P)	9.2×10^{-6}	II
923	15.0 (P)	1.31×10^{-6}	II
923	12.5 (P)	$4.1 \quad 10^{-7}$	II-I
923	03.22 (P)	4.26×10^{-8}	I
923	02.01 (P)	2.2×10^{-8}	I
923	01.5 (P)	2.46×10^{-8}	I
923	00.95 (P)	1.39×10^{-8}	I
925	03.65 (S)	8.6×10^{-8}	I
925	02.11 (S)	4.06×10^{-8}	I
925	01.28 (S)	2.26×10^{-8}	I

P - denotes polycrystals

S - denotes single crystals

Errata

Table I.c. Lead data.

Temperature (°K)	Applied Stress (psi)	Creep Rate sec^{-1}	Region
554	21.4	5.7×10^{-8}	II
554	26.0	4.77×10^{-7}	II
554	30.6	9.2×10^{-7}	II
554	32.7	3.56×10^{-6}	II
554	37.2	5.17×10^{-6}	II
554	23.5	3.75×10^{-7}	II
554	46.4	2.66×10^{-5}	II
554	55.5	5.5×10^{-5}	II
554	21.4	2.94×10^{-7}	II
587	15.4	2.05×10^{-7}	II
587	17.6	4.44×10^{-6}	II
587	22.3	4.70×10^{-7}	II
587	24.5	2.20×10^{-6}	II
587	26.3	3.55×10^{-6}	II
587	31.3	9.15×10^{-6}	II
587	35.7	2.04×10^{-5}	II
587	44.6	4.37×10^{-5}	II
587	54.0	1.80×10^{-4}	II
587	68.0	9.99×10^{-5}	II
514	35.0	2.00×10^{-7}	II
514	39.7	9.8×10^{-7}	II
514	44.3	1.16×10^{-6}	II
514	57.3	5.45×10^{-6}	II
473	44.3	3.16×10^{-7}	II
473	57.8	1.11×10^{-6}	II
473	66.5	1.15×10^{-6}	II
473	71.2	2.00×10^{-6}	II

Table I.c continued

Temperature (°K)	Applied Stress (psi)	Creep Rate sec^{-1}	Region
554	3.85	8.3×10^{-9}	I
554	5.00	1.02×10^{-8}	I
554	7.3	1.53×10^{-8}	I
554	10.17	2.7×10^{-8}	I
554	14.6	3.34×10^{-8}	I
587	1.8	1.77×10^{-8}	I
587	4.1	3.2×10^{-8}	I
587	6.3	4.88×10^{-8}	I
587	8.54	8.7×10^{-8}	I

Table I.c. Lead data.

Temperature (°K)	Applied Stress (psi)	Creep Rate sec^{-1}	Region
554	21.4	5.7×10^{-8}	II
554	26.0	4.77×10^{-7}	II
554	30.6	9.2×10^{-7}	II
554	32.7	3.56×10^{-6}	II
554	37.2	5.17×10^{-6}	II
554	23.5	3.75×10^{-7}	II
554	46.4	2.66×10^{-5}	II
554	55.5	5.5×10^{-5}	II
554	21.4	2.94×10^{-7}	II
587	15.4	2.26×10^{-5}	II
587	17.6	2.59×10^{-5}	II
587	22.3	3.28×10^{-5}	II
587	24.5	3.60×10^{-5}	II
587	26.3	3.87×10^{-5}	II
587	31.3	4.6×10^{-5}	II
587	35.7	5.25×10^{-5}	II
587	44.6	6.56×10^{-5}	II
587	54.0	6.94×10^{-5}	II
587	68.0	9.99×10^{-5}	II
514	35.0	2.00×10^{-7}	II
514	39.7	9.8×10^{-7}	II
514	44.3	1.16×10^{-6}	II
514	57.3	5.45×10^{-6}	II
473	44.3	3.16×10^{-7}	II
473	57.8	1.11×10^{-6}	II
473	66.5	1.15×10^{-6}	II
473	71.2	2.00×10^{-6}	II

Table I.c continued

Temperature (°K)	Applied Stress (psi)	Creep Rate sec^{-1}	Region
554	3.85	8.3×10^{-9}	I
554	5.00	1.02×10^{-9}	I
554	7.3	1.53×10^{-8}	I
554	10.17	2.7×10^{-8}	I
554	14.6	3.34×10^{-8}	I
587	1.8	1.77×10^{-8}	I
587	4.1	3.2×10^{-8}	I
587	6.3	4.88×10^{-8}	I
587	8.54	8.7×10^{-8}	I

Table I.d. Tin data.

Temperature (°K)	Applied Stress (psi)	Creep Rate sec^{-1}	Region
495	30.9	1.6×10^{-8}	II
495	40.0	9.25×10^{-8}	II
495	62.8	2.27×10^{-6}	II
495	98.3	4.45×10^{-5}	II
495	85.0	1.62×10^{-5}	II
495	48.6	2.00×10^{-7}	II
495	44.0	8.00×10^{-8}	II
495	71.6	8.9×10^{-6}	II
495	35.7	4.8×10^{-8}	II
495	67.5	2.94×10^{-6}	II
495	54.0	5.3×10^{-7}	II
427	175.0	2.27×10^{-5}	II
427	150.0	5.00×10^{-6}	II
427	114.0	9.25×10^{-6}	II
427	102.0	2.37×10^{-7}	II
427	132.3	3.34×10^{-6}	II
461	126.0	2.56×10^{-5}	II
461	61.8	1.00×10^{-7}	II
461	107.0	7.6×10^{-6}	II
461	73.0	3.18×10^{-7}	II
461	85.0	1.72×10^{-6}	II
402	228.0	7.18×10^{-5}	II
402	244.0	2.14×10^{-5}	II
402	152.0	7.18×10^{-6}	II
402	182.0	6.00×10^{-6}	II
402	195.0	1.94×10^{-4}	II

Table 1.d continued

Temperature (°K)	Applied Stress (psi)	Creep Rate sec^{-1}	Region
495	17.6	8.3×10^{-9}	I
495	10.8	4.35×10^{-9}	I
495	5.38	2.78×10^{-9}	I
495	2.57	1.17×10^{-8}	I

Table II. Experimental values for various parameter in the three region for aluminum-3% magnesium.

Region	H kcal/mole	n	A
III	33.1 ±2.16	3.27±0.03	$51.4^{+18.1}_{-13.3}$
II	33.08±0.52	4.06±0.07	$\left(9.2^{+11.2}_{-5.1} \times 10^{4}\right)$
I	35.7 ±5.78	0.91±0.03	$\left(1.39^{+0.68}_{-0.45} \times 10^{-11}\right)$

Table III. Experimental values for (A) and (n) of the data on lead and tin.

Metal	Region I		Region II	
	n	A	n	A
Lead (d=1.5 mm)	0.97±0.08	$\left(2.88^{+4.88}_{-1.81}\right)\times10^{-11}$	4.92±0.57	$\left(1.38^{+405.2}_{-1.375}\right)\times10^{8}$
Tin (d=2 mm)	0.94±0.07	$\left(7.24^{+9.76}_{-4.22}\right)\times10^{-11}$	6.59±0.28	$\left(3.55^{+59.55}_{-3.35}\right)\times10^{17}$

Table IV. Diffusion controlled creep mechanisms

#	Mechanism	Relationship
A	Dislocation Climb	$\frac{\dot{\gamma}kT}{DGb} = 6 \times 10^{7} (\tau/G)^{4 \text{ to } 7}$
B	Jogged Screw Dislocation	$\frac{\dot{\gamma}kT}{DGb} = \frac{24 L_j}{b} (\tau/G)^3$ (a)
		$\frac{\dot{\gamma}kT}{D_c Gb} = \pi(\tau/G)^3$ (b)
C	Viscous Glide	$\frac{\dot{\gamma}kT}{DGb} = 6 (\tau/G)^3$
D	Nabarro-Herring	$\frac{\dot{\gamma}kT}{DGb} = 14 (b/d)^2 (\tau/G)$
E	Coble	$\frac{\dot{\gamma}kT}{D_b Gb} = 100 (b/d)^3 (\tau/G)$
F	Superplastic	$\frac{\dot{\gamma}kT}{D_b Gb} = \sim 200 (b/d)^2 (\tau/G)^2$
G	Nabarro-Subgrain	$\frac{\dot{\gamma}kT}{DGb} = 14 (b/\delta)^2 (\tau/G)$
		$(\delta/b) = 10 (\tau/G)^{-1}$
H	Nabarro-Bardeen-Herring	$\frac{\dot{\gamma}kT}{DGb} = \frac{1}{\pi \ln (4G/\pi\tau)}$

(a) if jogs on the screw dislocation are all either vacancy emitting or adsorbing type.
(b) for the case when equal numbers of both types of jogs are present.
D_c = core Diffusivity
D_b = grain boundary diffusivity
L_j = mean distance between jogs
d = mean grain diameter
δ = subgrain diameter

Table V. Values of (A) and (n) obtained from the least square analyses of creep data from materials which show apparent Harper-Dorn creep. The values predicted on the assumption of Nabarro-Herring creep are included.

Metal	Region I (Harper-Dorn)		Region II (Climb)		Nabarro	
	n	A	n	A	n	A
Aluminum (d=9 mm)	1.01±0.07	$5.05^{+9.65}_{-3.95} \times 10^{-11}$	4.5	10^{8}	1	1.42×10^{-14}
Aluminum-3% Magnesium (d=3 mm)	0.91±0.03	$\left(1.39^{+0.68}_{-0.45}\right) \times 10^{-11}$	4.06±0.08	$\left(9.2^{+11.2}_{-5.1}\right) \times 10^{4}$	1	1.26×10^{-13}
Lead (d=1.5 mm)	0.97±0.08	$2.88^{+4.88}_{-1.81} \times 10^{-11}$	4.92±0.57	$1.38^{+405.62}_{-1.375} \times 10^{8}$	1	8×10^{-13}
Tin (d=2 mm)	0.94±0.07	$7.24^{+9.76}_{-4.22} \times 10^{-11}$	6.59±0.28	$3.55^{+59.55}_{-3.35} \times 10^{17}$	1	3.15×10^{-13}
Silver (d=0.2 mm)	1	6.6×10^{-11}	Uncertain		1	2.95×10^{-11}

Table VI

Mechanisms of Harper - Dorn Creep

Mechanism	Relationship	A	Type of Mechanism	Appendix
Jogged Screw Dislocation (Harper, et al)	$\frac{\dot{\gamma}kT}{DGb} = 12\pi\rho bLj\,(\tau/G)$	$12\pi\rho bLj \sim 3.1\times10^{-10}$ $(Lj \approx b)$	Dislocation- Dominated (Screw)	A
Climb of Jogged Edge (Hirth and Lothe)	$\frac{\dot{\gamma}kT}{DGb} = \frac{12\pi\rho b^3}{Lj}\,(\tau/G)$	$\frac{12\pi\rho b^3}{Lj} \sim 1.54\times10^{-11}$ $(Lj \approx 20b)$	Dislocation-Dominated (Edge)	B
Subgrain Creep (Friedel)	$\frac{\dot{\gamma}kT}{DGb} = 14\left(\frac{b}{\delta}\right)^2\,(\tau/G)$	$14\left(\frac{b}{\delta}\right)^2 \sim 5.1\times10^{-13}$ $(\delta_{Average} \approx 1.5mm)$	Nabarro-Herring Type	C
Dynamic Balance (Barrett, et al)	$\frac{\dot{\gamma}kT}{DGb} = 3\rho_o b^2\delta_o(\tau/G)$	$3\rho_o b^2\delta_o \sim 2.4\times10^{-11}$ $(\delta_o = 10, \rho_o = 10^3 cm^{-2})$	Dislocation - Dominated	D
Climb of Saturated Dislocation (Present Thesis)	$\frac{\dot{\gamma}kT}{DGb} = \frac{-6\pi\rho b^2}{\ln\sqrt{\rho}b}(\tau/G)$	$\frac{-6\pi\rho b^2}{\ln\sqrt{\rho}b} \sim 1.21\times10^{-11}$	Dislocation- Dominated	E

XBL 7210-7123

FIGURE CAPTIONS

Fig. 1 Thermal activation process.

Fig. 2 Nabarro creep.

Fig. 3 Motion of jogged screw dislocations.

Fig. 4 Climb of edge dislocation.

Fig. 5 Viscous glide process.

Fig. 6a Idealized creep curve.

Fig. 6b Typical creep curves.

Fig. 7a Viscous glide vs climb in nickel-gold.

Fig. 7b Harper-Dorn data on pure aluminum.

Fig. 8 A typical stress-strain curve during differential strain-rate tests in Al-3% Mg. Inset shows the drawing of the double-shear type specimens.

Fig. 9 Creep machine.

Fig. 10 Plot of log $\dot{\gamma}$ vs log τ for Al-3% Mg at T=857°K indicating the two transitions.

Fig. 11 Schematic representation of the creep curves observed in the three regions.

Fig. 12 Typical intermittent-stress test in region III showing no or brief transients after reloading.

Fig. 13 Typical intermittent-stress test in Al-5% Mg depicting the observation of inverted primary creep after reloading.

Fig. 14 Intermittent-stress test in region II showing the existence of normal primary creep even after prior deformation.

Fig. 15 Stress law for viscous glide region.

Fig. 16a Arrhenius plot of log $\dot{\gamma}G^2T$ vs $\frac{1000}{T}$ in region III. Slope of the line gives a value of 33.1 ± 2.2 kcal/mole for the activation energy for creep.

Fig. 16b Plot of log $\dot{\gamma}G^3T$ vs $\frac{1000}{T}$ in region II at a constant stress. The value for the activation energy for creep was found to be 31.7 ± 0.5 kcal/mole.

Fig. 16c Plot of log $\frac{\dot{\gamma}T}{\tau}$ vs $\frac{1000}{T}$ in region III. The slope of the line yields a value of 35.7 kcal/mole for the activation energy for creep.

Fig. 17 Plot of log $\frac{\dot{\gamma}kT}{DGb}$ vs log τ/G depicting the three regions with slopes 3.2, 4.1 and 0.9 indicating the transitions from glide to climb and climb to Newtonian viscous creep mechanisms. Data of Harper and Dorn on pure aluminum are included for comparison.

Fig. 18 Plot of log $\frac{\dot{\gamma}kT}{DGb}$ vs log τ/G for pure aluminum. Data of Harper and Dorn are included for comparison.

Fig. 19 The effect of stress on the steady-state creep rate of lead.

Fig. 20 The effect of stress on the steady-state creep rate of tin.

Fig. 21 Typical creep curves for lead observed in high-stress region (τ = 46.4 psi, T = 554°K) and low-stress region (τ = 7.3 psi, T = 554°K).

Fig. 22 Typical creep curves for tin observed in high-stress region (τ = 126 psi, T = 461°K) and low-stress region (τ = 10.8 psi, T = 495°K).

Fig. 23 Effect of temperature on the steady-state creep rate of lead and tin in high stress region.

Fig. 24 Plot of log $\frac{\dot{\gamma}kT}{DGb}$ vs log τ/G for lead and tin, indicating the transition from climb to Harper-Dorn mechanism.

Fig. 25 Data on creep of lead and tin compared to creep behavior of aluminum and aluminum-3% magnesium.

Fig. 26 Data of three investigations of the low-stress, high-temperature creep of coarse-grained aluminum.

Fig. 27 High-temperature, low-stress data on silver.

Fig. 28 Data on metals which shows apparent Harper-Dorn creep.

Fig. 29 Stress dependence of dislocation density.

Fig. 30 The data of Burton on the creep of fine-grained foils of aluminum in vacuum (data points) compared to creep behavior of aluminum in bulk (solid line).

Fig. 31 Nabarro creep vs. Harper-Dorn creep.

Fig. 32 Diffusivity of pure aluminum.

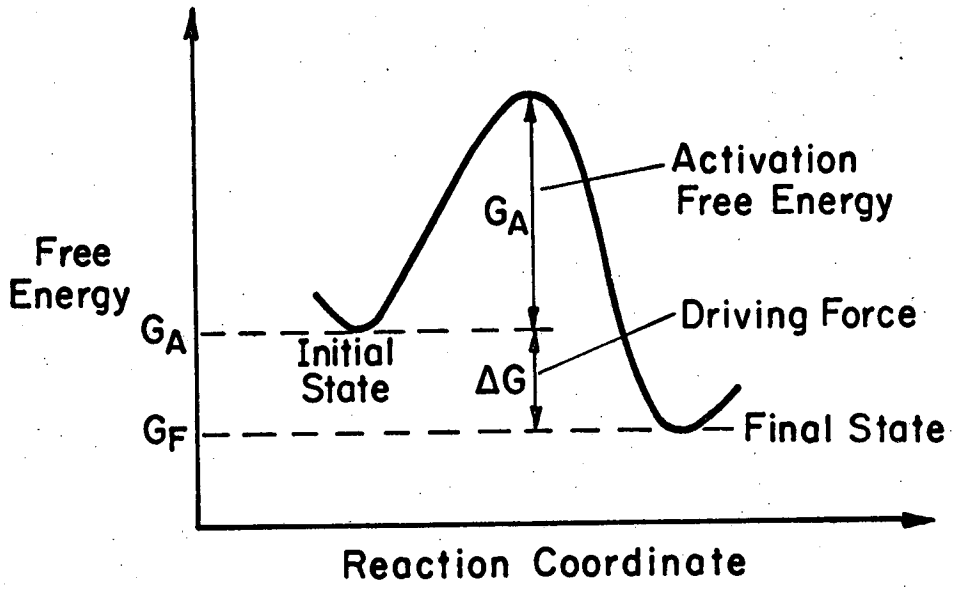

Thermally Activated Process

$$\dot{\gamma}_i = f_i^+ \{\tau, T, st\}\, e^{-\frac{h_i^+(\tau, T, st)}{kT}} - f_i^- \{\tau, T, st\}\, e^{-\frac{h_i^-(\tau, T, st)}{kT}}$$

Forward Rate — Reverse Rate

Processes which are sequential: Slowest controls

Processes which are parallel: Sum of all contributions

XBL724-6175

Fig. 1

(a) STRESS-DIRECTED DIFFUSION OF VACANCIES IN POLYCRYSTALS

Nabarro Creep

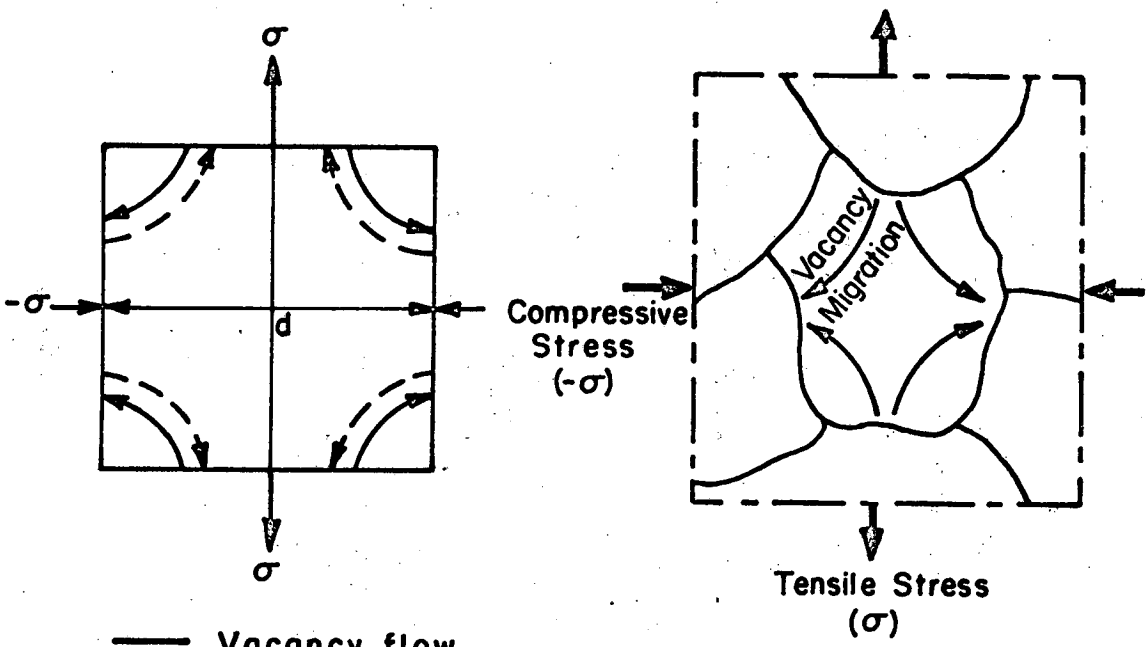

—— Vacancy flow

– – – Atom flow

$$\dot{\gamma} = A_N \frac{b^2}{d^2} \frac{\tau}{kT} D$$

$A_N = 14 - 21$

XBL724-6170

Fig. 2

(b) CREEP DUE TO THE MOTION OF JOGGED SCREW DISLOCATIONS

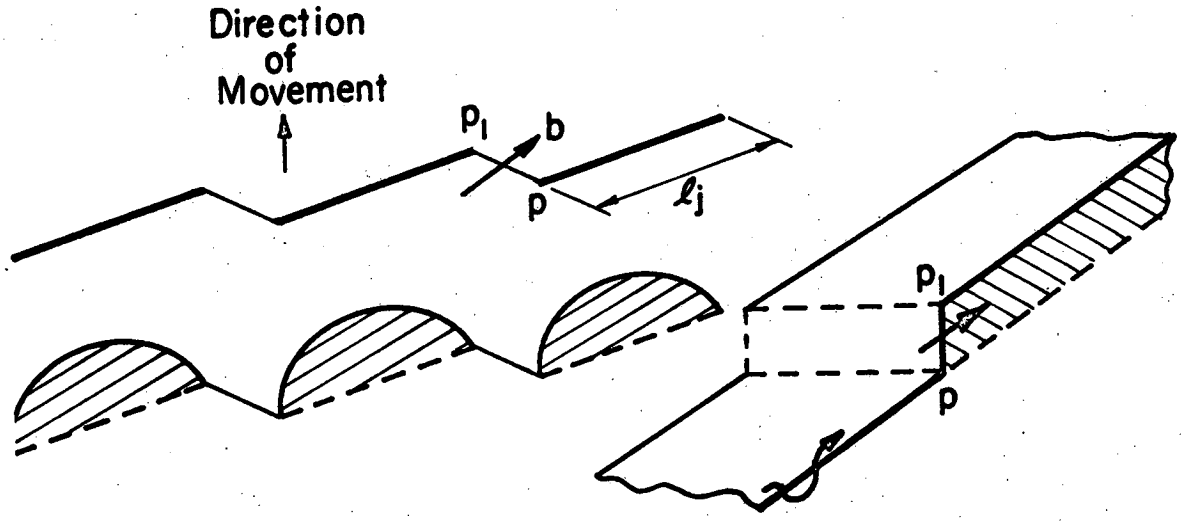

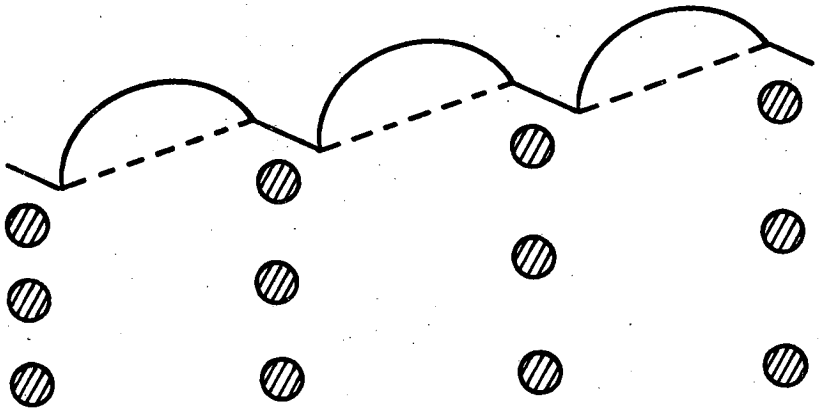

Vacancy has to Diffuse Away

$$\dot{\gamma} = 6\rho_s D\,(e^{\tau \ell_j b^2/kT} - 1)$$

XBL724-6171

Fig. 3

(a) CREEP AS A RESULT OF CLIMB OF EDGE DISLOCATIONS

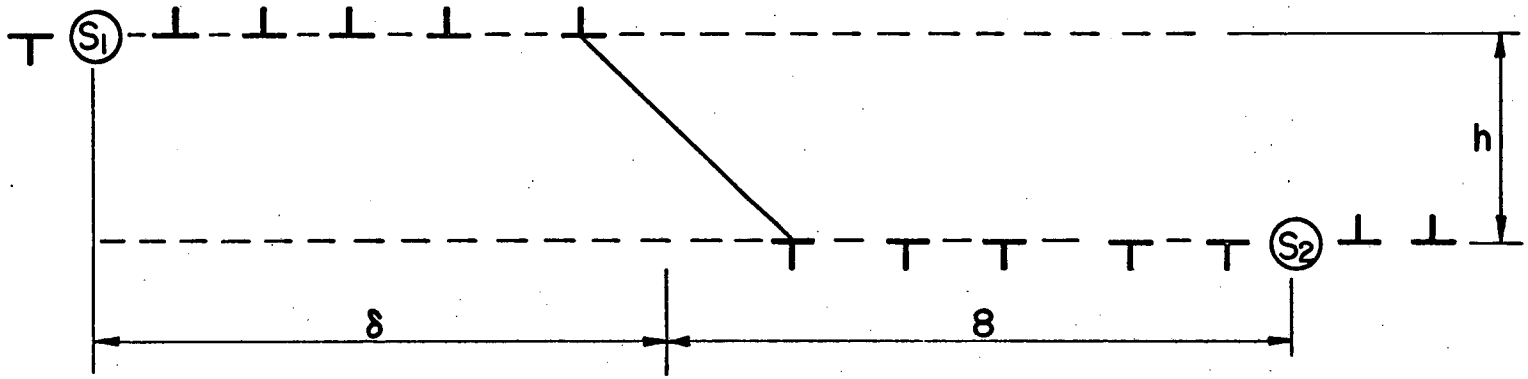

$$\dot{\gamma} = A_c \frac{\tau^5}{G^4} \left(\frac{1}{kT}\right) D$$

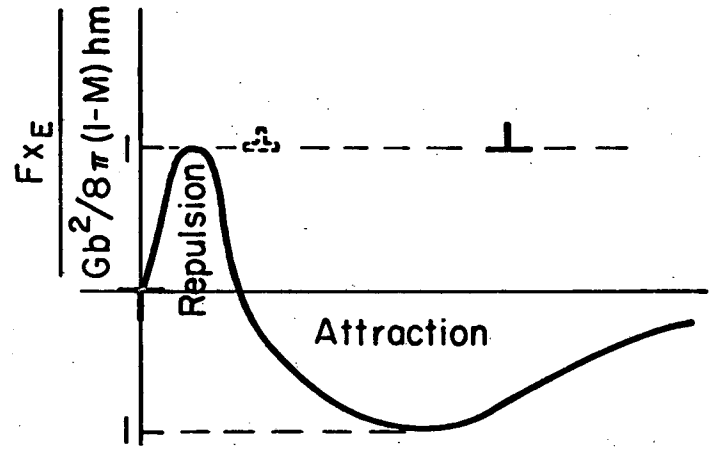

XBL724-6172

Fig. 4

(d) SOLUTE ATOM DIFFUSIONAL PROCESS AND VISCOUS DRAG

$$\dot{\gamma} = 6 \cdot \frac{D}{kT} \frac{\tau^3}{G^2}$$

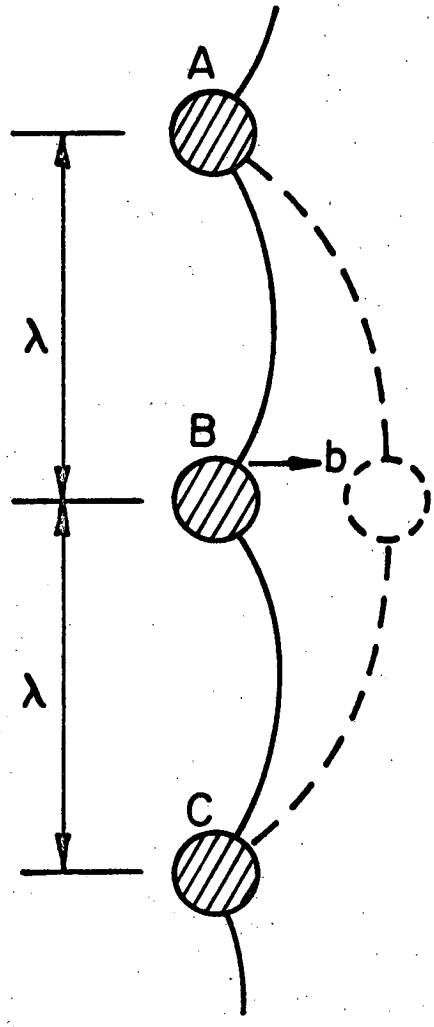

XBL724-6173

Fig. 5

CREEP CURVES

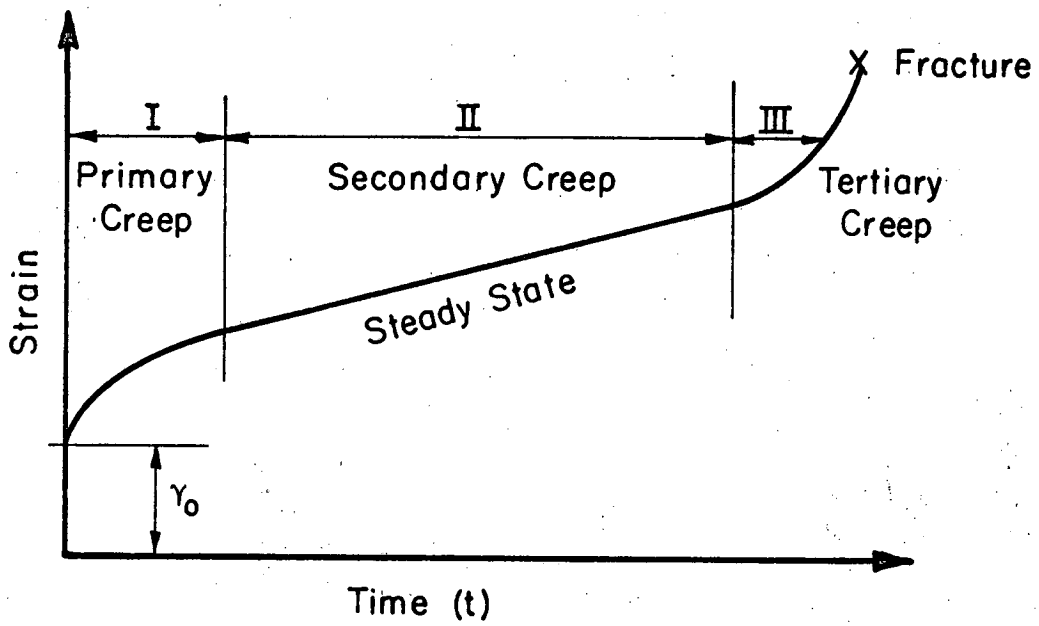

Fig. 6a

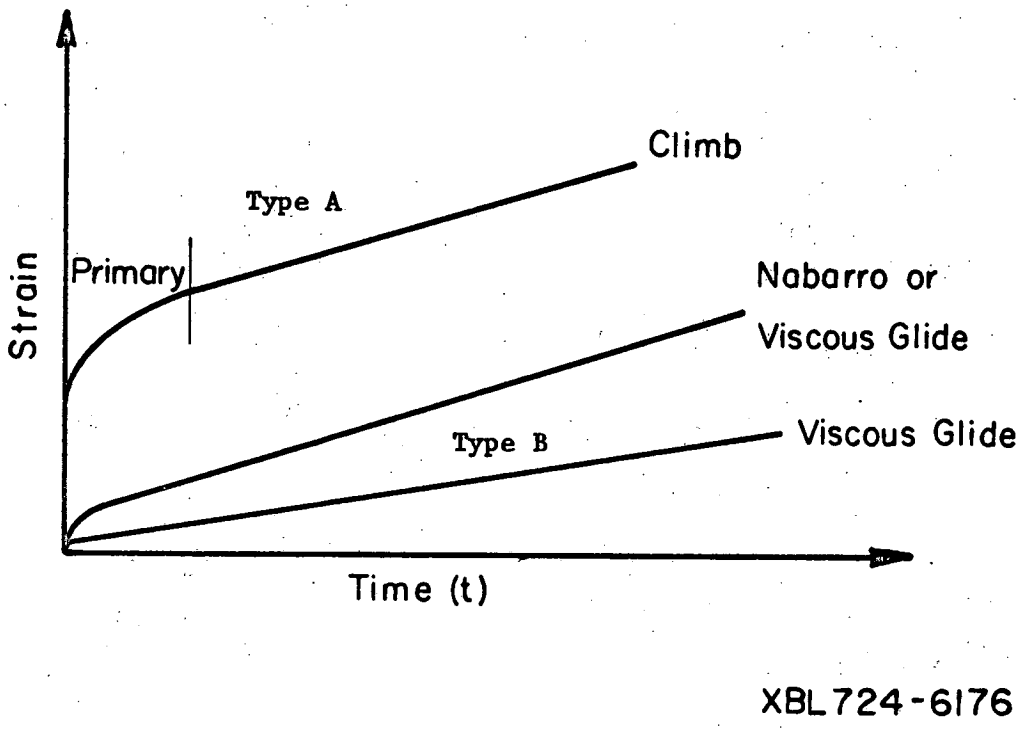

Fig. 6b

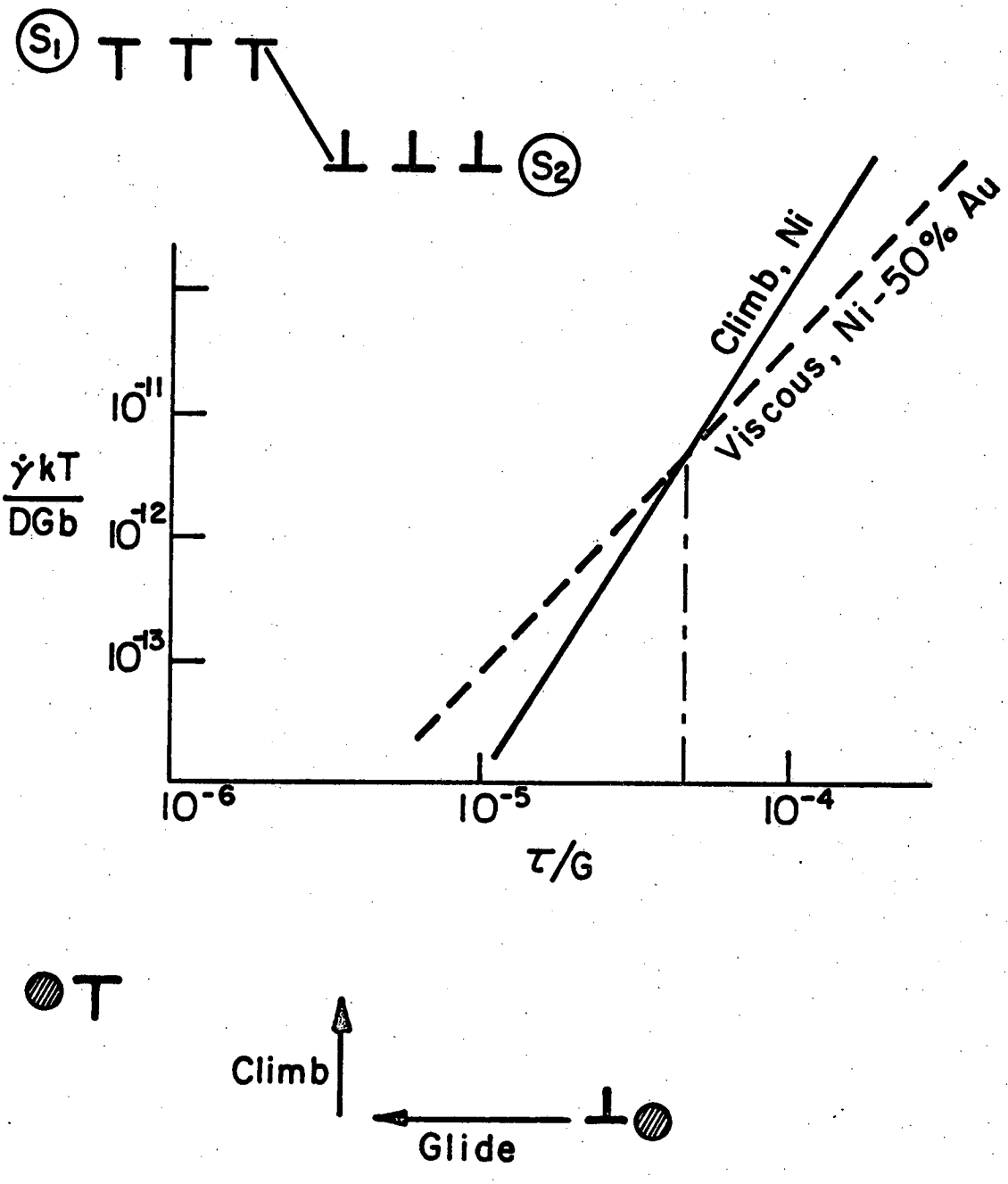

XBL724-6174

Fig. 7a

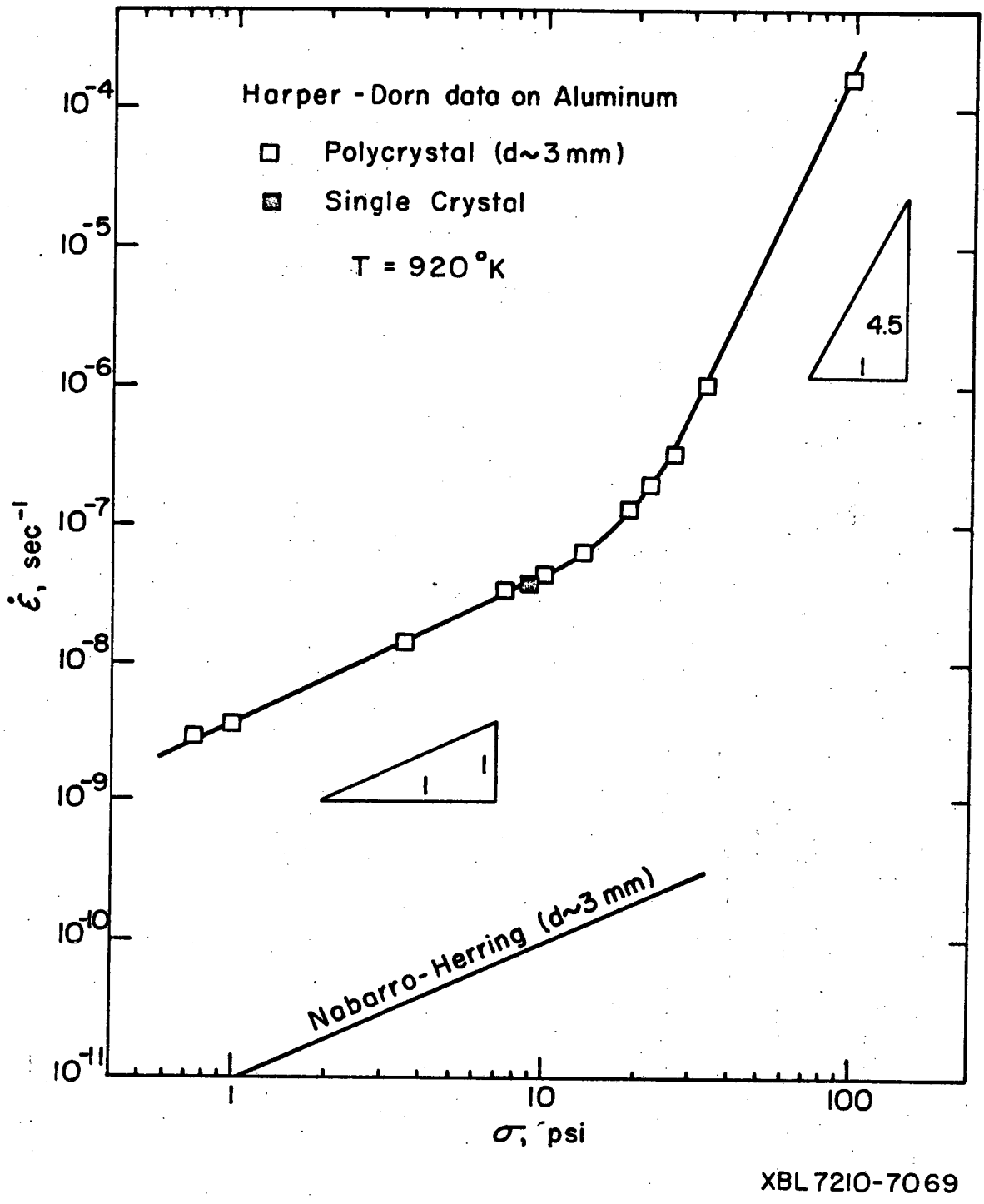
Harper - Dorn data on Aluminum
Polycrystal (d~3 mm)
Single Crystal
T = 920°K
4.5
1
1
1
Nabarro-Herring (d~3 mm)
10^{-4}
10^{-5}
10^{-6}
10^{-7}
10^{-8}
10^{-9}
10^{-10}
10^{-11}
$\dot{\varepsilon}$, sec^{-1}
1
10
100
σ, psi
XBL 7210-7069

Fig. 7b

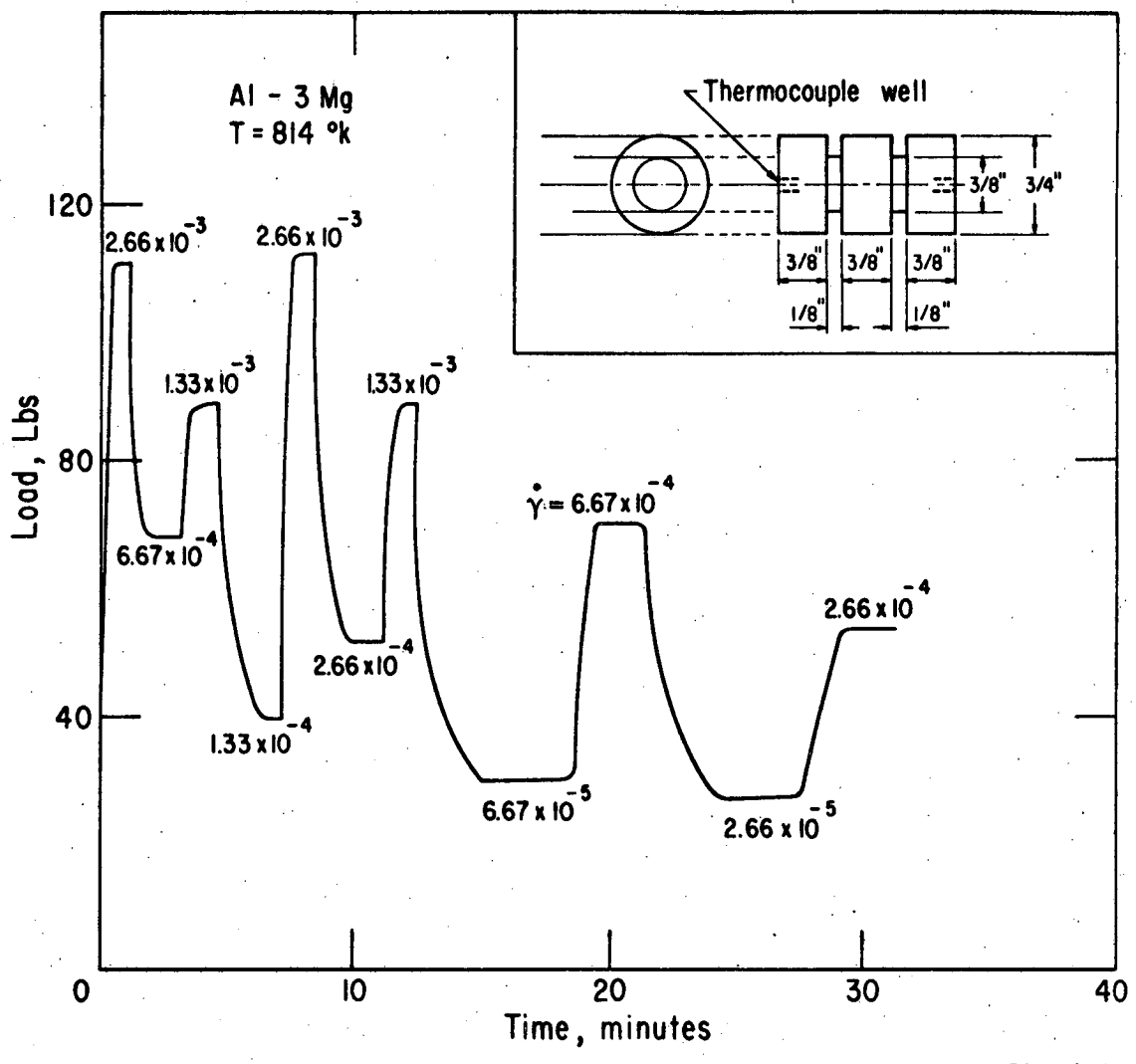
Al - 3 Mg
T = 814 °k
Thermocouple well
3/8"
3/4"
3/8"
3/8"
3/8"
1/8"
1/8"
120
80
40
Load, Lbs
2.66 x 10^-3
2.66 x 10^-3
1.33 x 10^-3
1.33 x 10^-3
6.67 x 10^-4
1.33 x 10^-4
2.66 x 10^-4
γ̇ = 6.67 x 10^-4
2.66 x 10^-4
6.67 x 10^-5
2.66 x 10^-5
0
10
20
30
40
Time, minutes
XBL 721 - 5929

Fig. 8

Instron-machine $\dot{\gamma} = 10^{-3} - 10^{-5}\ sec^{-1}$

Creep-machine $\dot{\gamma} = 10^{-4} - 10^{-9}\ sec^{-1}$

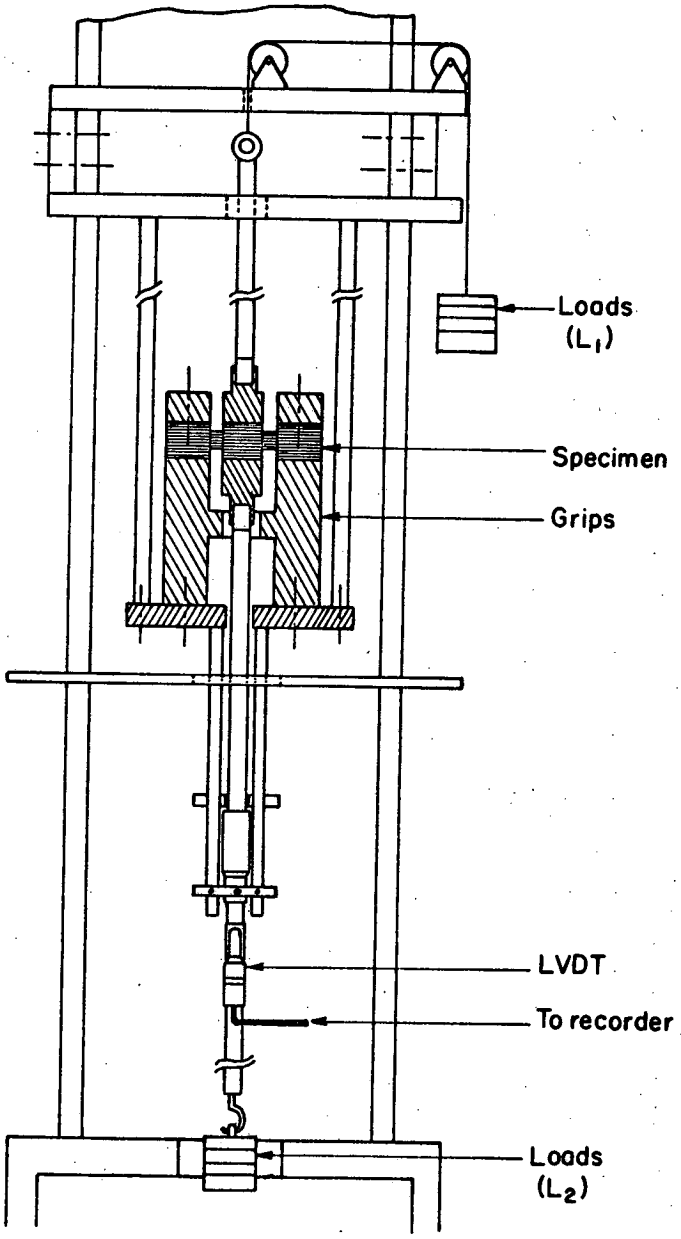

XBL727-6475

Fig. 9

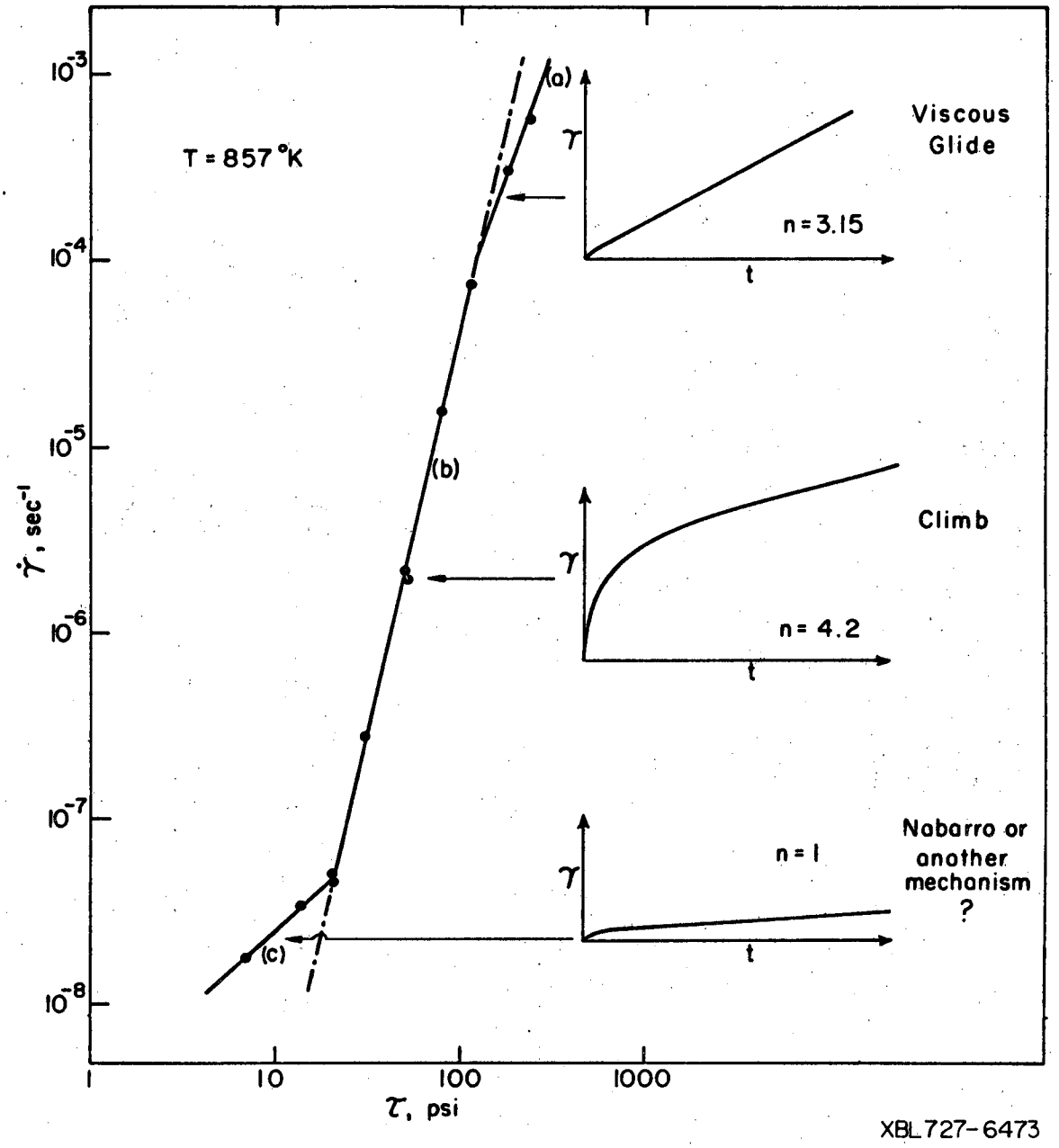

Fig. 10

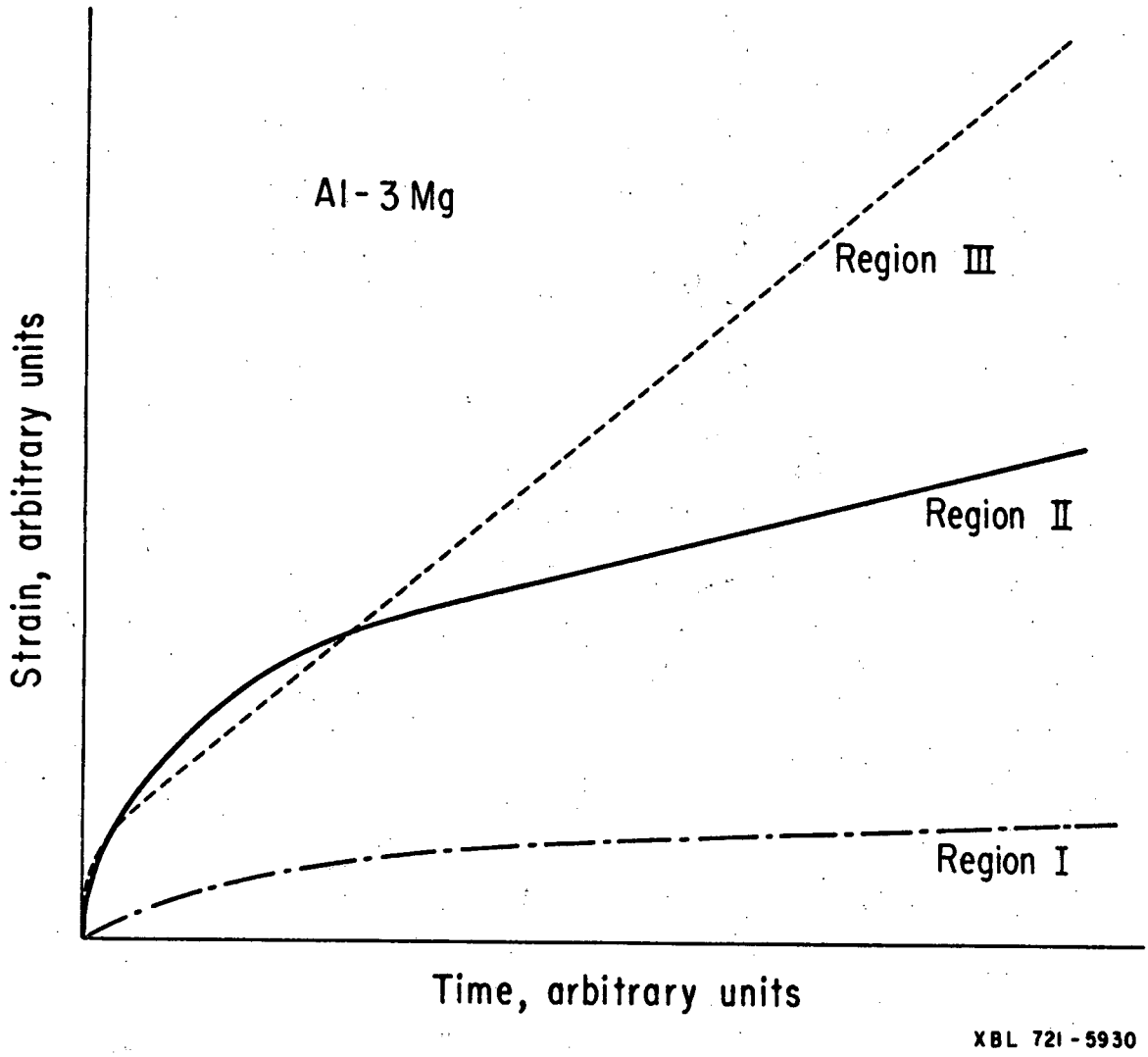
Al - 3 Mg
Region III
Region II
Region I
Strain, arbitrary units
Time, arbitrary units
XBL 721-5930

Fig. 11

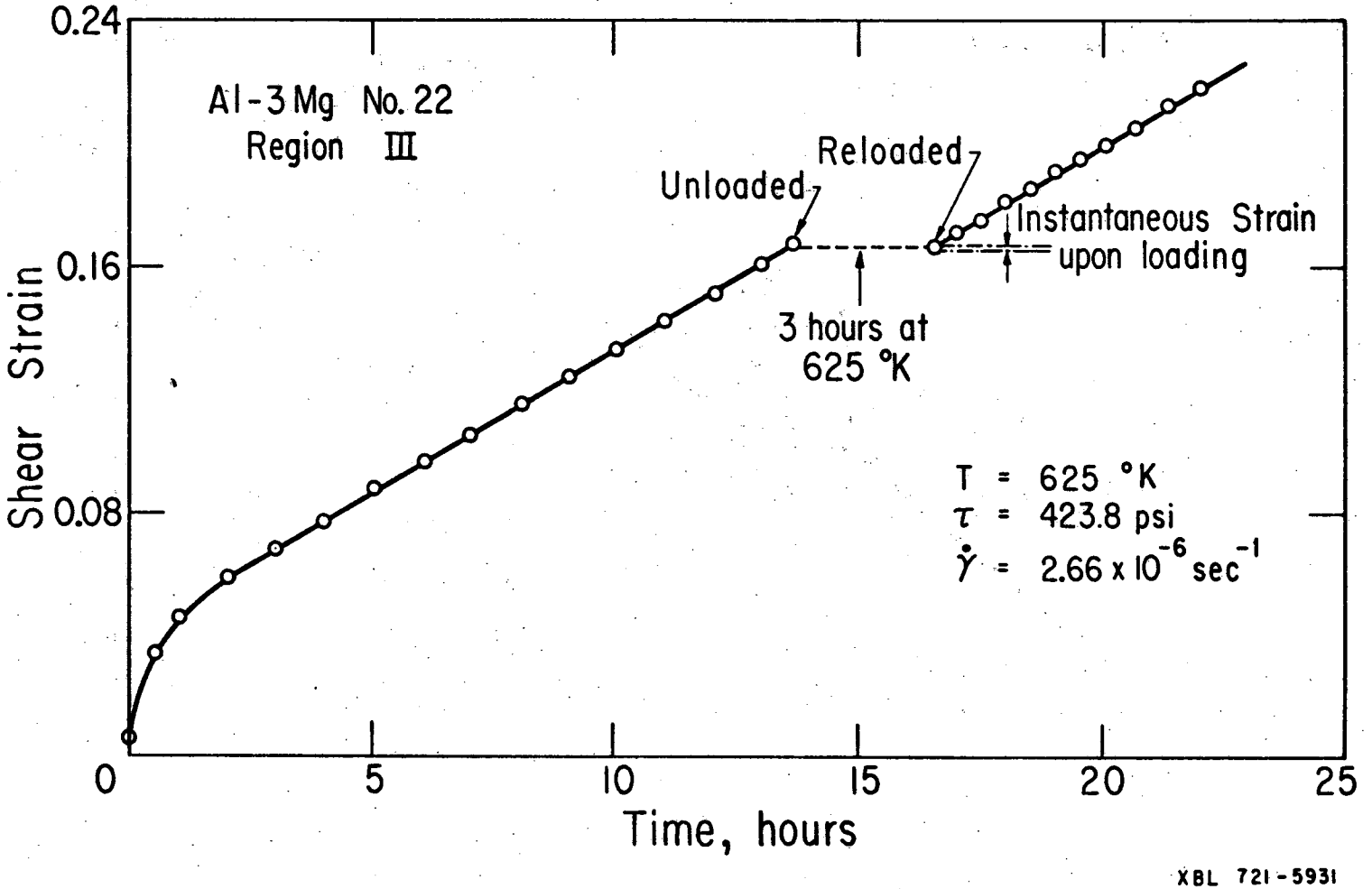
0.24
0.16
0.08
0
Shear Strain
Al-3 Mg No. 22
Region III
Unloaded
Reloaded
Instantaneous Strain
upon loading
3 hours at
625 °K
T = 625 °K
τ = 423.8 psi
γ̇ = 2.66 x 10^-6 sec^-1
0
5
10
15
20
25
Time, hours
XBL 721-5931

Fig. 12

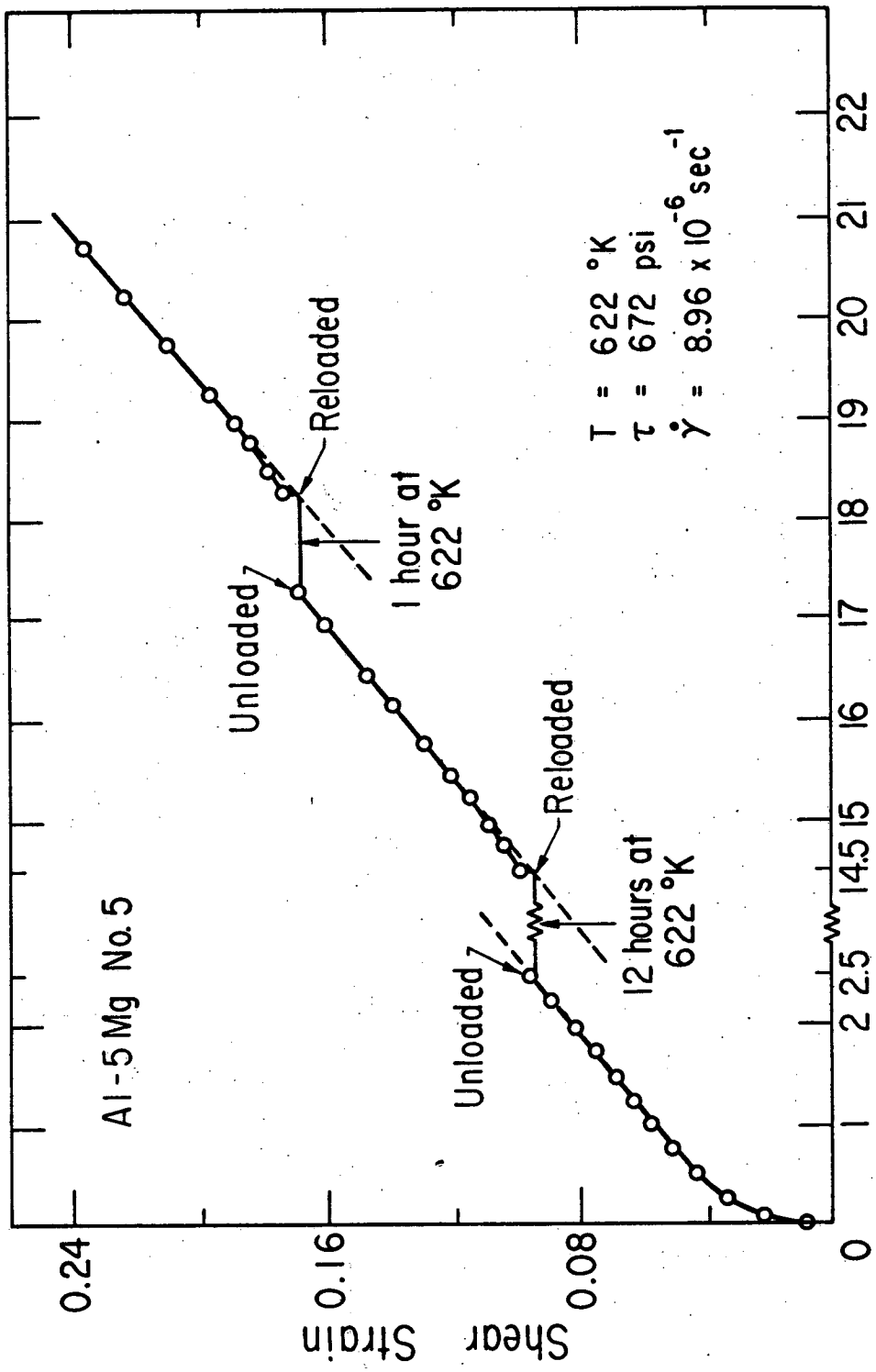

XBL 721-5927

Fig. 13

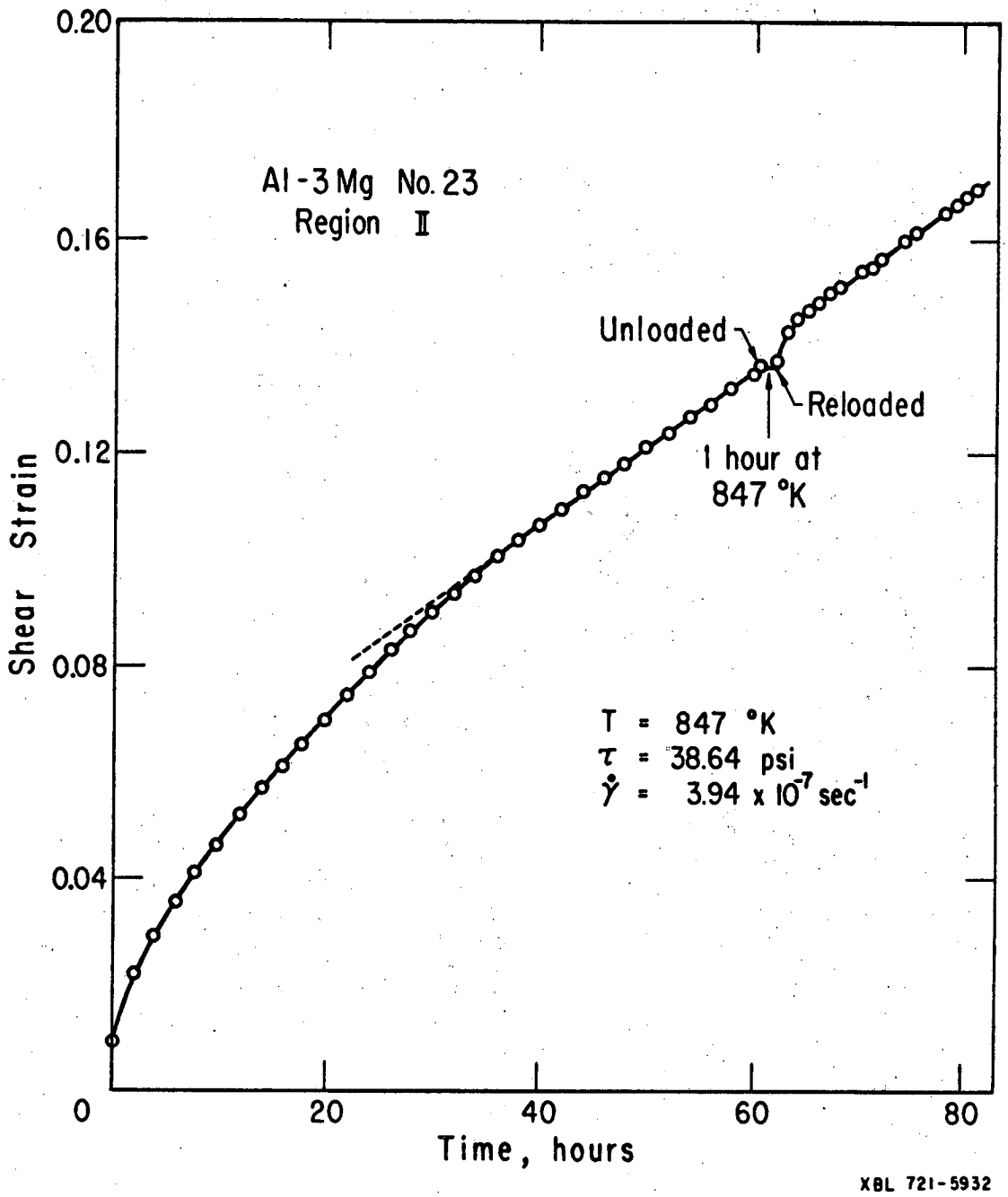
Al - 3 Mg No. 23
Region II
Unloaded
Reloaded
1 hour at
847 °K
T = 847 °K
τ = 38.64 psi
γ̇ = 3.94 x 10⁻⁷ sec⁻¹
Shear Strain
0.20
0.16
0.12
0.08
0.04
0
20
40
60
80
Time, hours
XBL 721-5932

Fig. 14

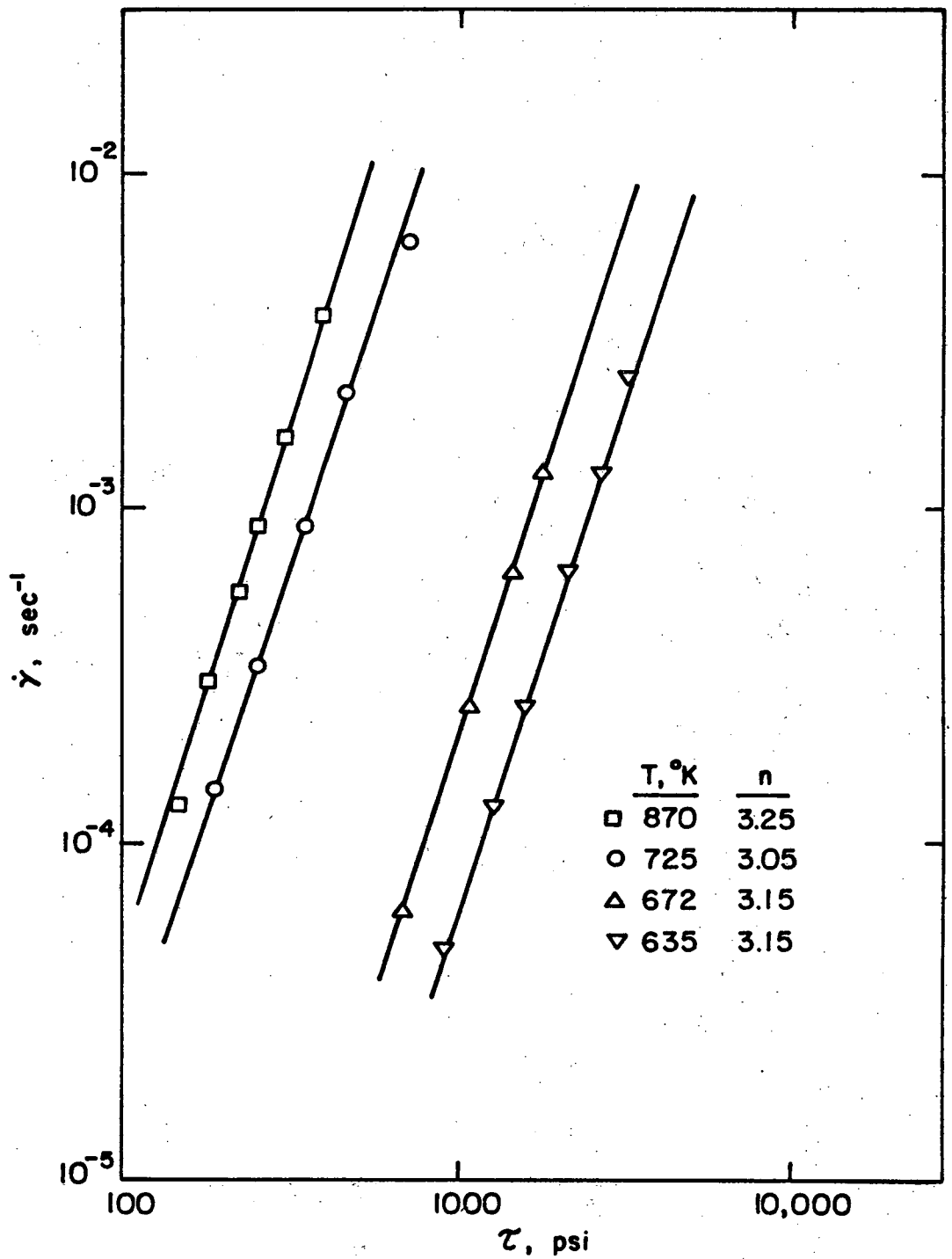
10^{-2}
10^{-3}
10^{-4}
10^{-5}
$\dot{\gamma}$, sec^{-1}
100
1000
10,000
τ, psi
T, °K
n
870
3.25
725
3.05
672
3.15
635
3.15
XBL 727-6474

Fig. 15

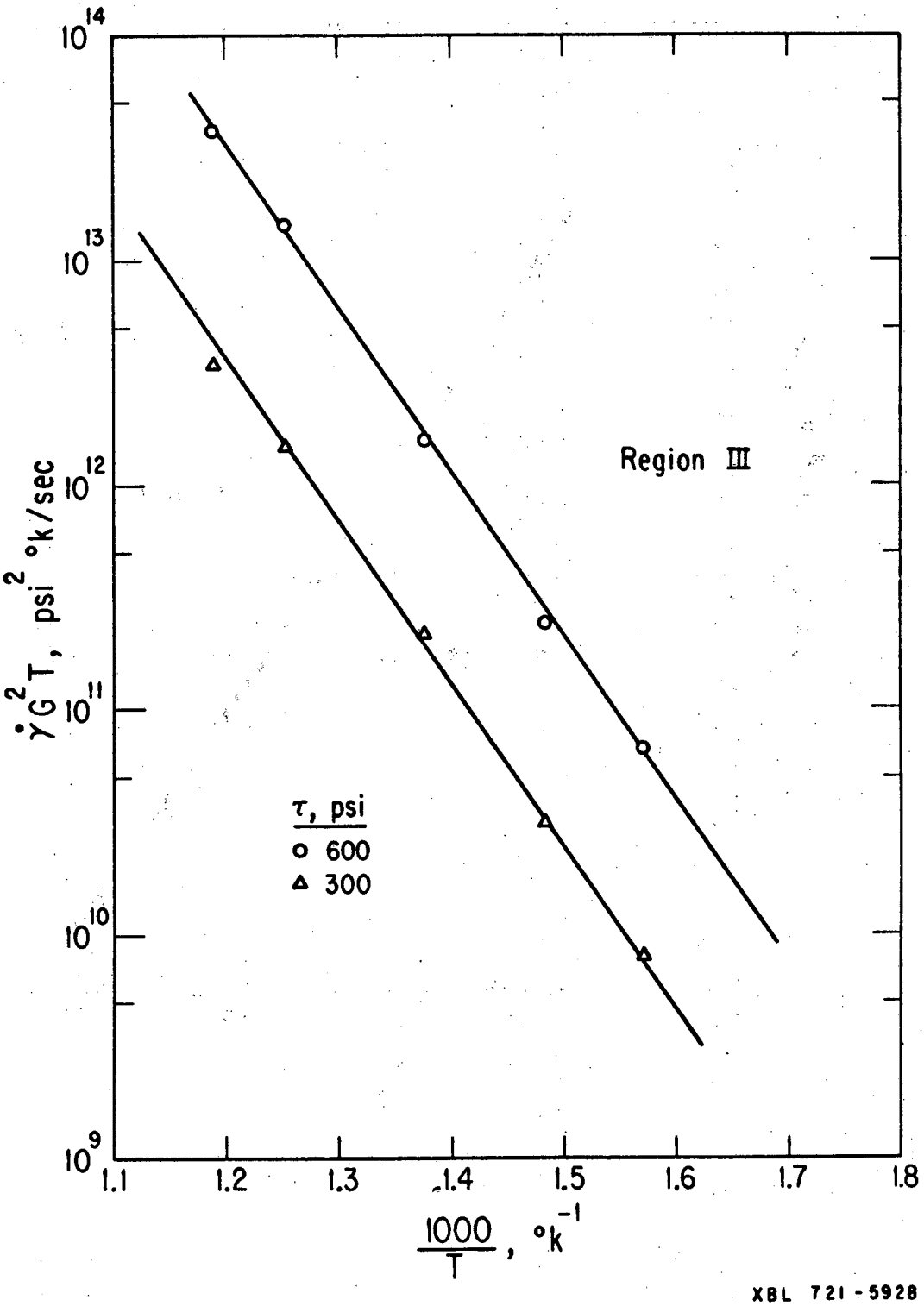
10^{14}
10^{13}
10^{12}
10^{11}
10^{10}
10^{9}
$\dot{\gamma}_G^2 T$, psi^2 °k/sec
Region III
τ, psi
o 600
Δ 300
1.1
1.2
1.3
1.4
1.5
1.6
1.7
1.8
$\frac{1000}{T}$, °k^{-1}
XBL 721-5928

Fig. 16a

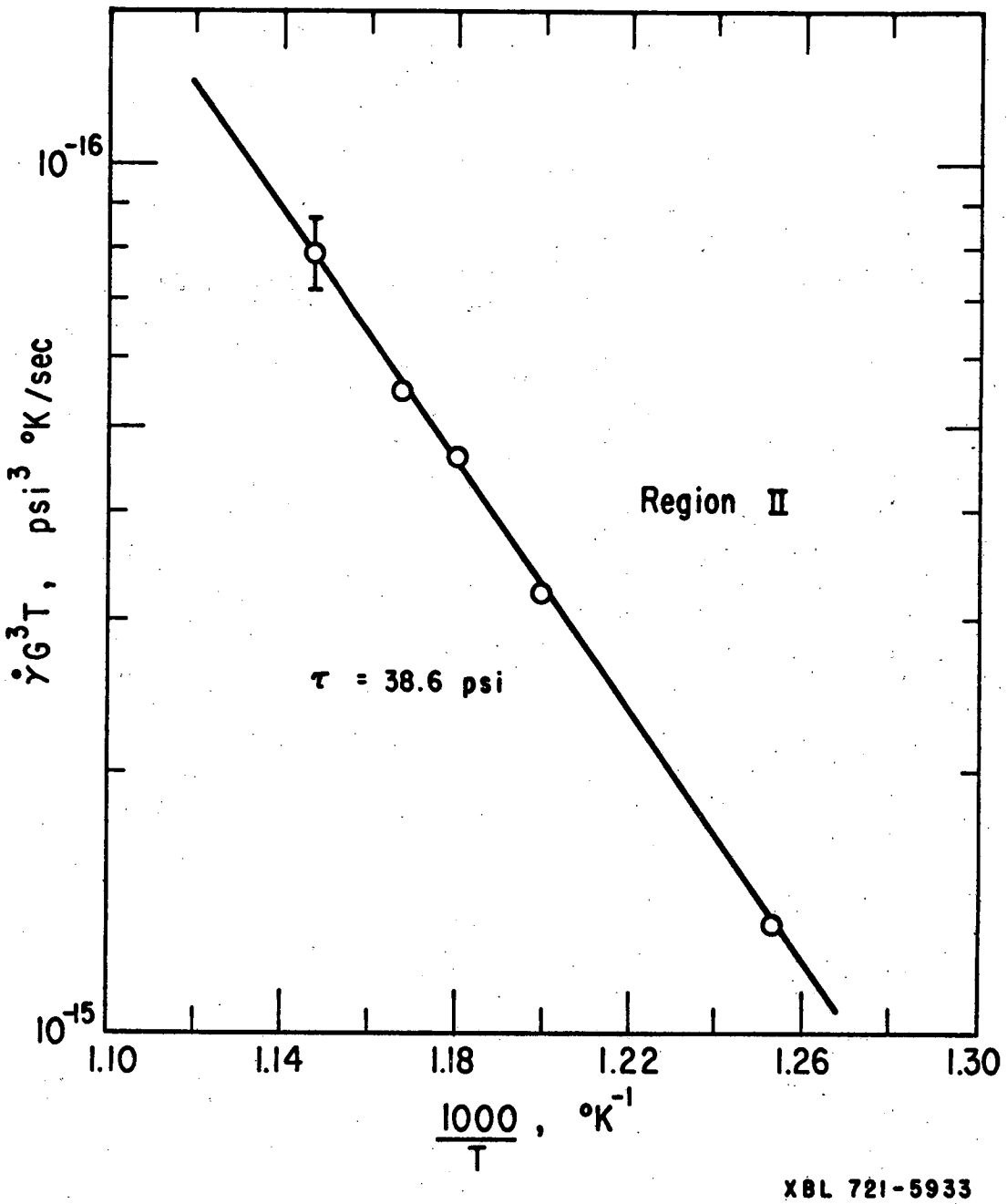
10^{-16}
10^{-15}
$\dot{\gamma}_G^3 T$, psi^3 °K/sec
Region II
τ = 38.6 psi
1.10
1.14
1.18
1.22
1.26
1.30
$\frac{1000}{T}$, °K^{-1}
XBL 721-5933

Fig. 16b

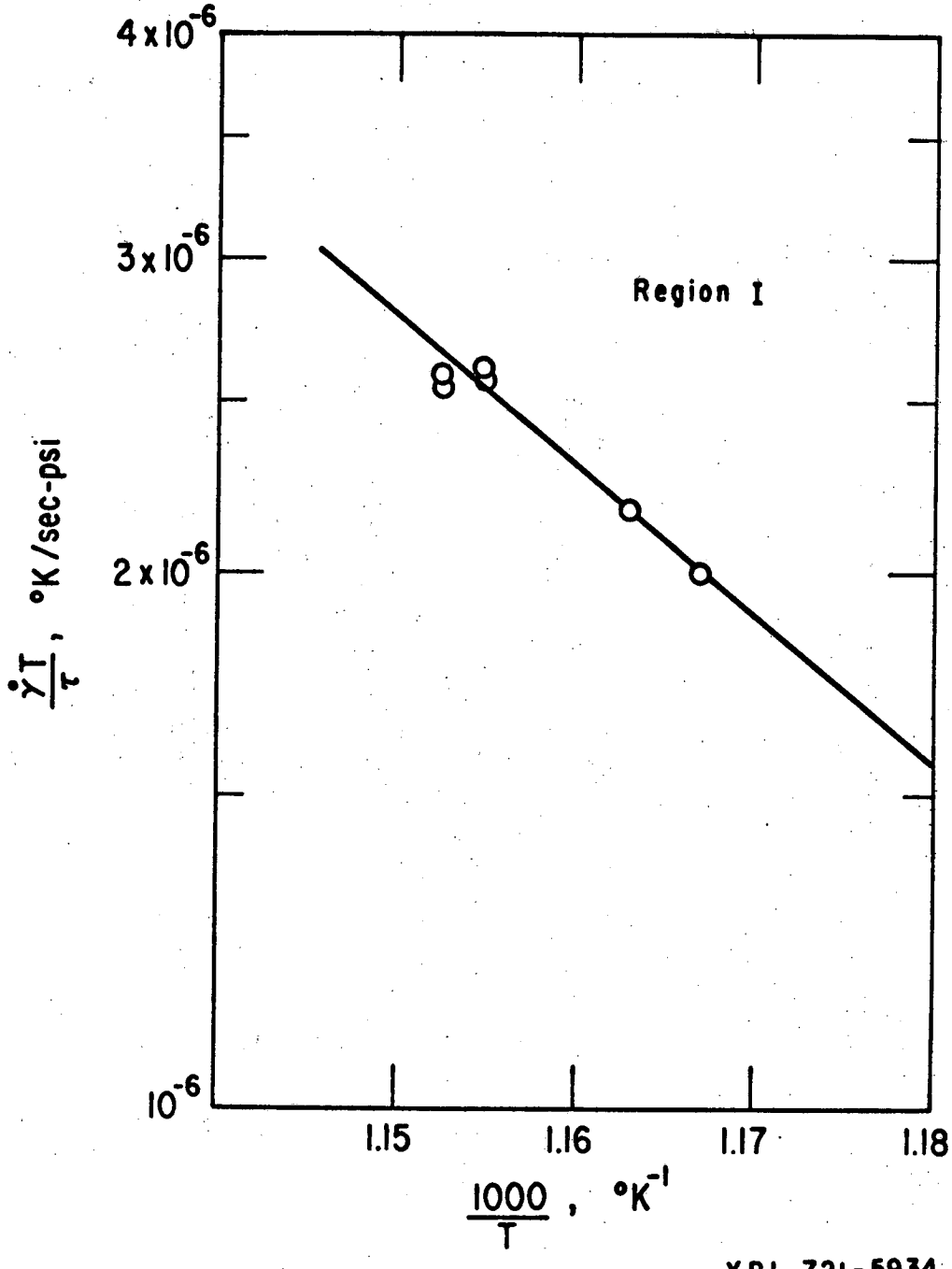
4x10^-6
3x10^-6
2x10^-6
10^-6
Region I
γ̇T/τ, °K/sec-psi
1.15
1.16
1.17
1.18
1000/T, °K^-1
XBL 721-5934

Fig. 16c

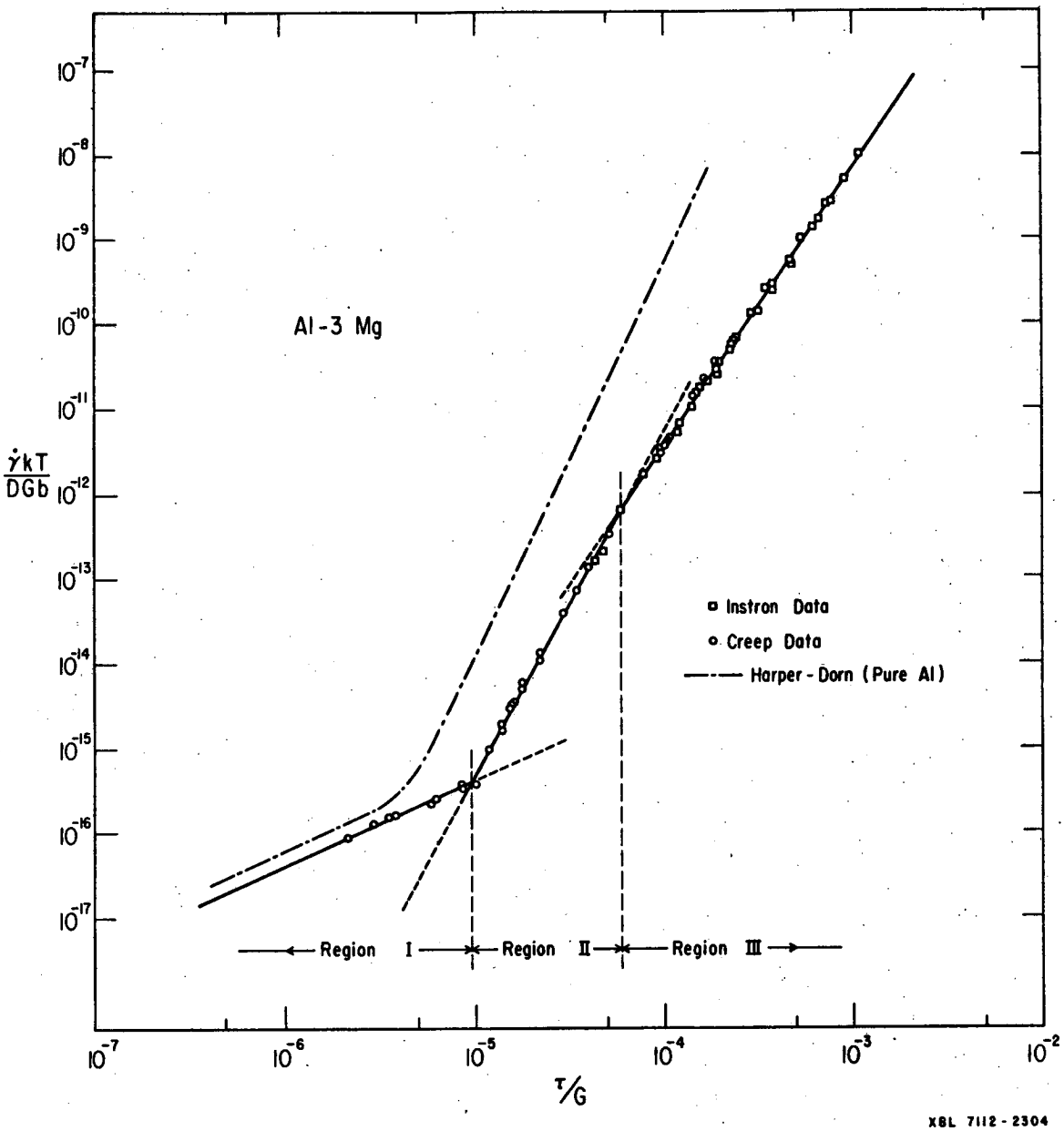
Al - 3 Mg
Instron Data
Creep Data
Harper - Dorn (Pure Al)
Region I
Region II
Region III
$\frac{\dot{\gamma}kT}{DGb}$
τ/G
10^{-7}
10^{-8}
10^{-9}
10^{-10}
10^{-11}
10^{-12}
10^{-13}
10^{-14}
10^{-15}
10^{-16}
10^{-17}
10^{-7}
10^{-6}
10^{-5}
10^{-4}
10^{-3}
10^{-2}
XBL 7112 - 2304

Fig. 17

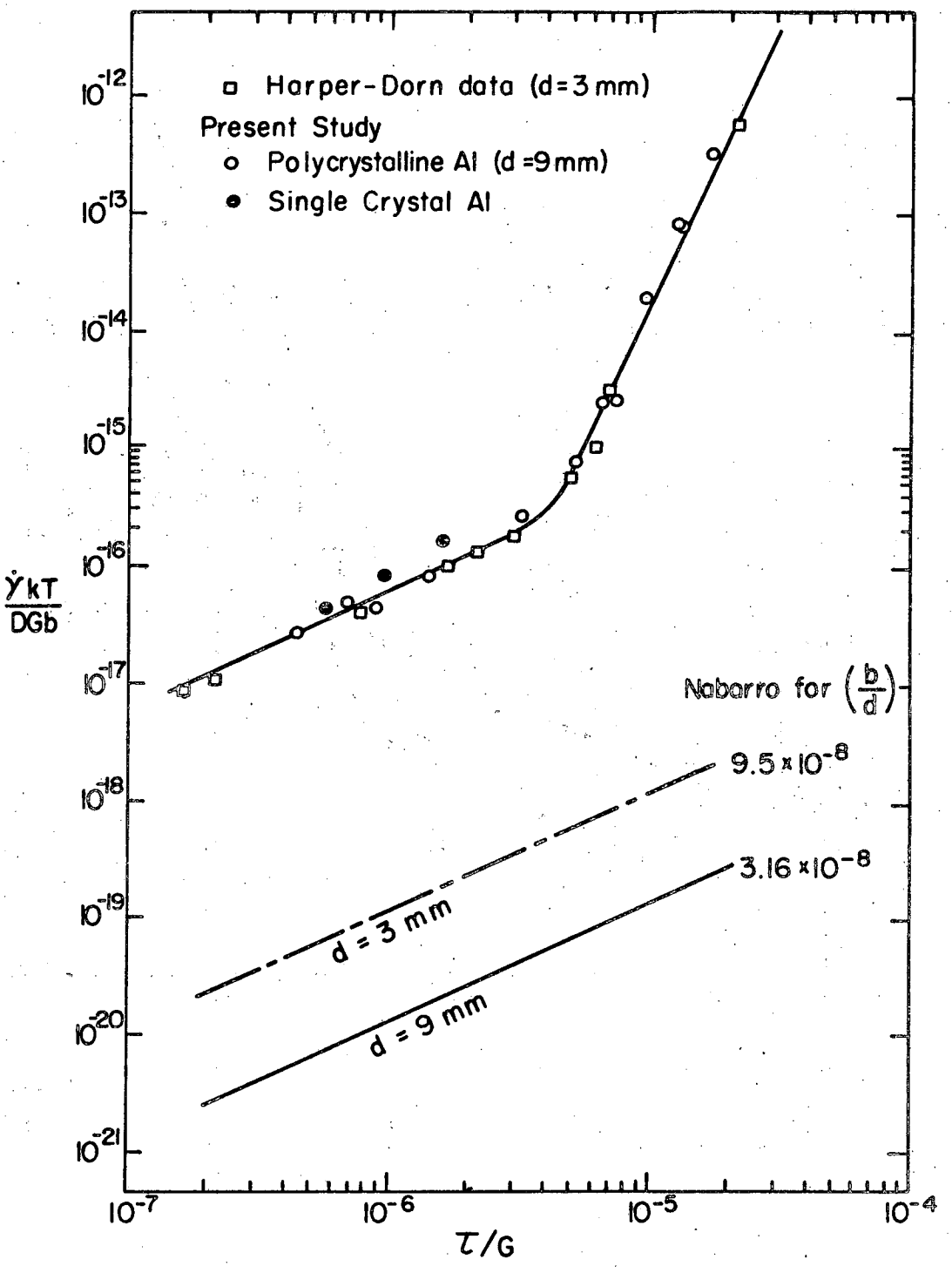

XBL724-6178B

Fig. 18

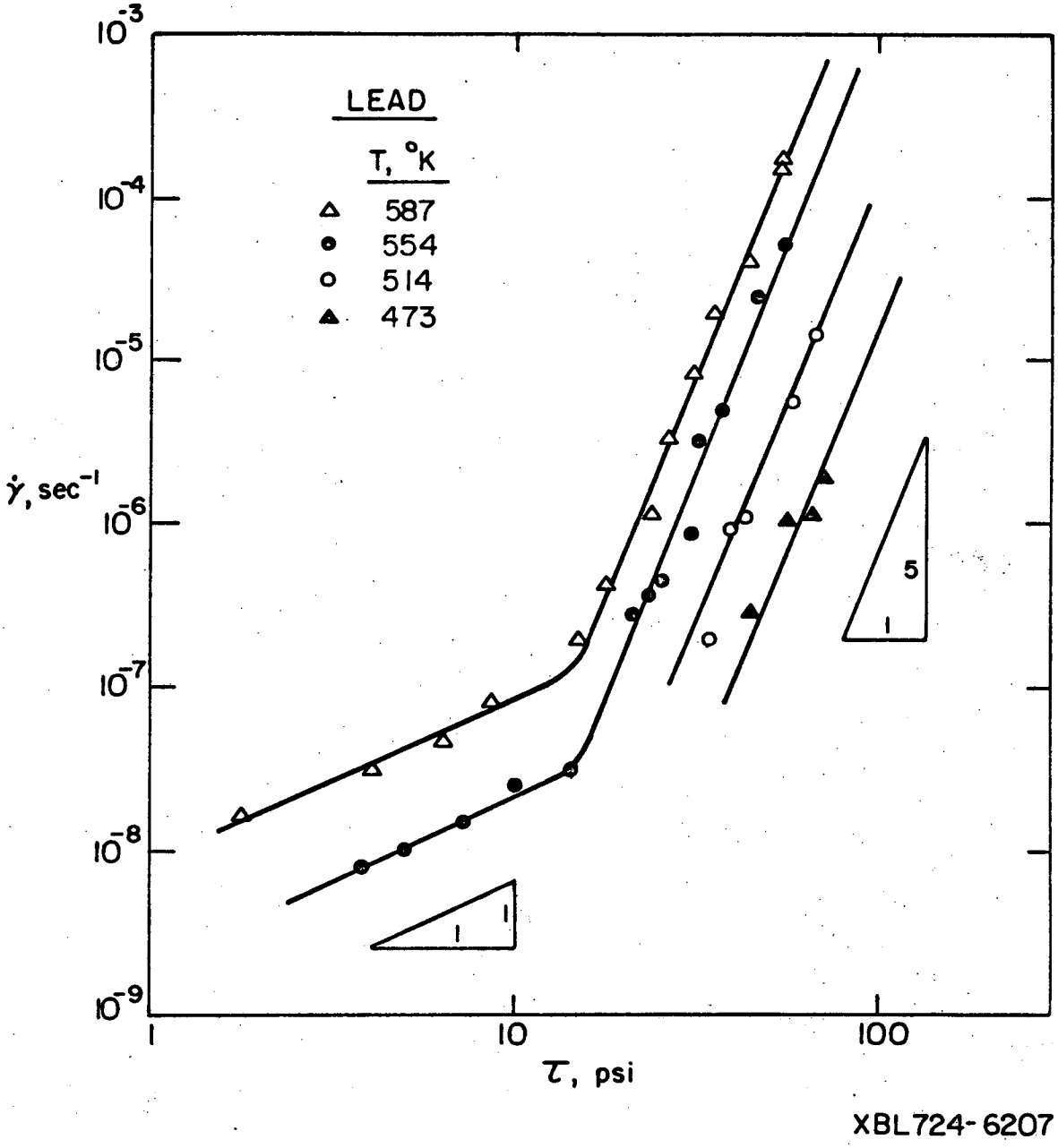
LEAD
T, °K
587
554
514
473
10^{-3}
10^{-4}
10^{-5}
10^{-6}
10^{-7}
10^{-8}
10^{-9}
$\dot{\gamma}$, sec^{-1}
1
10
100
τ, psi
5
1
1
1
XBL724-6207

Fig. 19

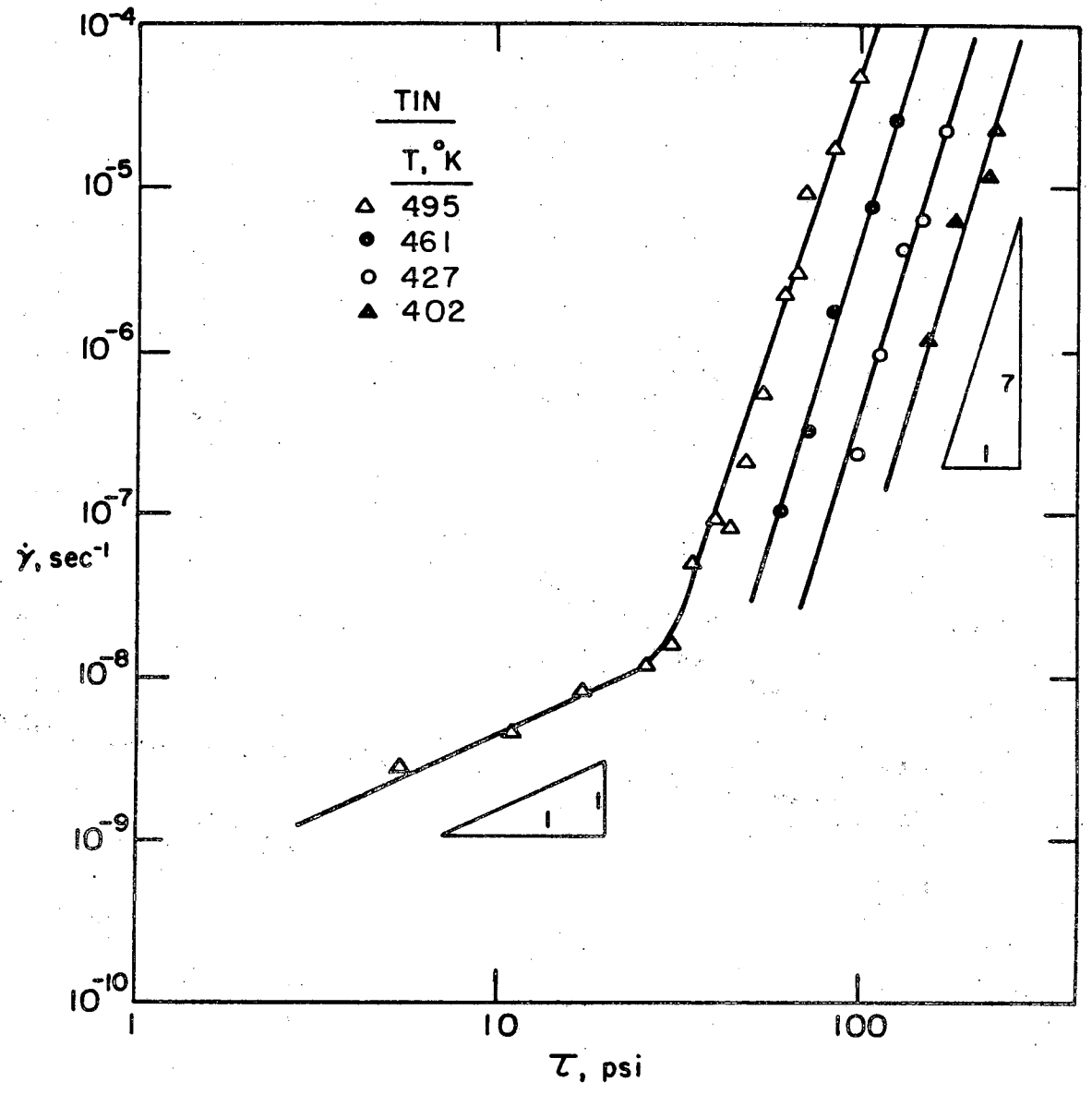
TIN
T, °K
495
461
427
402
7
1
1
1
10^{-4}
10^{-5}
10^{-6}
10^{-7}
10^{-8}
10^{-9}
10^{-10}
$\dot{\gamma}$, sec^{-1}
1
10
100
τ, psi
XBL724-6208

Fig. 20

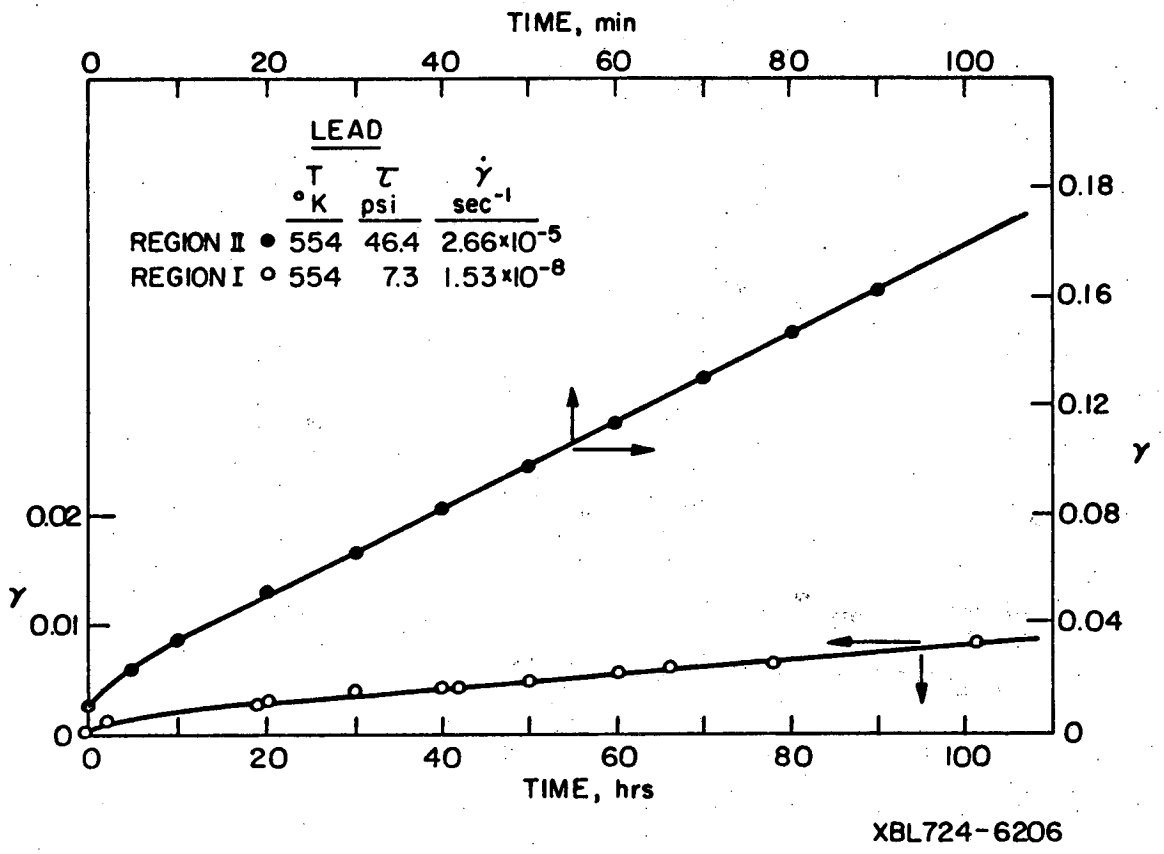
TIME, min
0
20
40
60
80
100
LEAD
T °K
τ psi
γ̇ sec⁻¹
REGION II ● 554 46.4 2.66×10⁻⁵
REGION I ○ 554 7.3 1.53×10⁻⁸
0.18
0.16
0.12
γ
0.08
0.02
γ
0.01
0.04
0
0
TIME, hrs
XBL724-6206

Fig. 21

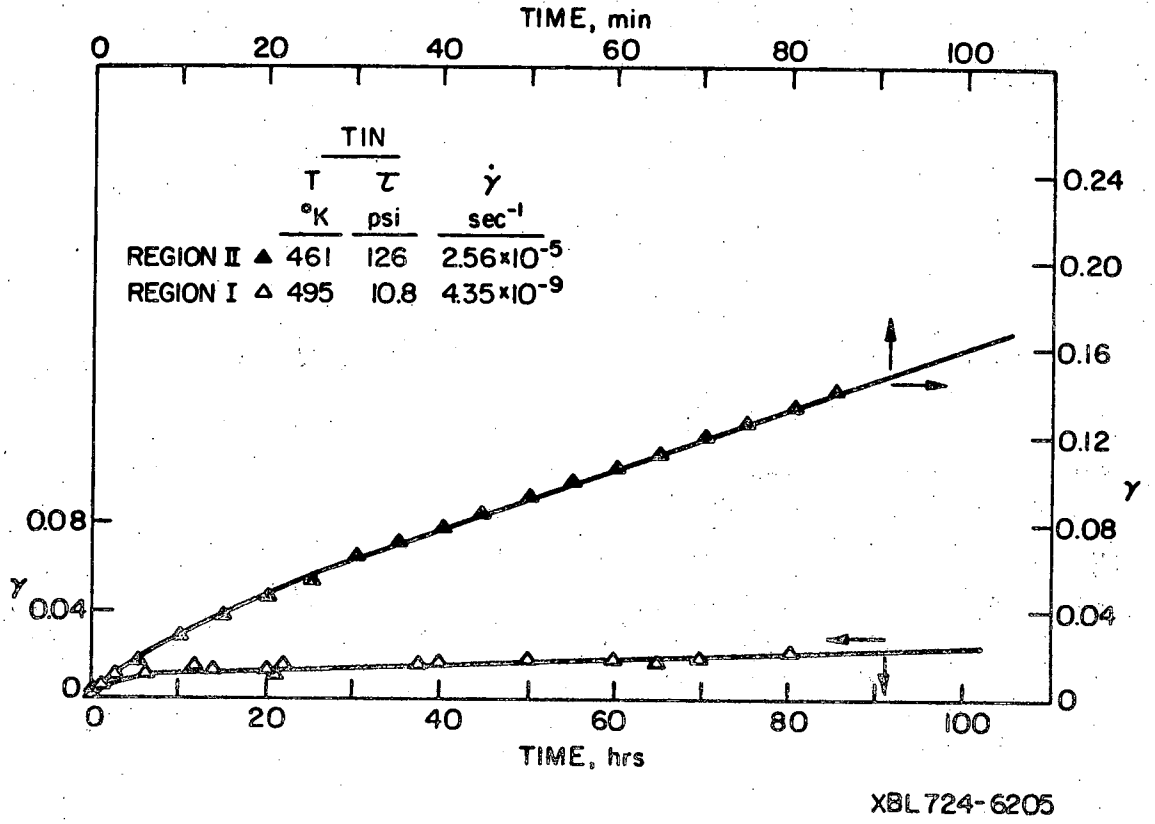
TIME, min
0
20
40
60
80
100
TIN
T °K
τ psi
γ̇ sec⁻¹
REGION II ▲ 461 126 2.56×10⁻⁵
REGION I △ 495 10.8 4.35×10⁻⁹
0.24
0.20
0.16
0.12
0.08
0.04
0
γ
TIME, hrs
XBL724-6205

Fig. 22

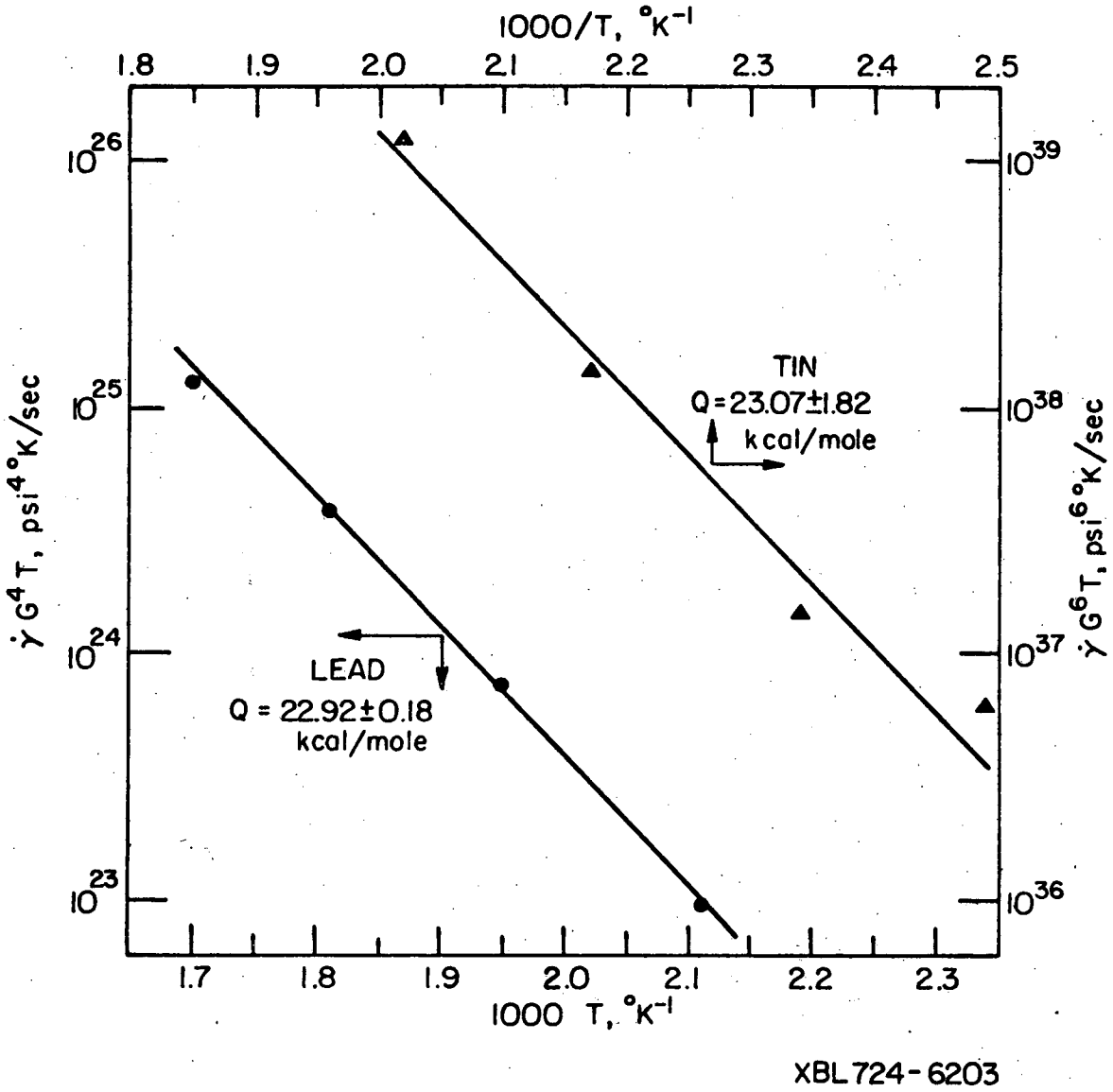
1000/T, °K⁻¹
1.8
1.9
2.0
2.1
2.2
2.3
2.4
2.5
10²⁶
10²⁵
10²⁴
10²³
10³⁹
10³⁸
10³⁷
10³⁶
TIN
Q=23.07±1.82
kcal/mole
LEAD
Q = 22.92±0.18
kcal/mole
1.7
1.8
1.9
2.0
2.1
2.2
2.3
1000 T, °K⁻¹
γ̇ G⁴T, psi⁴°K/sec
γ̇ G⁶T, psi⁶°K/sec
XBL724-6203

Fig. 23

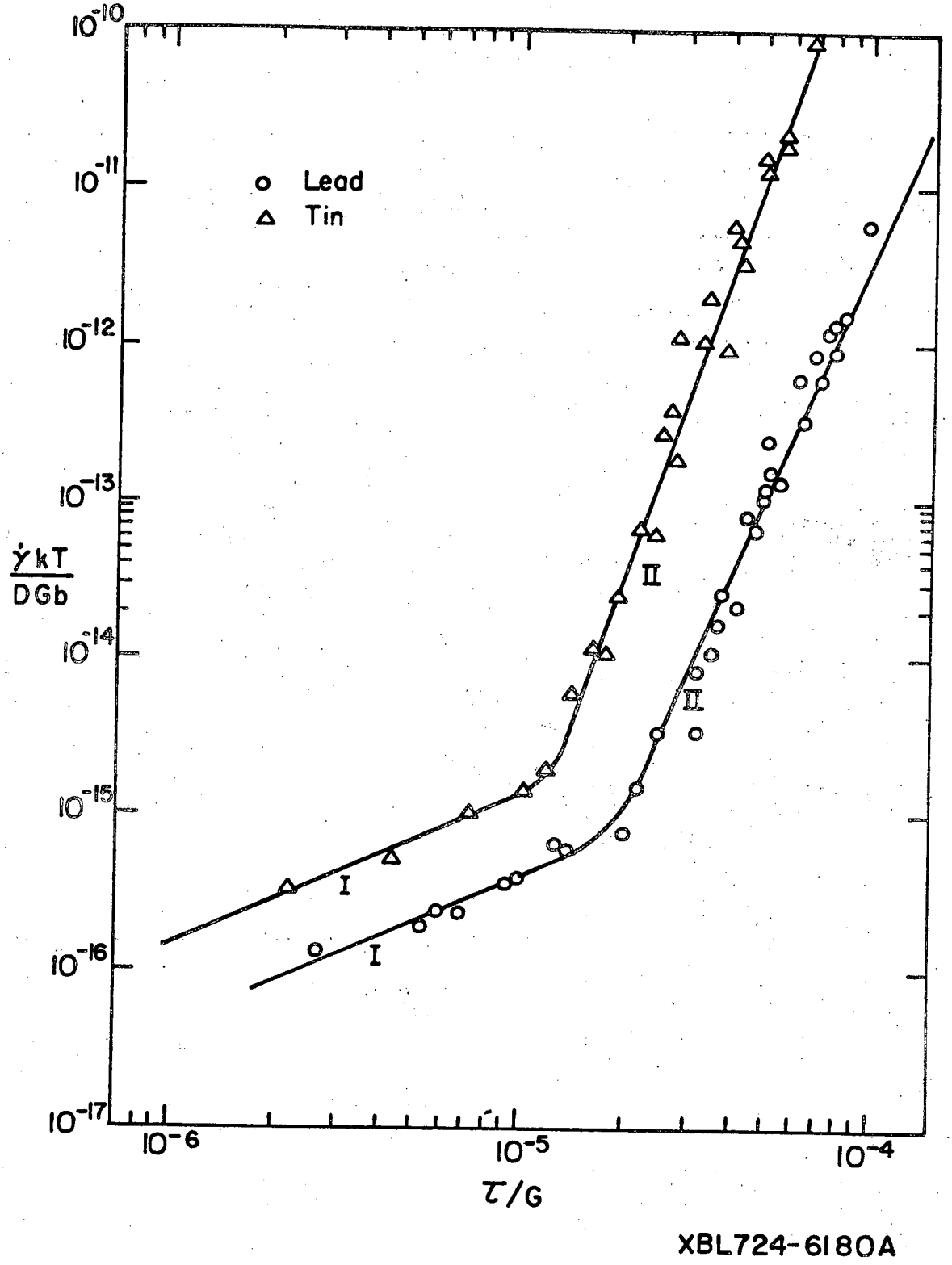
10^{-10}
10^{-11}
10^{-12}
10^{-13}
10^{-14}
10^{-15}
10^{-16}
10^{-17}
$\frac{\dot{\gamma} kT}{DGb}$
o Lead
Δ Tin
I
II
I
II
10^{-6}
10^{-5}
10^{-4}
τ/G
XBL724-6180A

Fig. 24

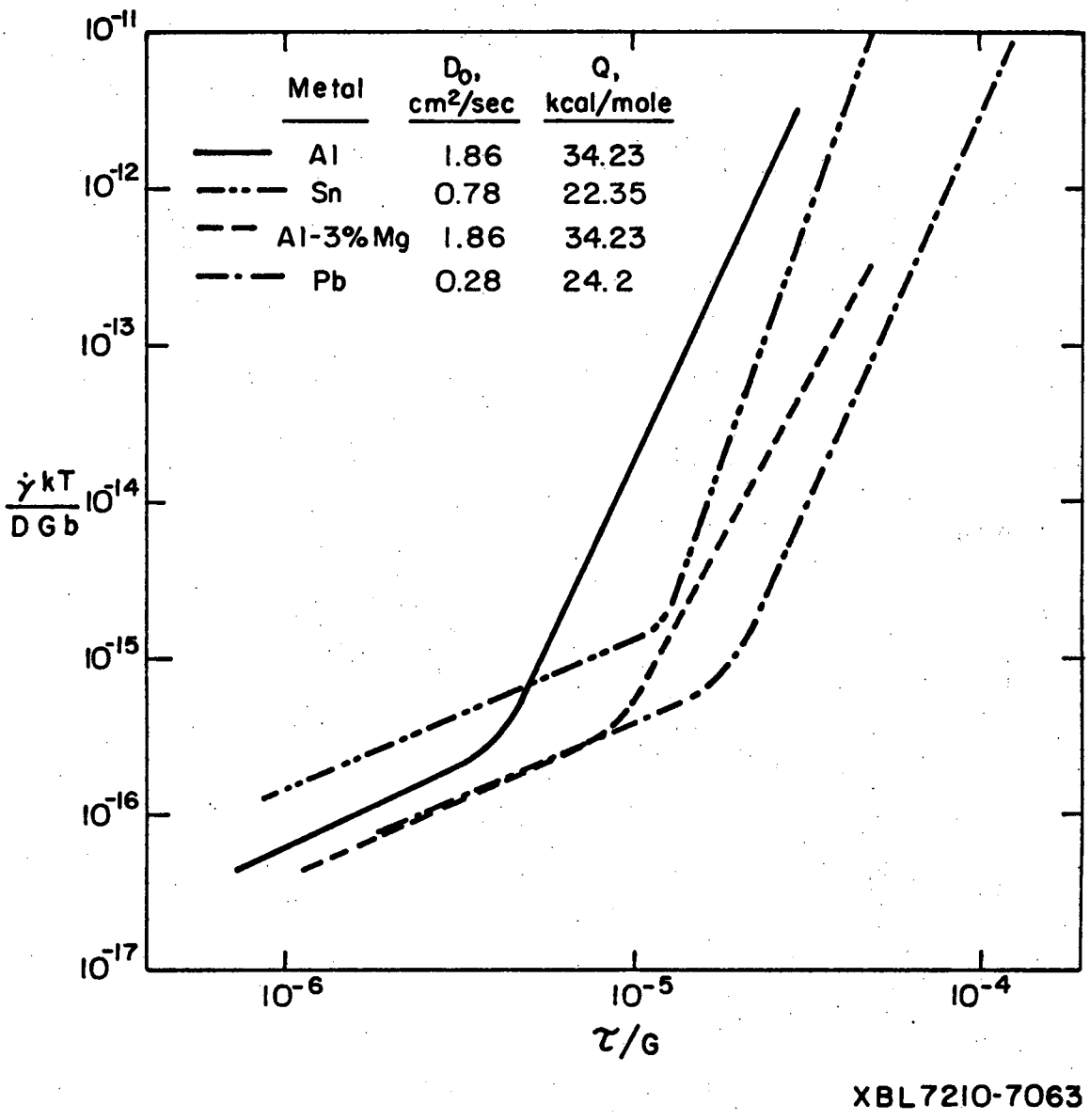
Metal
D_0, cm²/sec
Q, kcal/mole
Al 1.86 34.23
Sn 0.78 22.35
Al-3%Mg 1.86 34.23
Pb 0.28 24.2
10^{-11}
10^{-12}
10^{-13}
10^{-14}
10^{-15}
10^{-16}
10^{-17}
$\frac{\dot{\gamma} kT}{D G b}$
10^{-6}
10^{-5}
10^{-4}
τ/G
XBL7210-7063

Fig. 25

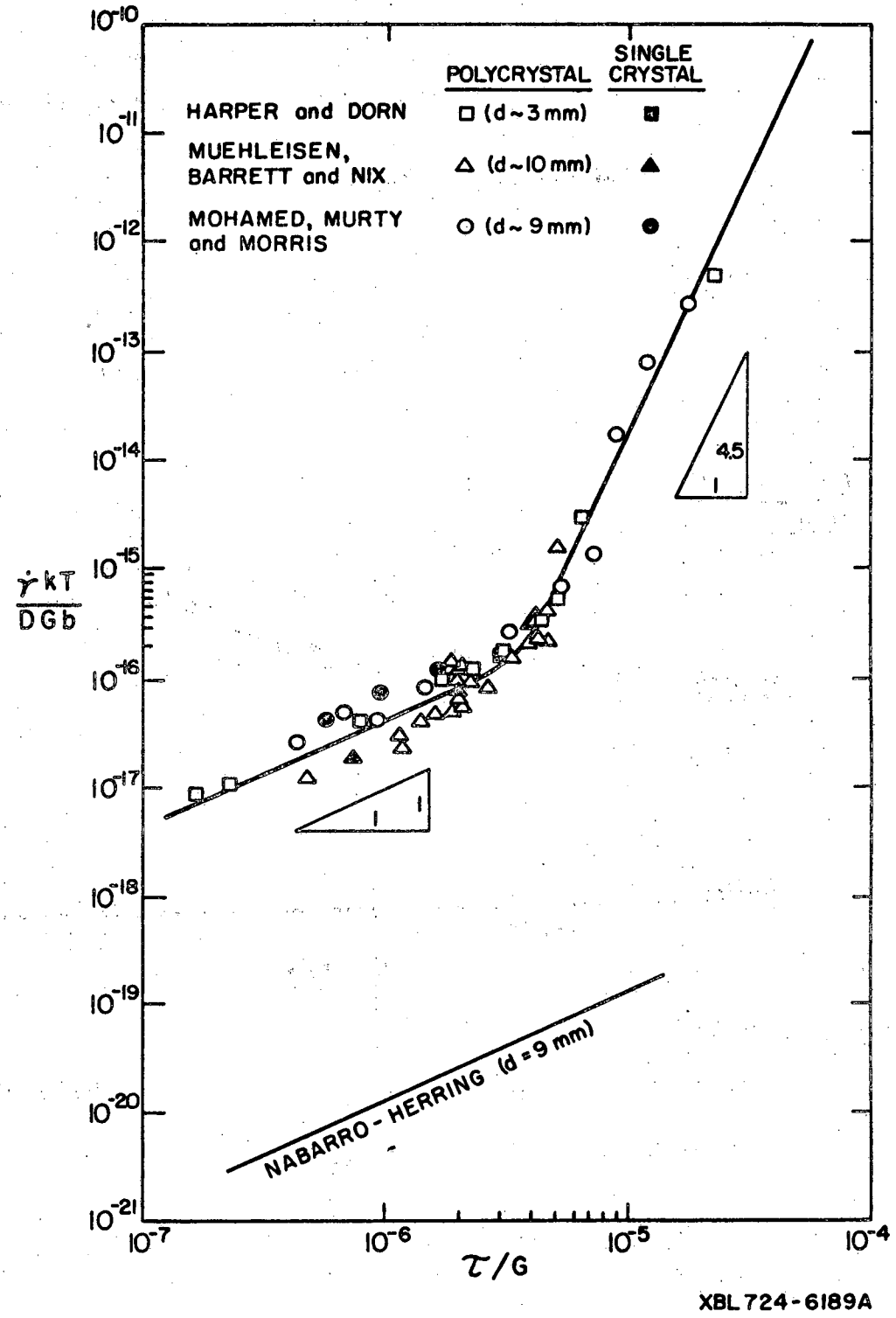
POLYCRYSTAL
SINGLE CRYSTAL
HARPER and DORN
□ (d ~ 3 mm)
■
MUEHLEISEN, BARRETT and NIX
△ (d ~ 10 mm)
▲
MOHAMED, MURTY and MORRIS
○ (d ~ 9 mm)
●
4.5
1
1
1
NABARRO - HERRING (d = 9 mm)
$\frac{\dot{\gamma} kT}{DGb}$
τ/G
10^{-10}
10^{-11}
10^{-12}
10^{-13}
10^{-14}
10^{-15}
10^{-16}
10^{-17}
10^{-18}
10^{-19}
10^{-20}
10^{-21}
10^{-7}
10^{-6}
10^{-5}
10^{-4}
XBL 724-6189A

Fig. 26

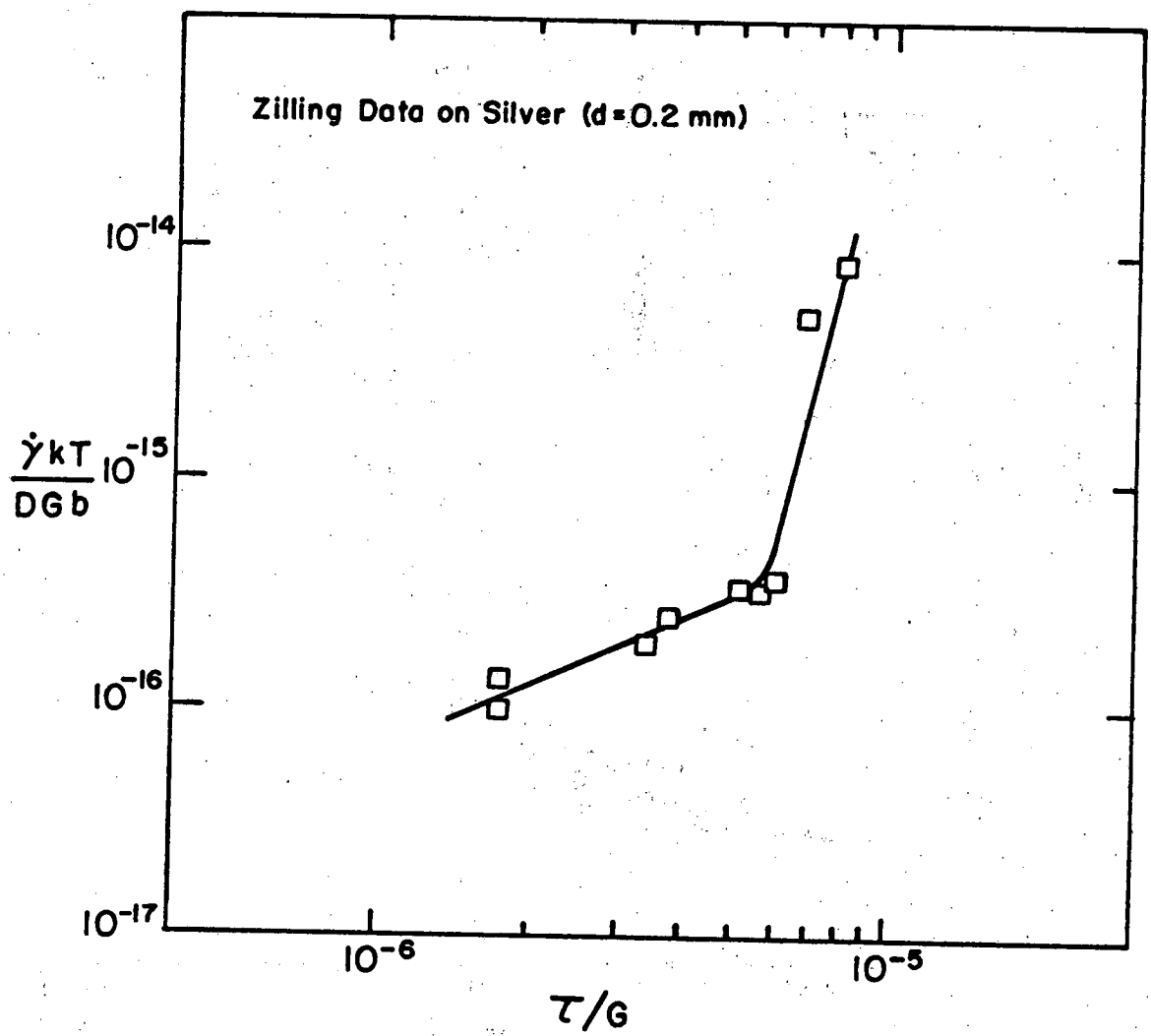
Zilling Data on Silver (d=0.2 mm)
10^{-14}
$\frac{\dot{\gamma} kT}{DGb}$ 10^{-15}
10^{-16}
10^{-17}
10^{-6}
10^{-5}
τ/G
XBL729-6919

Fig. 27

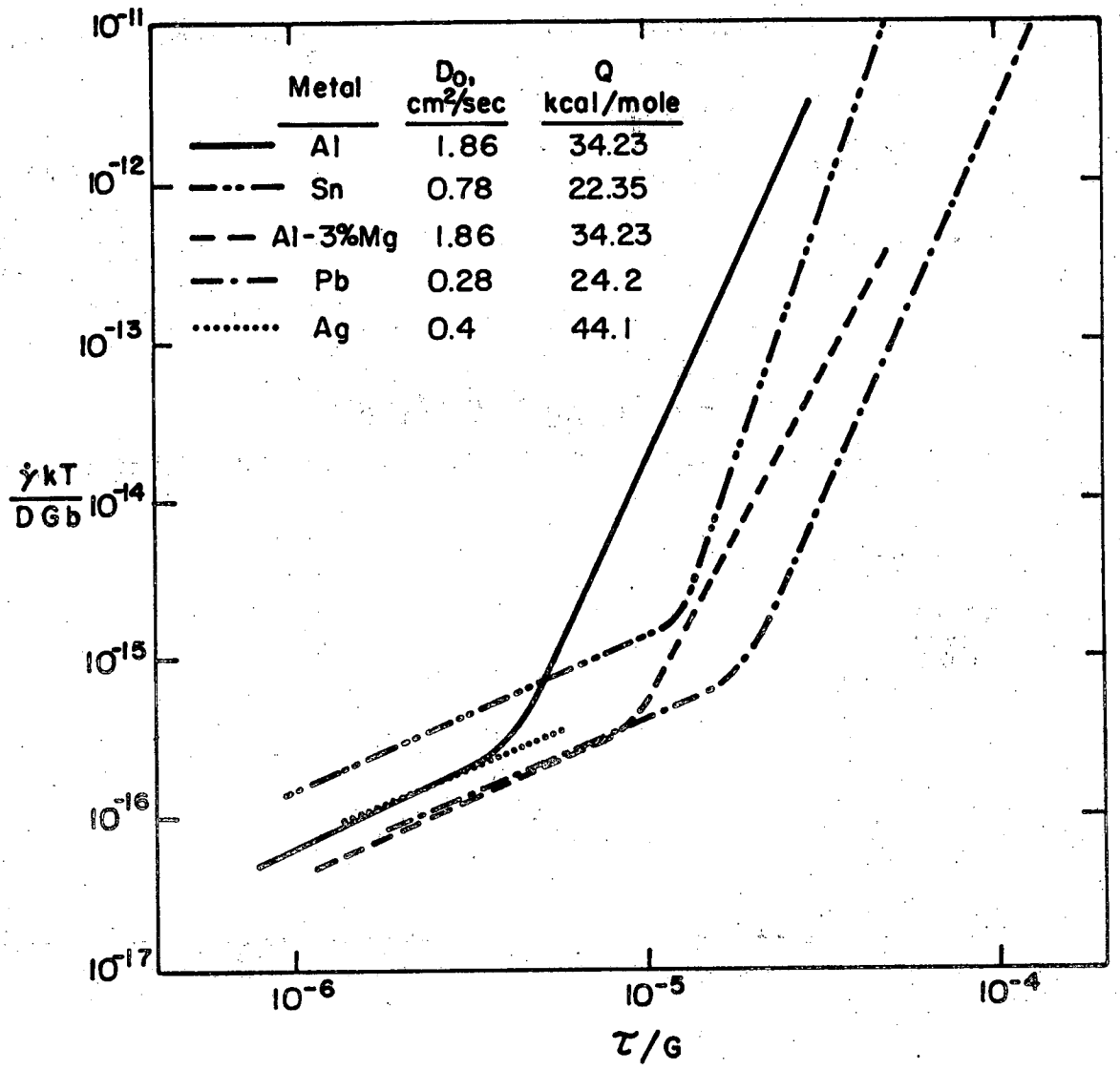

XBL7210-7062

Fig. 28

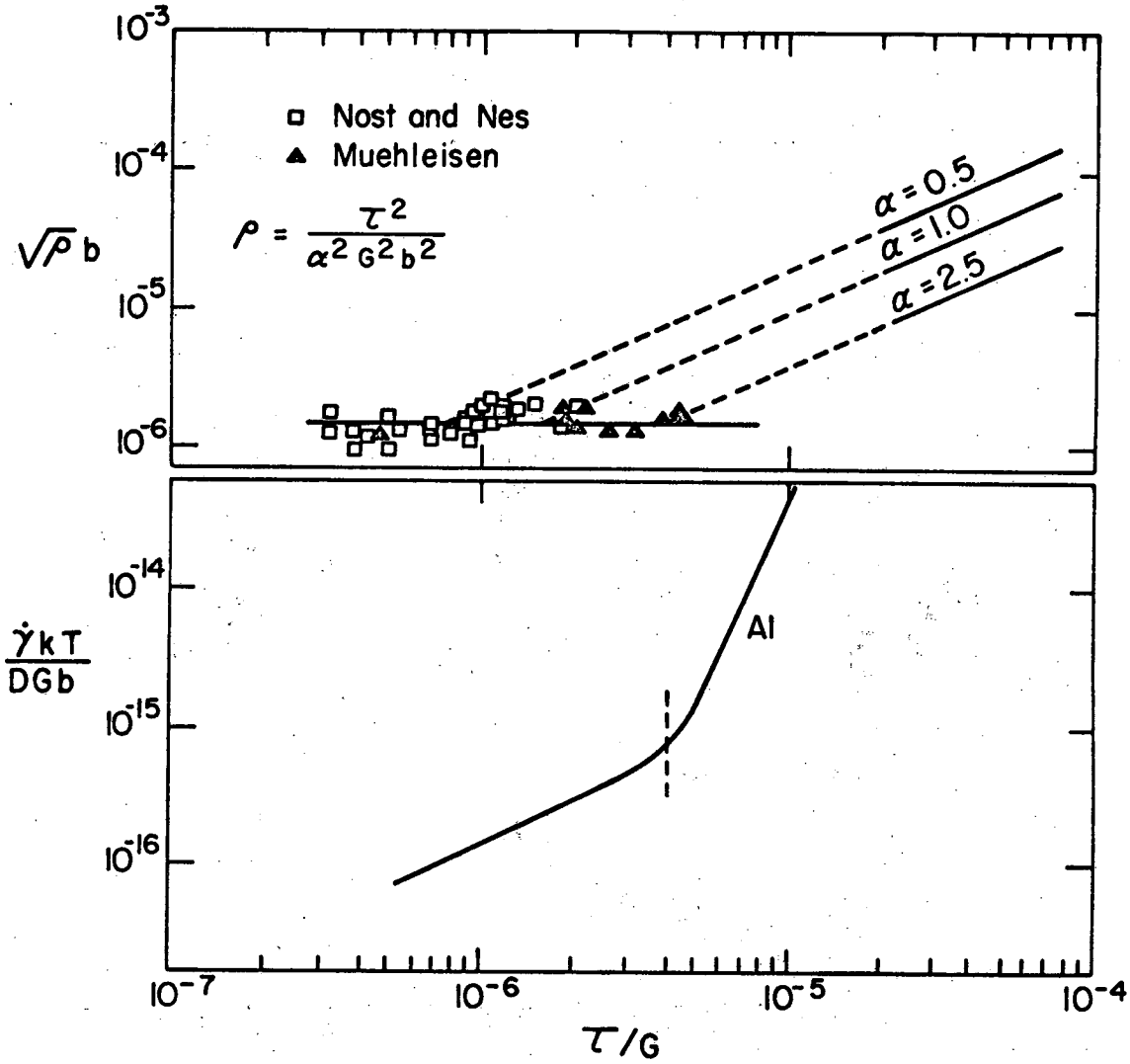
Nost and Nes
Muehleisen
$\rho = \frac{\tau^2}{\alpha^2 G^2 b^2}$
$\alpha = 0.5$
$\alpha = 1.0$
$\alpha = 2.5$
$\sqrt{\rho}\, b$
$\frac{\dot{\gamma} k T}{D G b}$
Al
τ/G
XBL 724-6204A

Fig. 29

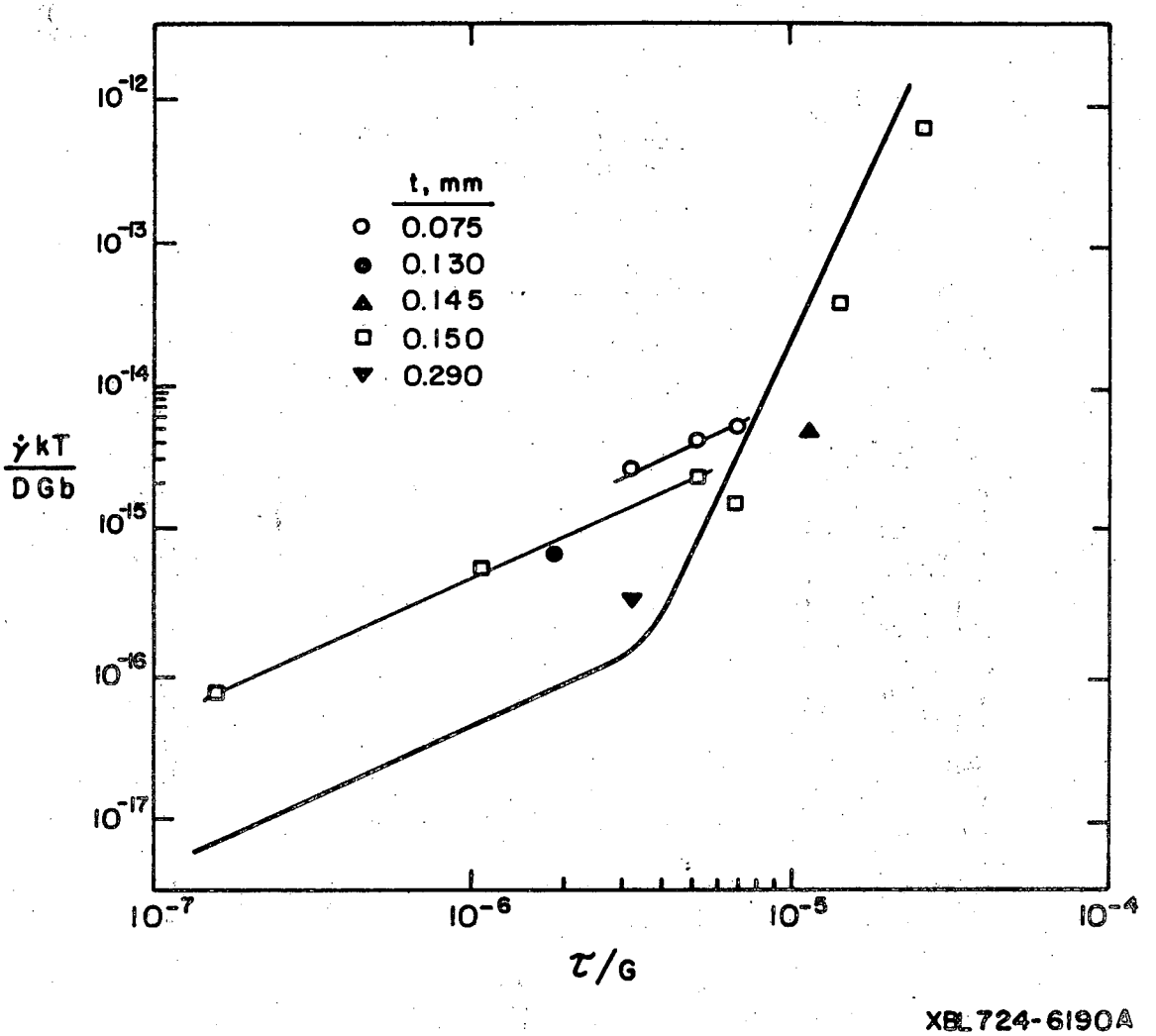

XBL724-6190A

Fig. 30

Harper–Dorn Creep vs Nabarro in Pure Aluminum

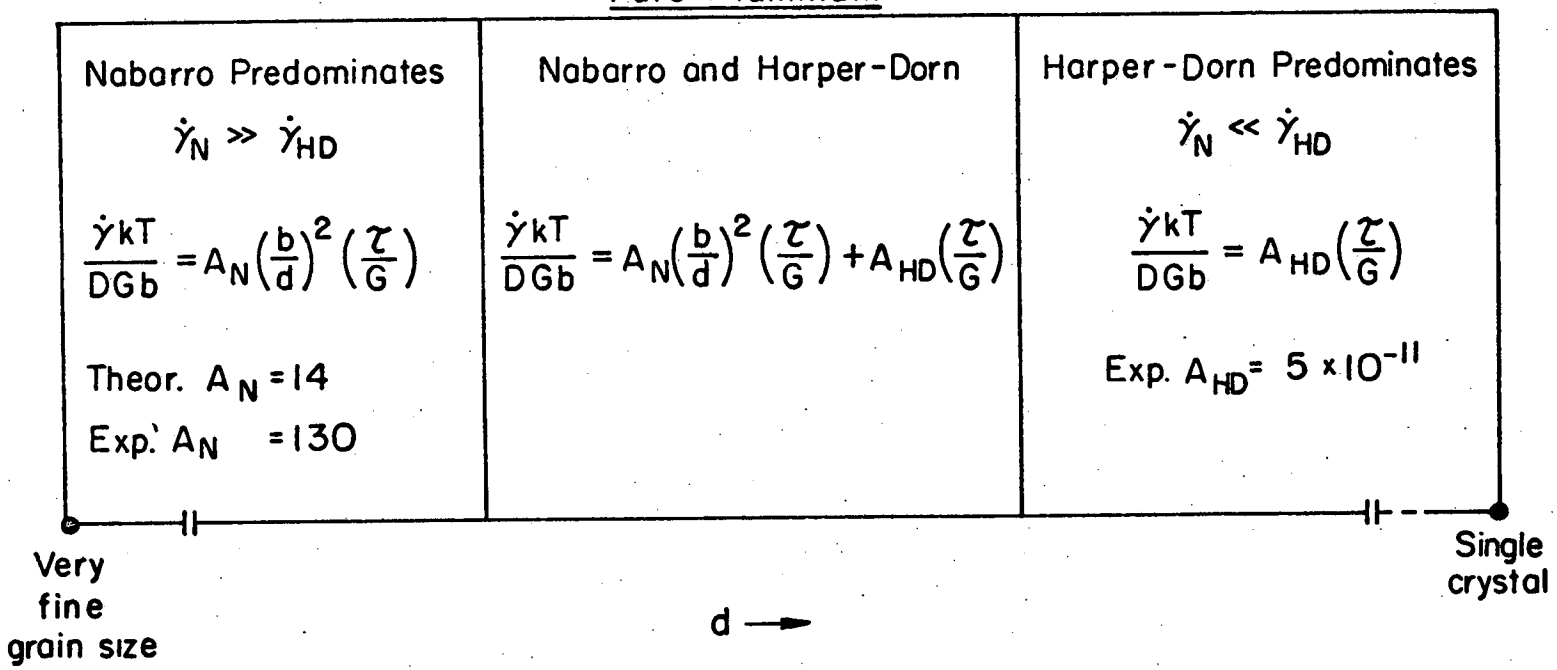

Critical grain size for pure Al ≅ 0.05 cm

XBL727-6472

Fig. 31

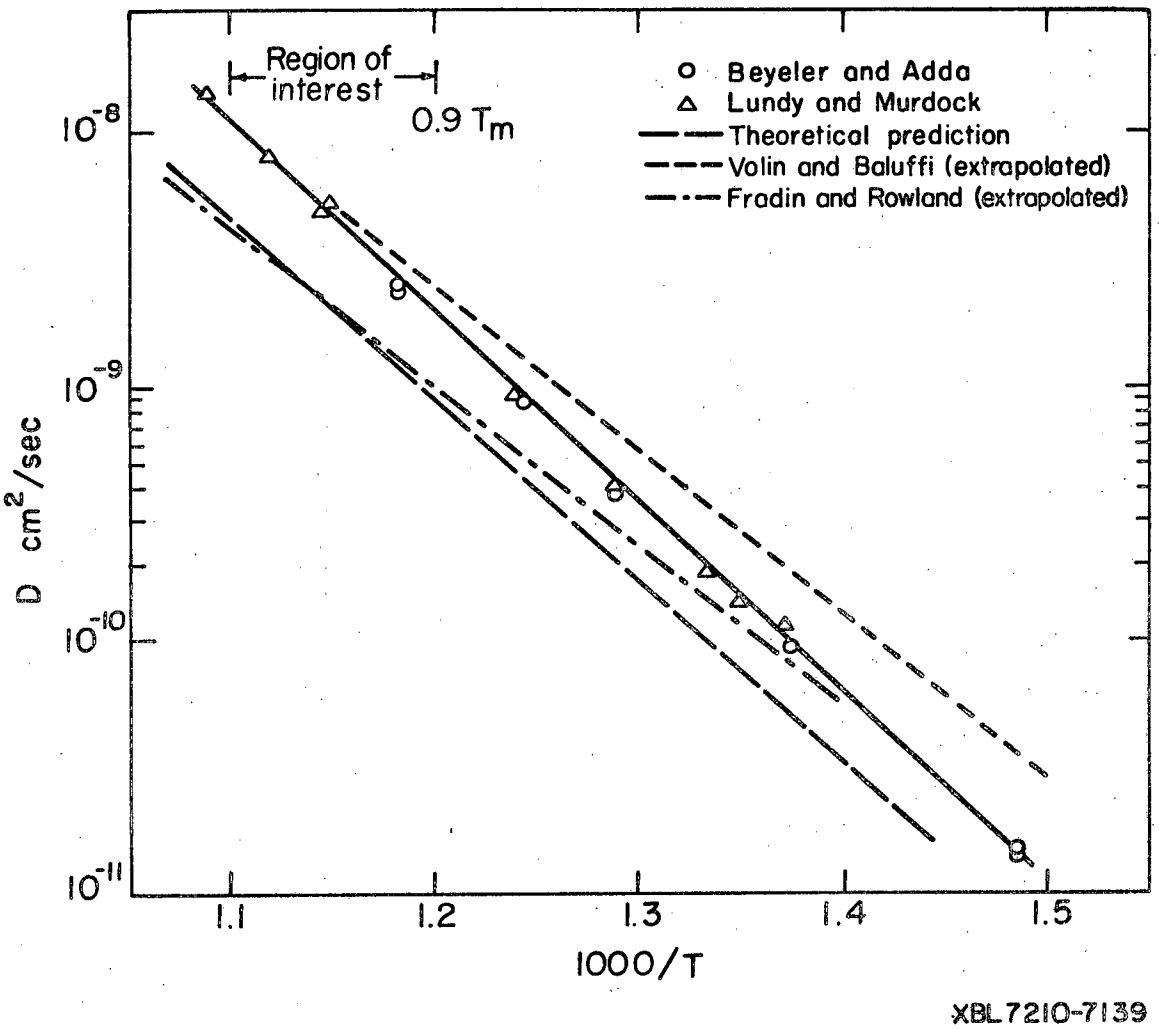
Region of interest
0.9 Tm
Beyeler and Adda
Lundy and Murdock
Theoretical prediction
Volin and Baluffi (extrapolated)
Fradin and Rowland (extrapolated)
D cm²/sec
10⁻⁸
10⁻⁹
10⁻¹⁰
10⁻¹¹
1.1
1.2
1.3
1.4
1.5
1000/T
XBL7210-7139

Fig. 32

TECHNICAL INFORMATION DIVISION
LAWRENCE BERKELEY LABORATORY
UNIVERSITY OF CALIFORNIA
BERKELEY, CALIFORNIA 94720